SSEC PUB #73.02.S1

POWER SPECTRAL ANALYSIS OF SIMULATED SMS DATA

A REPORT

from the space science and engineering center
the university of wisconsin-madison
madison, wisconsin

POWER SPECTRAL ANALYSIS OF SIMULATED SMS DATA

An Interim Report on NOAA Grant

NG-26-72

by

F. G. Stremler

G. R. Redinbo

Space Science and Engineering Center
University of Wisconsin
Madison, Wisconsin

15 February 1973

INTRODUCTION

This interim report contains preliminary results in the error analysis of the VISSR channel of the SMS. Photographs taken on the Apollo VI mission were studied to obtain a valid model of the spectral information of signals as viewed by the SMS. Some results of this study are shown.

Further work is continuing toward an estimation of aliasing error effects arising from spectral folding both for cloud patterns at the satellite subpoint and in a moré general geometry. The effects of sampling and of both spatial and spectral limiting are being considered especially as they degrade resolution. Actual system transfer functions will also be considered in this next phase of the analysis.

POWER SPECTRAL PLOTS FOR APOLLO VI TRANSPARENCIES

Color transparencies of Apollo VI cloud photographs were studied, and those containing interesting and typical cloud patterns were selected. Following consultations with representatives of NOAA and SSEC,* ten were selected for spectral analysis.

These ten 70 mm transparencies were copied using high resolution film (Panatomic X) and carefully mounted in glass mounts and sent to the DicoMed Corporation (Minneapolis) for digitizing. The transparencies were scanned on their Model 56 Image Digitizer in a 1024 x 1024 format using a slow scan (23 minutes per transparency). The data was quantized to 8 bits and recorded on magnetic tape. The scanning aperture used was 55 microns diameter. Bar patterns had been sent along for calibration purposes and these were digitized both at the beginning and end of the digitization runs.

The tape received from DicoMed was reformated for easy access in the UNIVAC 1108, as shown in Table 1. A sample line from each bar pattern was printed and these were checked for equipment drift problems. Differences in readings were on the order of two parts out of 256 or less. Also a FFT plot was made on the bar patterns to check the spatial frequencies of the harmonic content.

---

*Geoff Albert and Joe Silverman of NOAA, Verner E. Suomi, Thomas O. Haig, and Alfred Stamm of the Space Science and Engineering Center, University of Wisconsin.

TABLE 1

Apollo Picture Location for UNIVAC 1108

Tape #17		Tape #18	
File	Apollo Picture	File	Apollo Picture
1	56-2-877	1	56-2-1430
2	56-2-934	2	56-2-1467
3	56-2-948	3	56-2-1468
4	56-2-1064	4	56-2-1469
5	56-2-1429	5	56-2-1484 (horiz.)
		6	56-2-1484 (vert.)

Prints of seven of these Apollo VI transparencies are shown in Figures 1 and 2. The power spectra of selected regions of these transparencies were run on the UNIVAC 1108 and plotted. Results are shown in the following pages and reveal a gradual exponential decrease with increasing spatial frequency. A conversion chart to convert these scales to SMS at the satellite subpoint is shown in Figure 3. These conversions vary as a function of angle, and therefore are referred to the satellite subpoint. A graph showing the variation of the frequency conversion when the scan line passes through the earth's center is shown in Figure 4; a derivation of this correction can be found in Appendix C. From these conversions, our preliminary conclusion is that the power spectral density decreases about 10-15 dB within the 0-200 kHz range at the satellite subpoint.

The power spectra shown have been run with a rectangular window and 512 sample points. The line numbers and sample point locations are

Apollo 56-2-877

Apollo 56-2-934

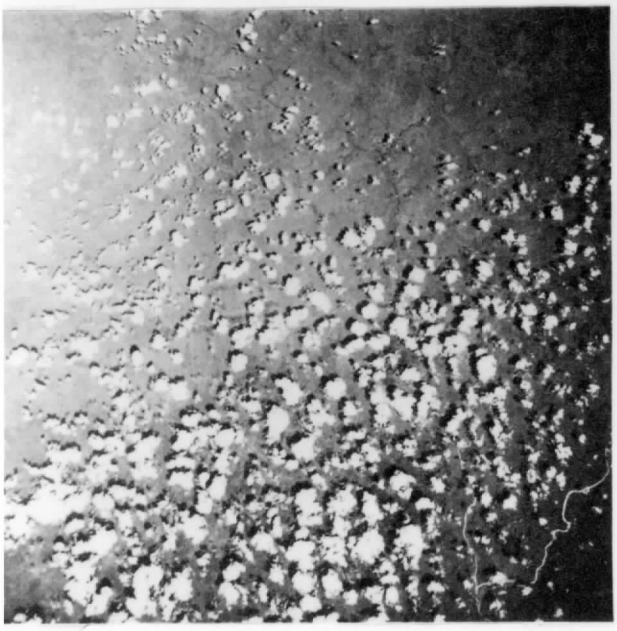

Apollo 56-2-948

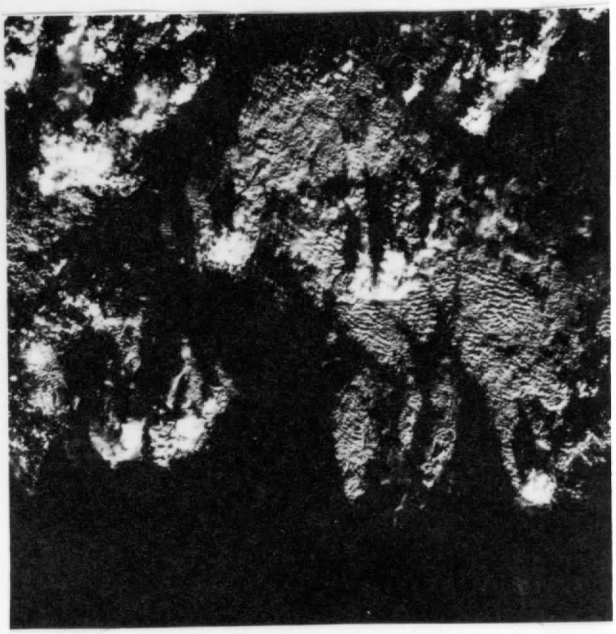

Apollo 56-2-1064

Figure 1

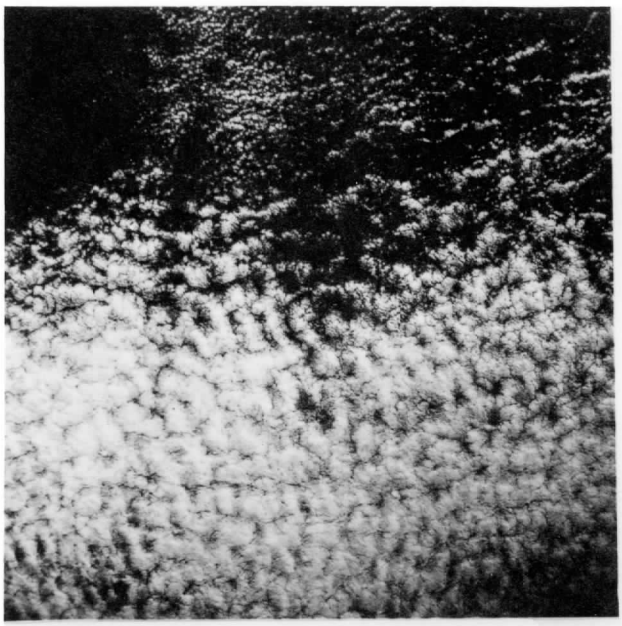

Apollo 56-2-1429

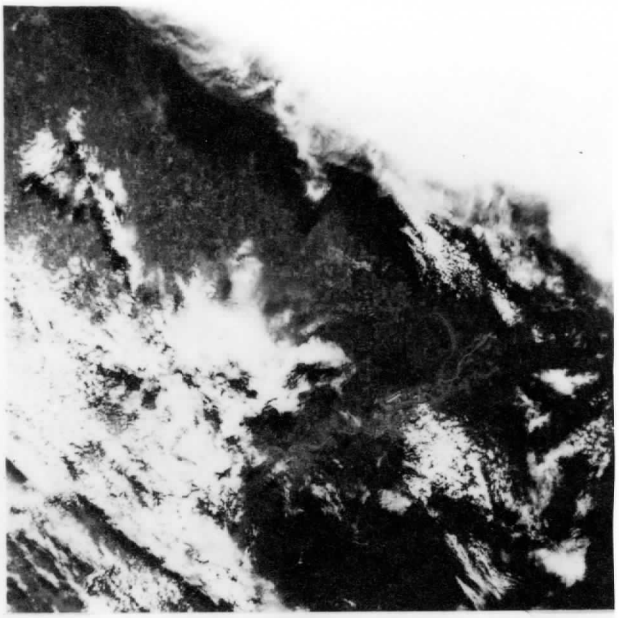

Apollo 56-2-1468

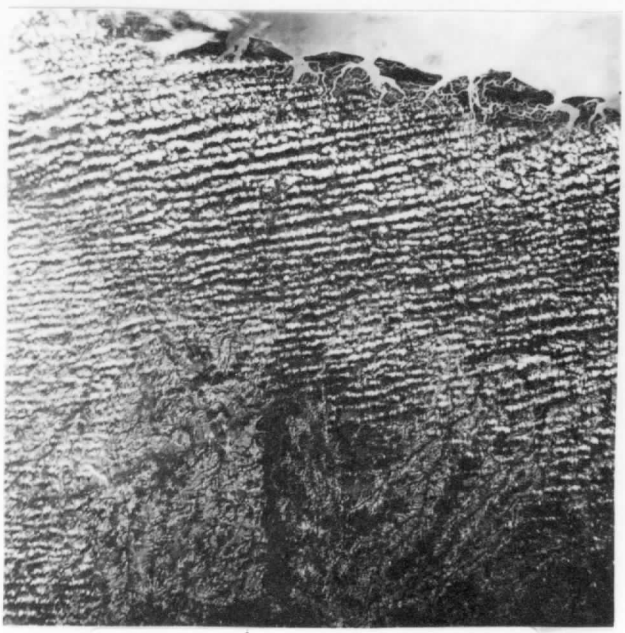

Apollo 56-2-1484 (horiz.)

Apollo 56-2-1484 (vert.)

Figure 2

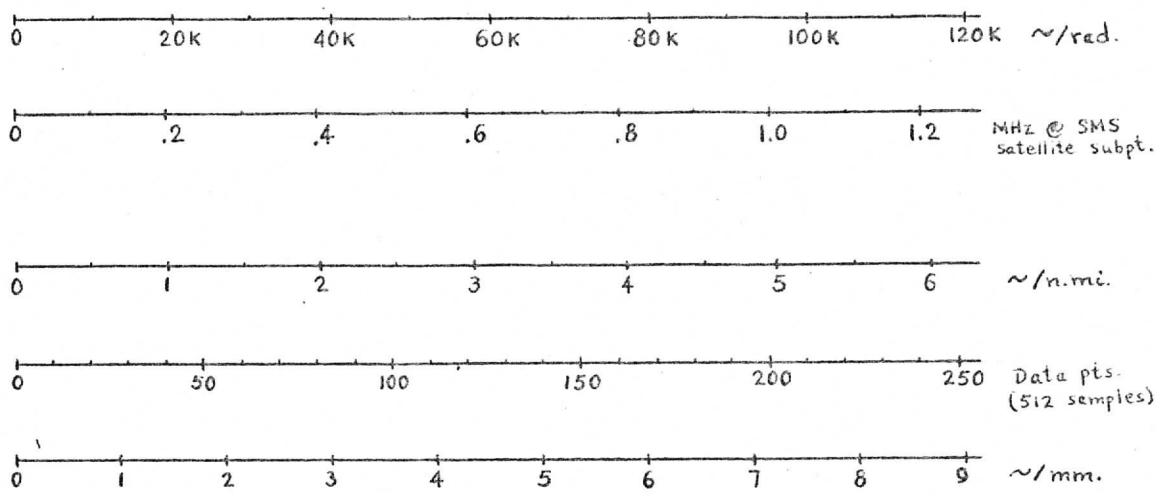

Figure 3. Conversion Chart for SMS Spectral Data.

shown on the graphs. Other window functions have been tested but not used on the spectral plots. The window functions considered are discussed in Appendix B. Sample runs on picture data using a Hanning and a Hamming window showed no significant changes. Use of the Papoulis window is under investigation at this time. It is expected that the use of various window functions will not alter these power spectral plots appreciably.

The spectral plots shown reflect the spatial frequency content of the scene to be viewed by SMS. The Apollo transparencies were sampled at .055 mm/sample (.079 n.mi/sample) yielding a maximum frequency of 9.15 cycles/mm (6.33 cycles/n.mi.). A sampling rate under 10 cycles per mm was judged well within the limitations of the film. On the other hand, this maximum frequency corresponds to a 1.28 MHz rate at the SMS subpoint

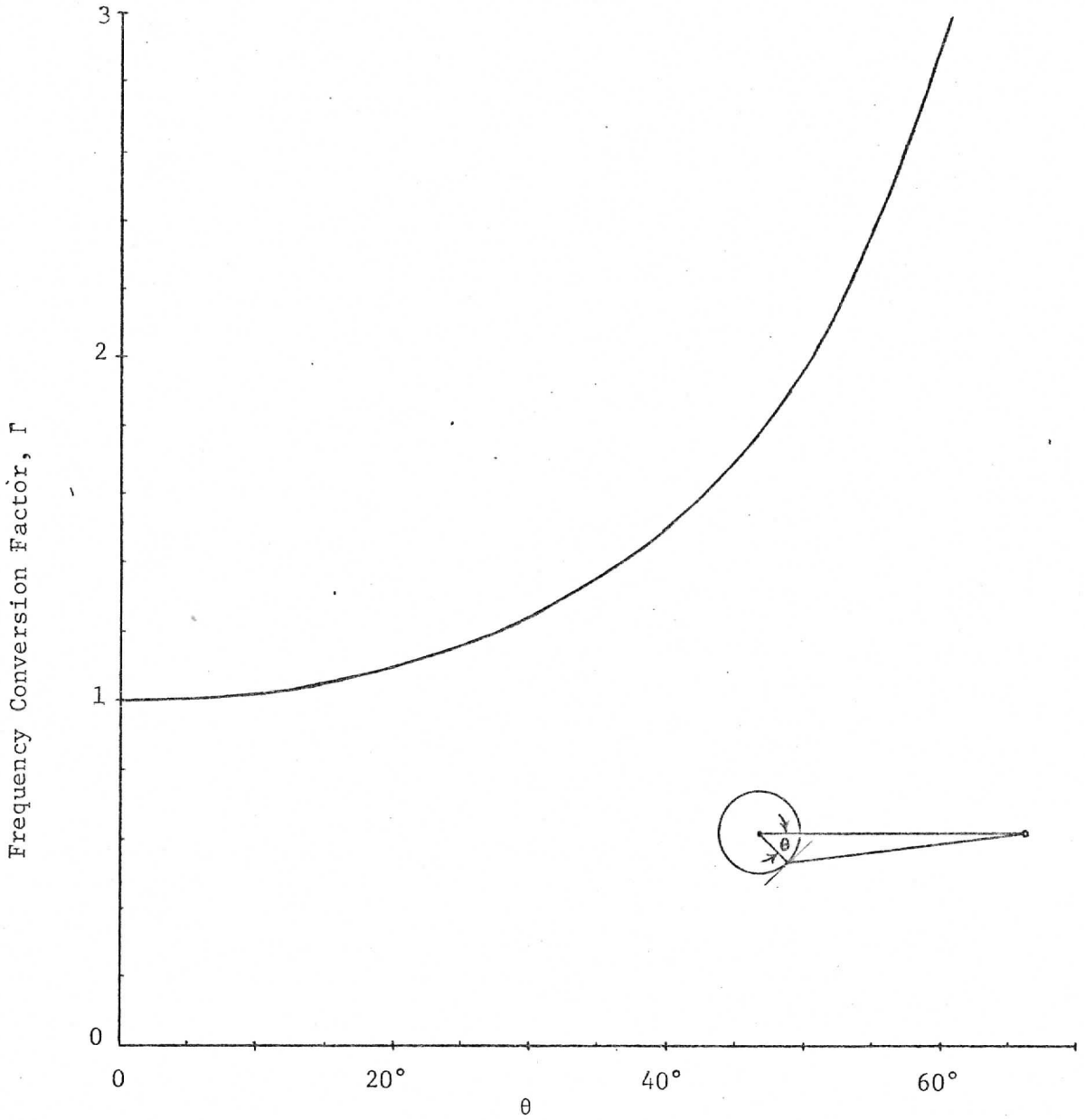

Figure 4. Frequency Conversion Factor for SMS.

which is about a factor of six higher than the maximum frequency of the pre-alias filters. This latter margin will allow us to use a discrete approximation to the pre-alias filters by merely frequency-sampling the transfer functions.

The effects of scanning apertures, both of the DicoMed scanner and of the SMS, have not been included in the spectral plots. These effects are not major; they are discussed in Appendix A.

The plots shown were generated using a 512-pt. FFT routine in the UNIVAC 1108. This is discussed in Appendix B.

The computer-generated plots follow the same order: (1) the (logarithmic) power spectral plot of the first sample line; (2) the autocorrelation function of the first sample line; (3) the (logarithmic) power spectral plot of the fifth sample line; (4) the log of the average power spectrum of five consecutive lines; (5) the average autocorrelation function of five consecutive lines. Averaging over five lines decreases the spectral randomness in the measurement and is essentially averaging over a scan of 5 x .079 = 0.395 n.mi. in width. A smoothing window to average in the along-scan direction will be tried so as to smooth the data. However, it was not used in this plotting routine.

Apollo 56-2-877, (rect.)
Locator: Tape 17, File 1
Records: 860 - 864 Date: 2/1/73
Elements: 510 - 1021
Plot: Log Power Spectrum, First Line

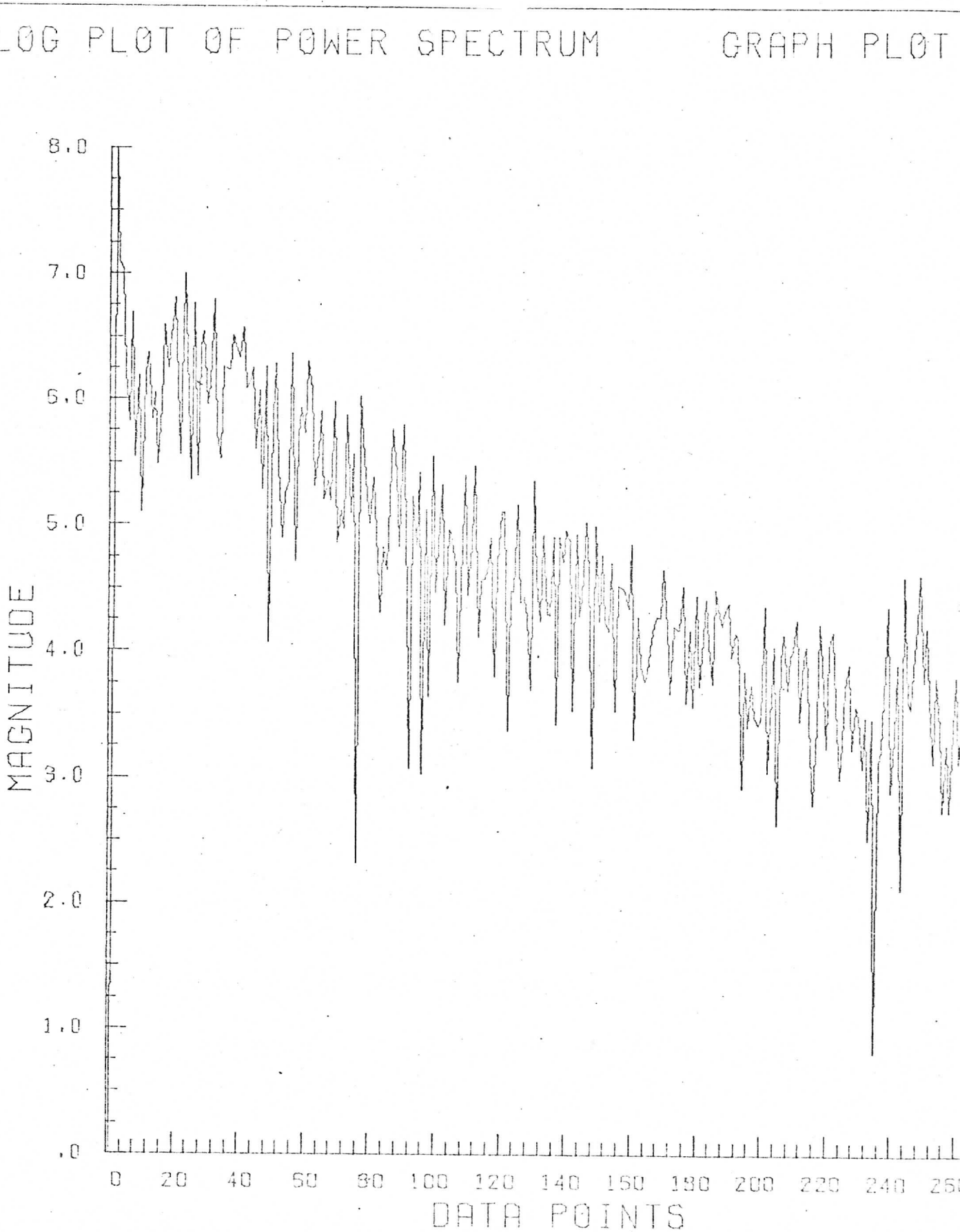

Apollo 56-2-877, (rect.)
Locator: Tape 17, File 1
Records: 860 - 864 Date: 2/1/73
Elements: 510 - 1021
Plot: Autocorrelation, First Line

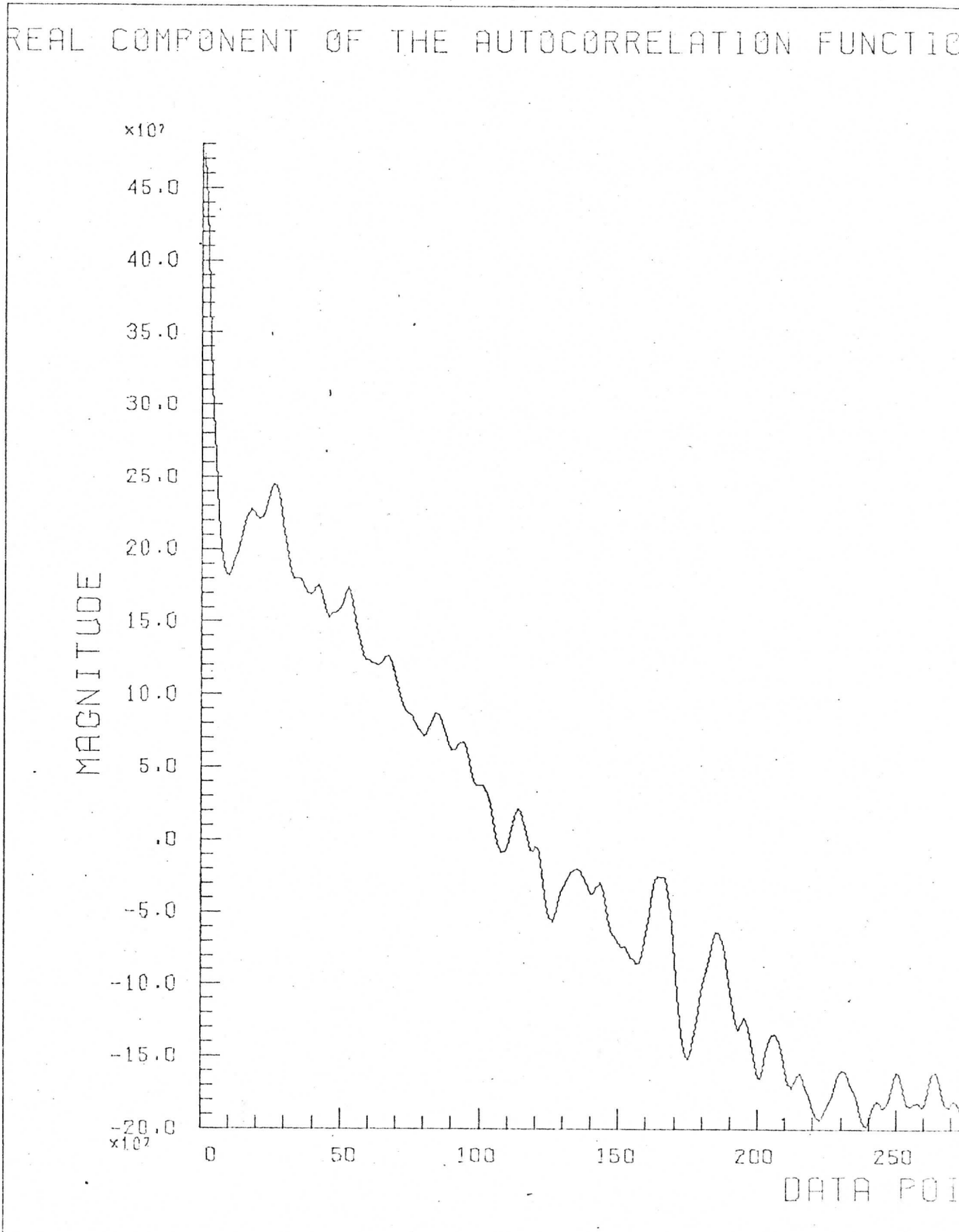

Apollo 56-2-877, (rect.)
Locator: Tape 17, File 1
Records 860 - 864 Date: 2/1/73
Elements: 510 - 1021
Plot: Log Power Spectrum, Fifth Line

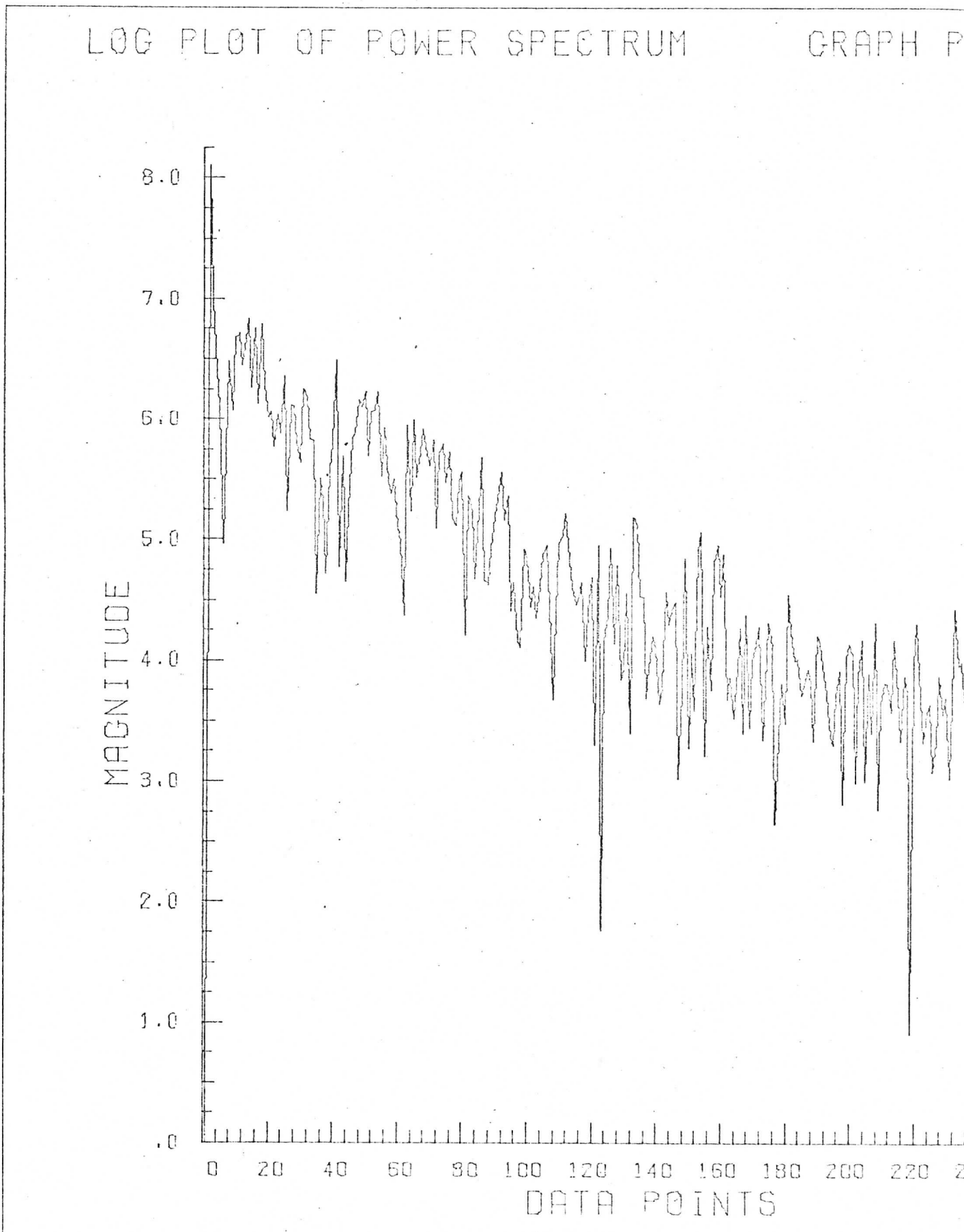

Apollo 56-2-877, (rect.)
Locator: Tape 17, File 1
Records: 860 - 864 Date: 2/1/73
Elements: 510 - 1021
Plot: Log Avg. Powen Spectrum

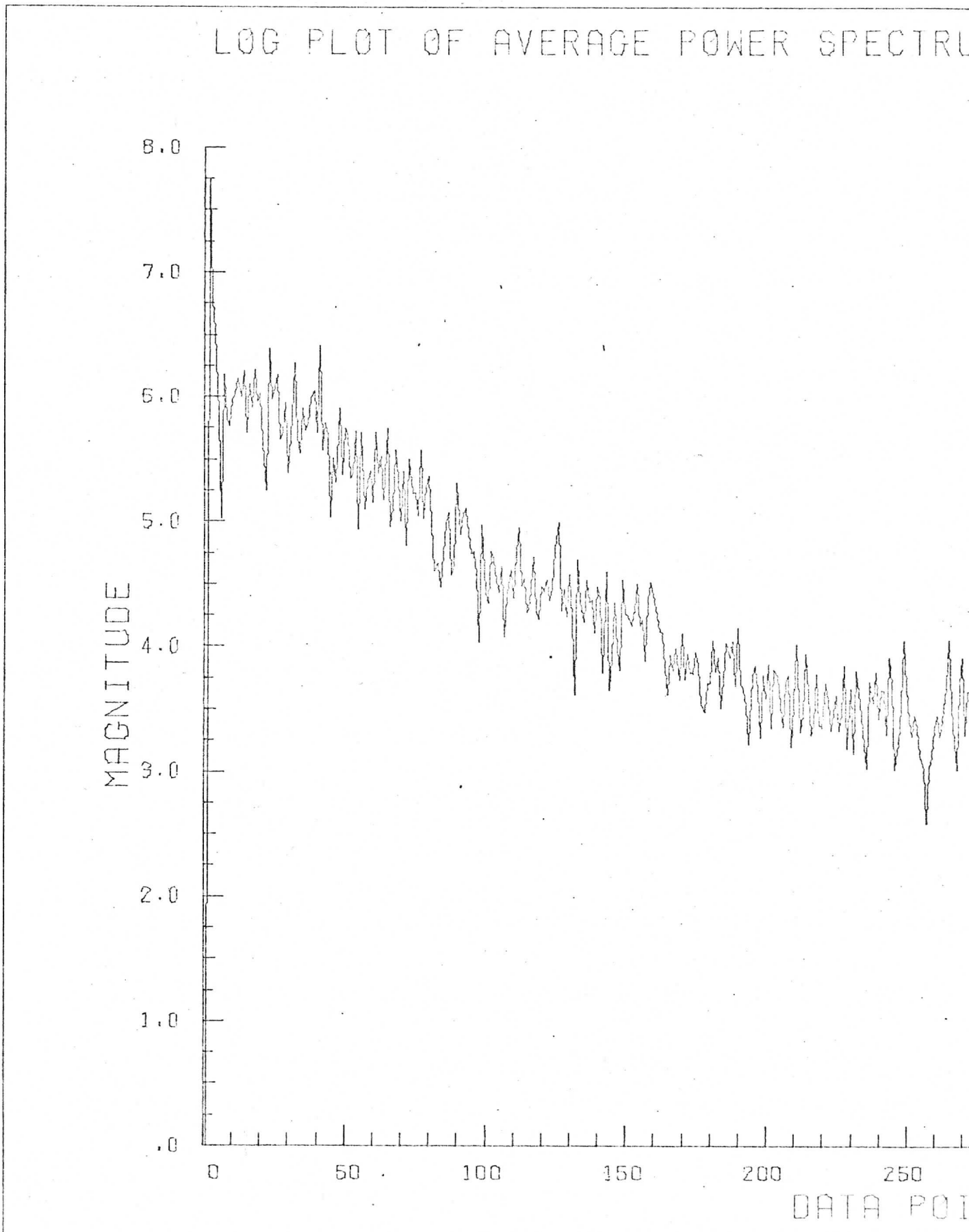

Apollo 56-2-877, (rect.)
Locator: Tape 17, File 1
Records: 860 - 864 Date: 2/1/73
Elements: 510 - 1021
Plot: Avg. Autocorrelation

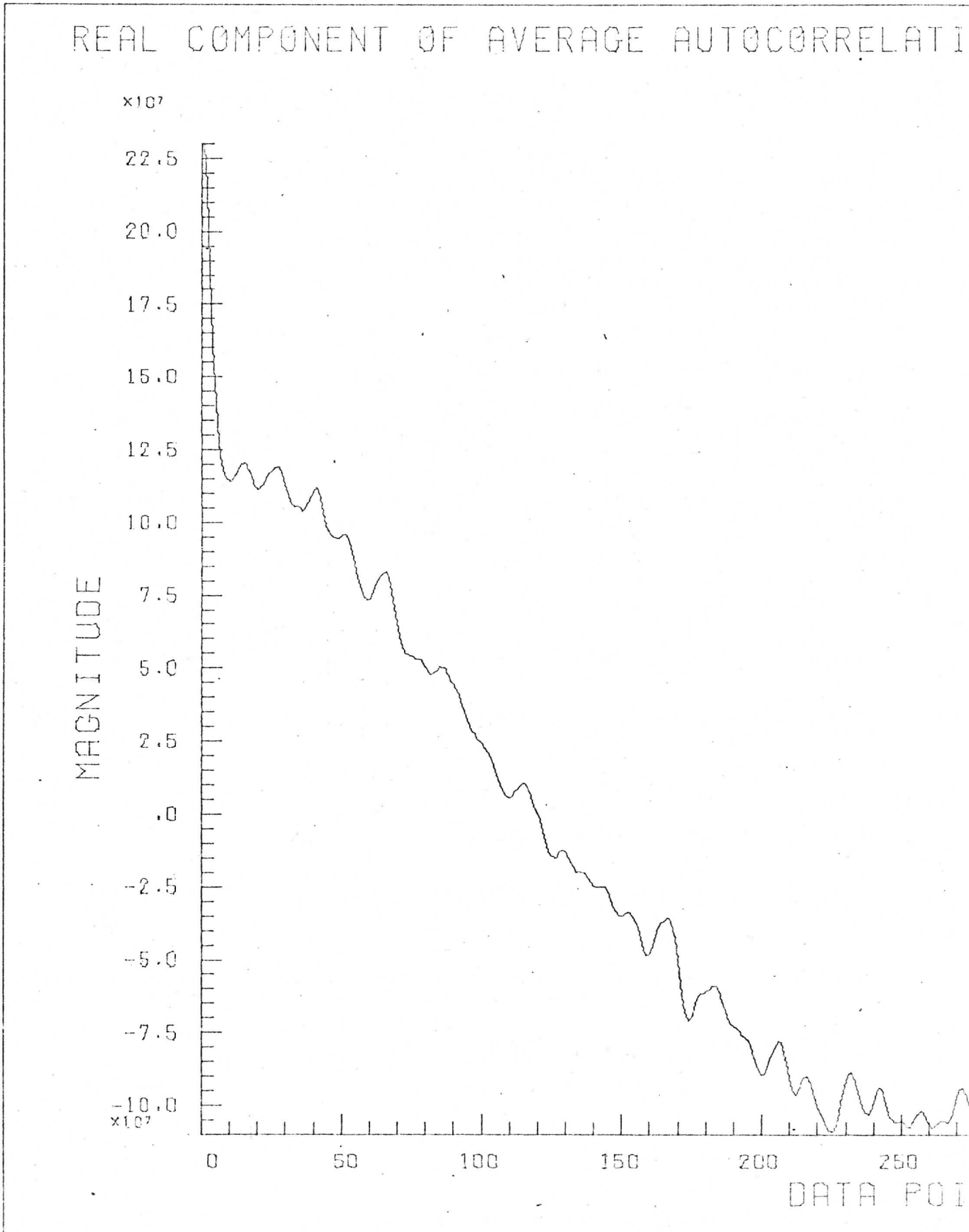

Apollo 56-2-934, (rect.)
Locator: Tape 17, File 2
Records: 100 - 104 Date: 2/1/73
Elements: 510 - 1021
Plot: Log Power Spectrum, First Line

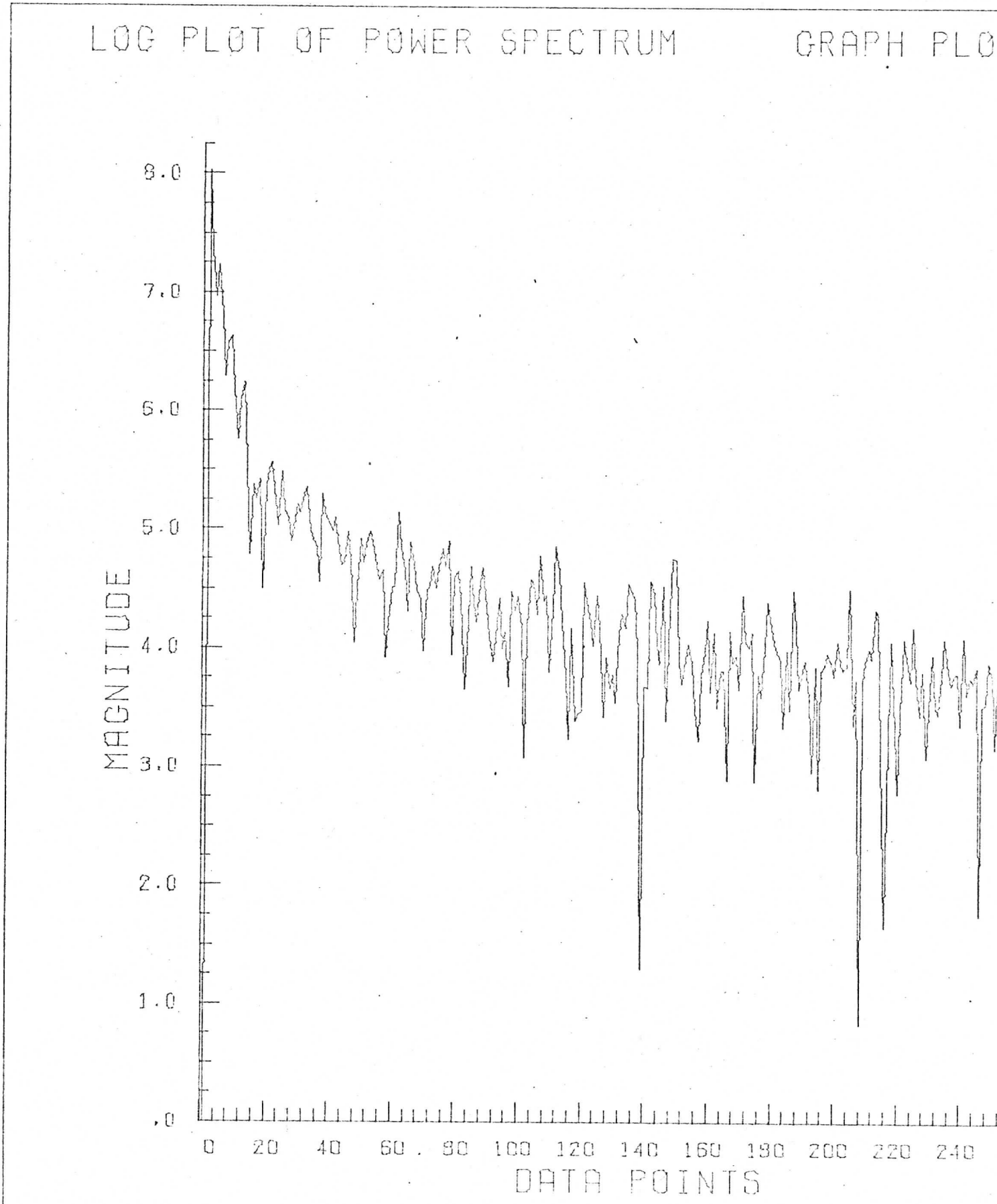

Apollo 56-2-934, (rect.)
Locator: Tape 17, File 2
Records: 100 - 104 Date: 2/1/73
Elements: 510 - 1021
Plot: Autocorrelation, First Line

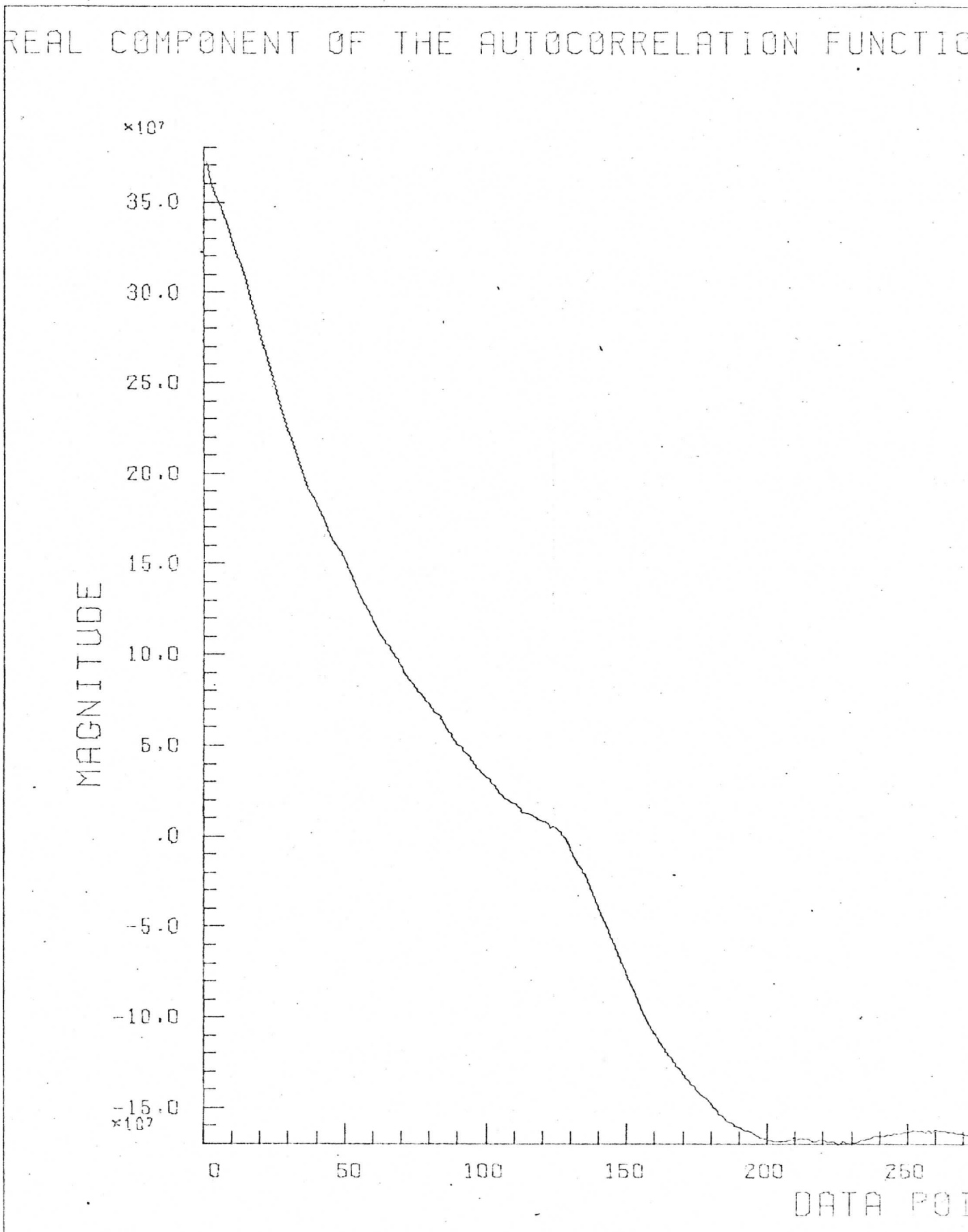

Apollo 56-2-934, (rect.)
Locator: Tape 17, File 2
Records: 100 - 104 Date: 2/1/73
Elements: 510 - 1021
Plot: Log Power Spectrum, Fifth Line

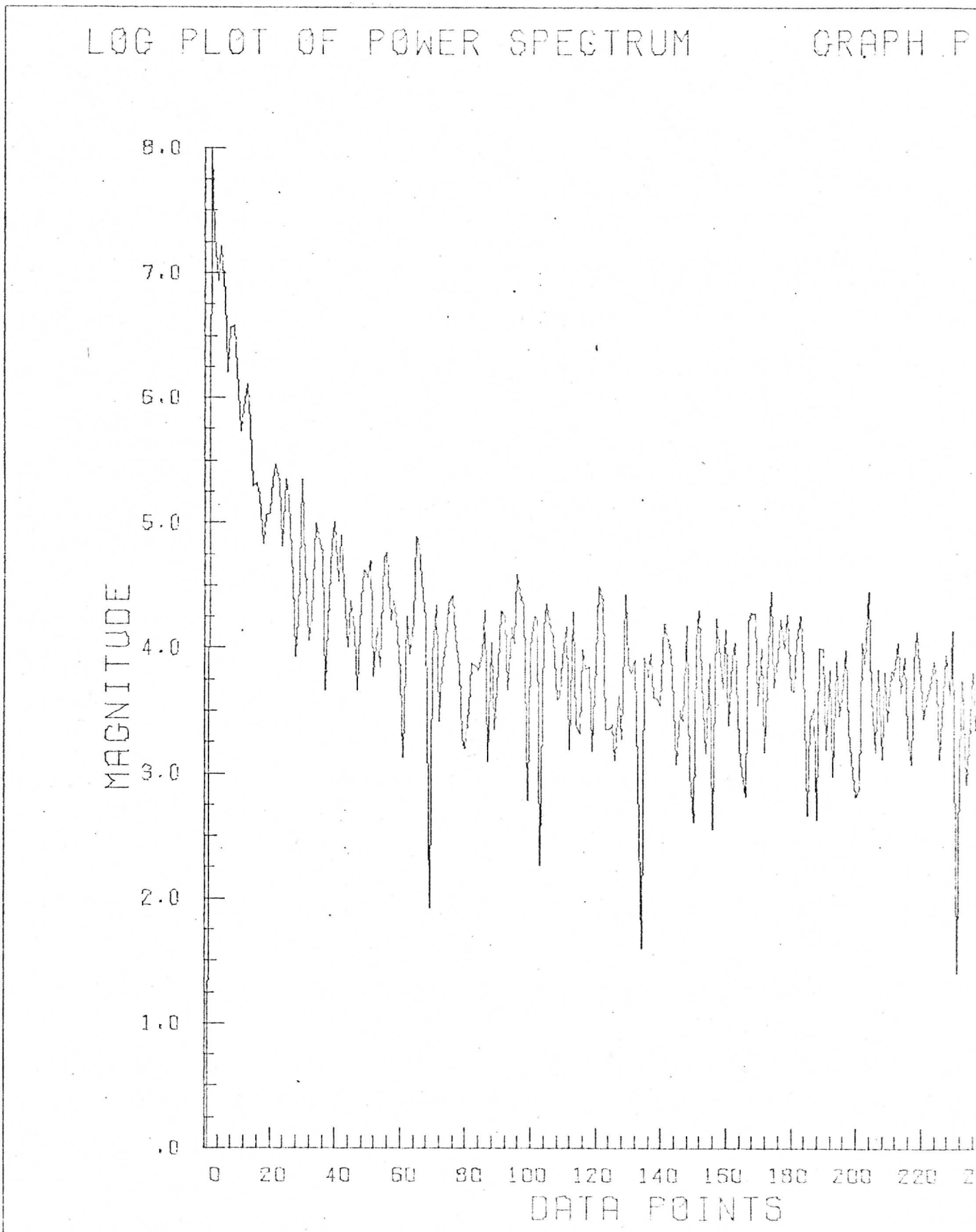

Apollo 56-2-934, (rect.)
Locator: Tape 17, File 2
Records: 100 - 104 Date: 2/1/73
Elements: 510 - 1021
Plot: Log Avg. Power Spectrum

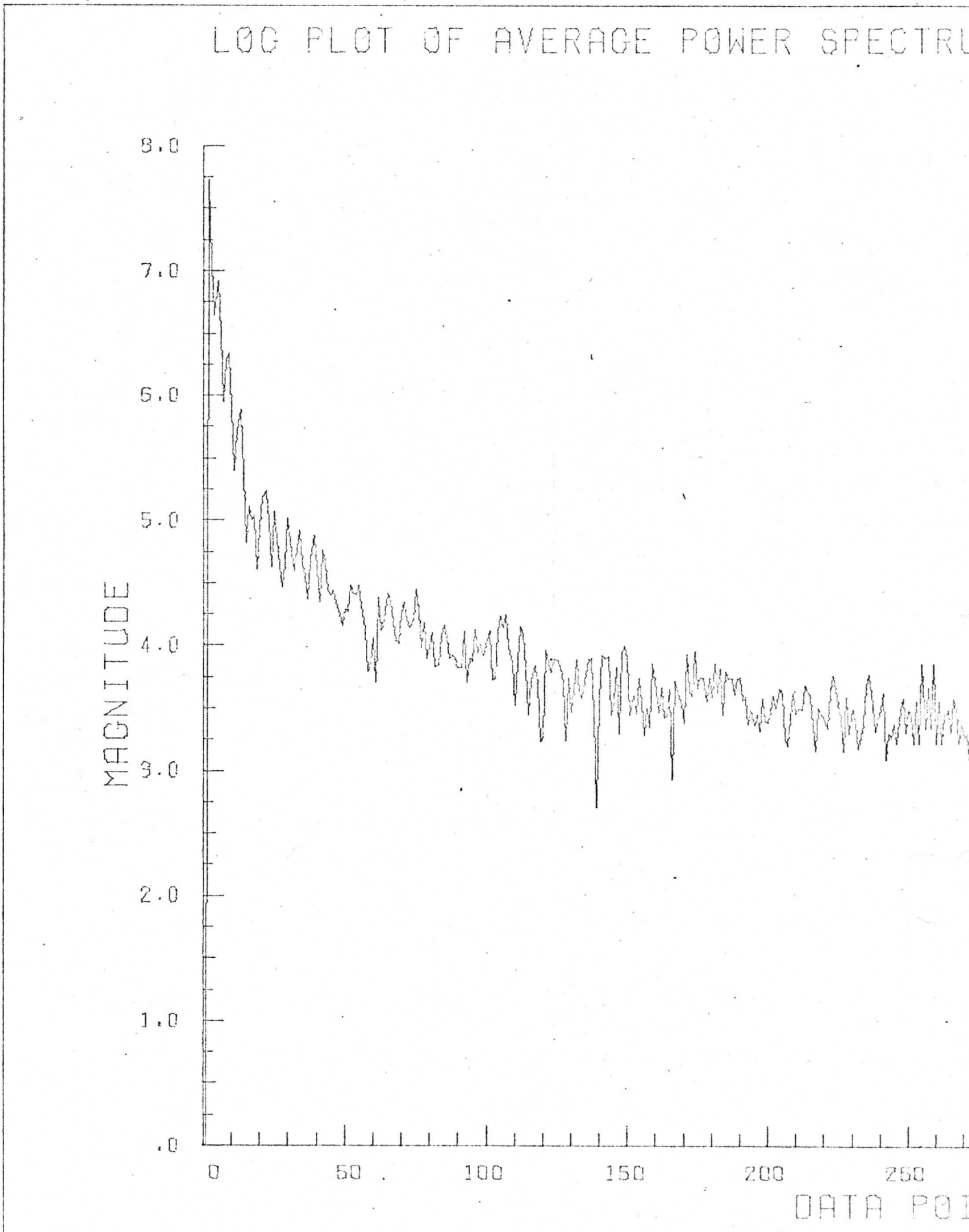

Apollo 56-2-934, (rect.)
Locator: Tape 17, File 2
Records: 100 - 104 Date: 2/1/73
Elements: 510 - 1021
Plot: Avg. Autocorrelation

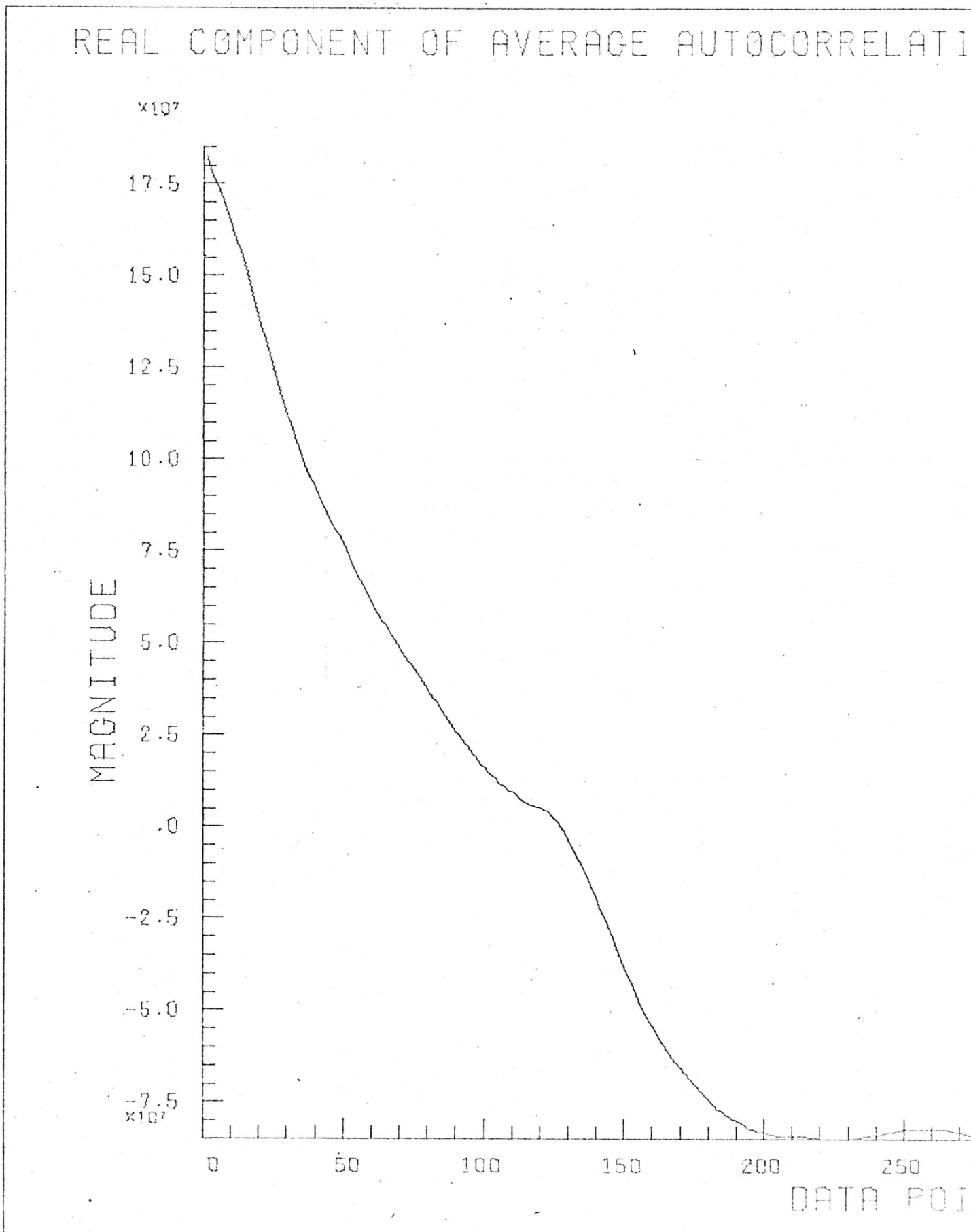

Apollo 56-2-948, (rect.)
Locator: Tape 17, File 3
Records: 800 - 804 Date: 2/1/73
Elements: 10 - 521
Plot: Log Power Spectrum, First Line

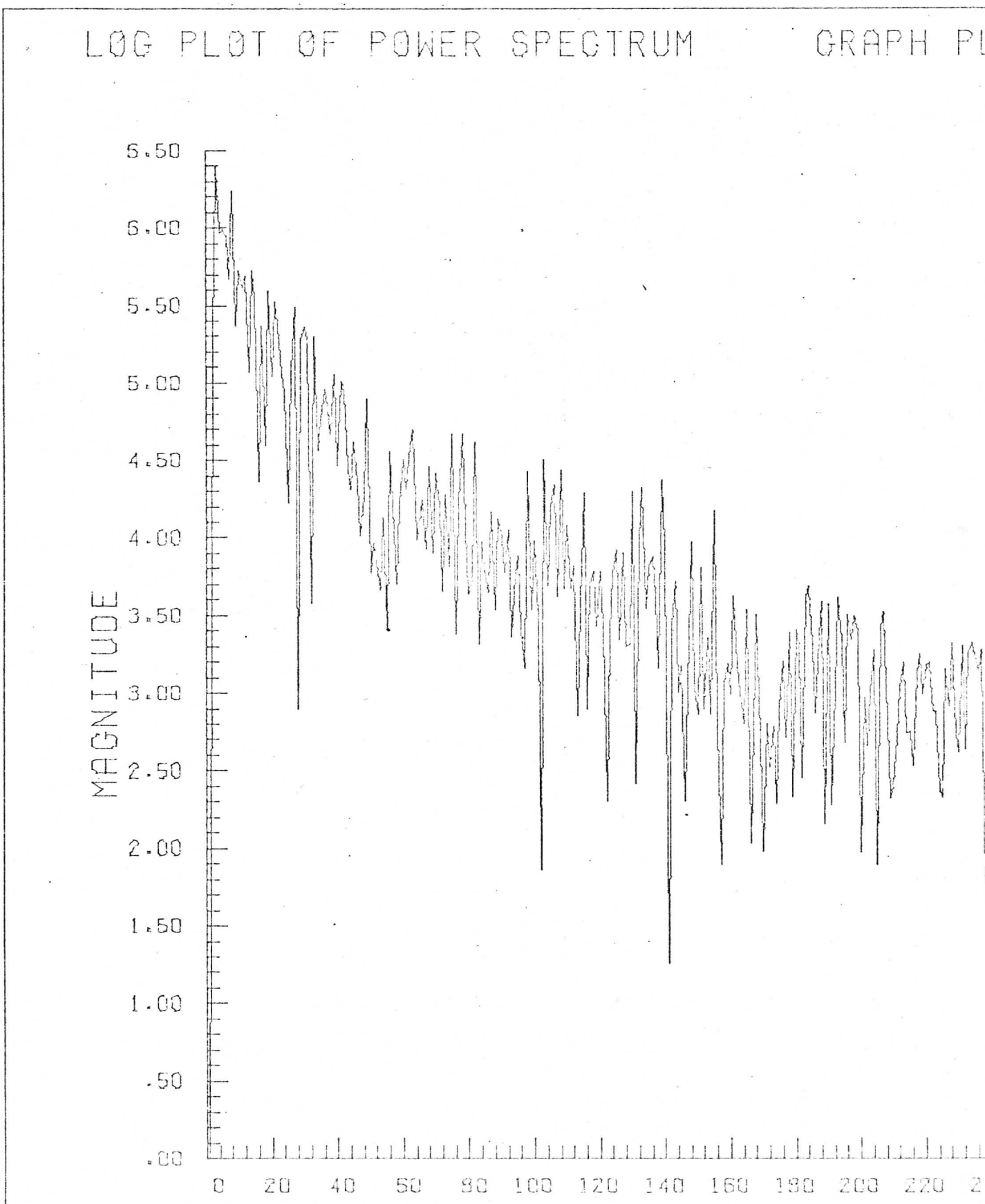

Apollo 56-2-948, (rect.)
Locator: Tape 17, File 3
Records: 800 - 804 Date: 2/1/73
Elements: 10 - 521
Plot: Autocorrelation, First Line

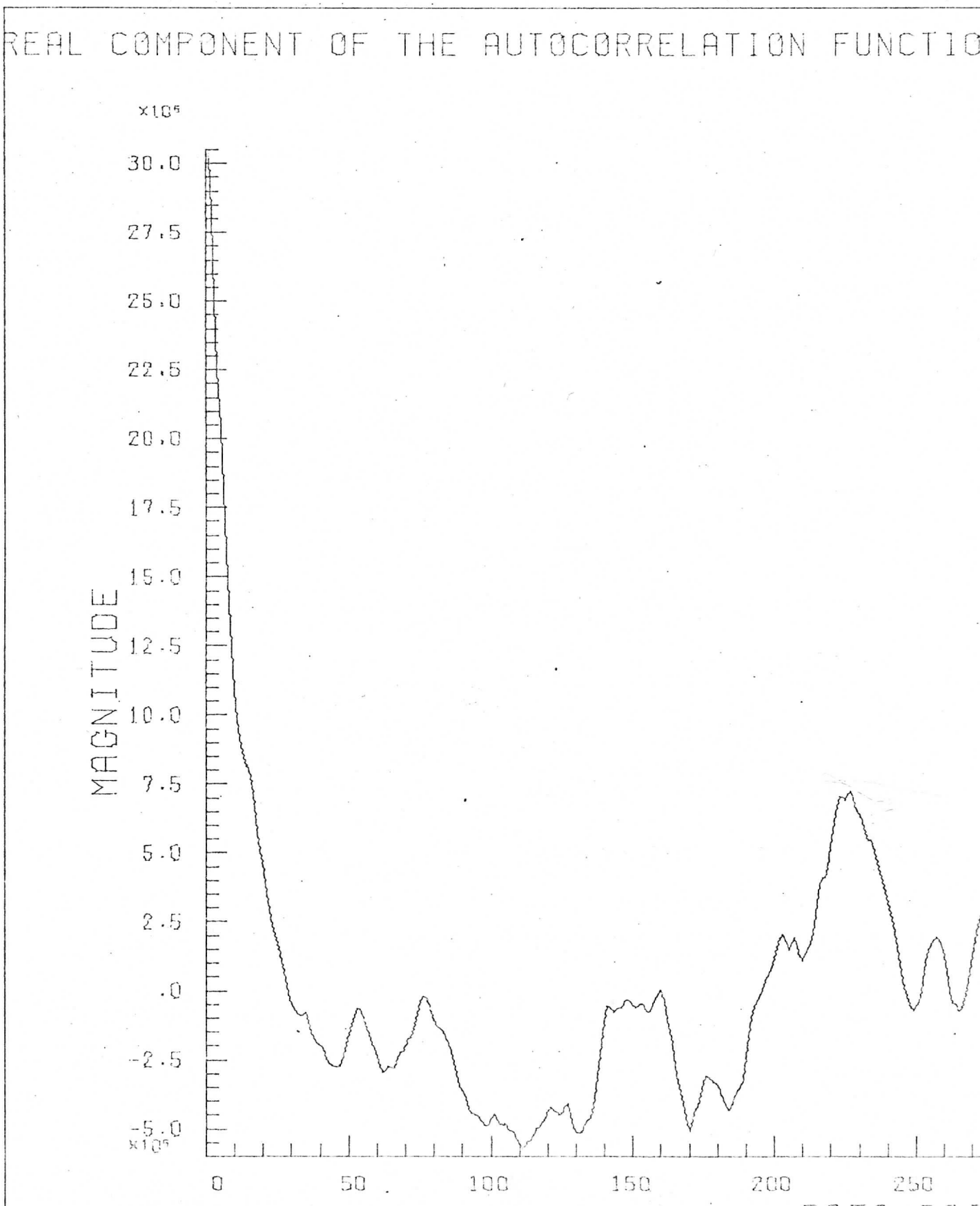

Apollo 56-2-948, (rect.)
Locator: Tape 17, File 3
Records: 800 - 804 Date: 2/1/73
Elements: 10 - 521
Plot: Log Power Spectrum, Fifth Line

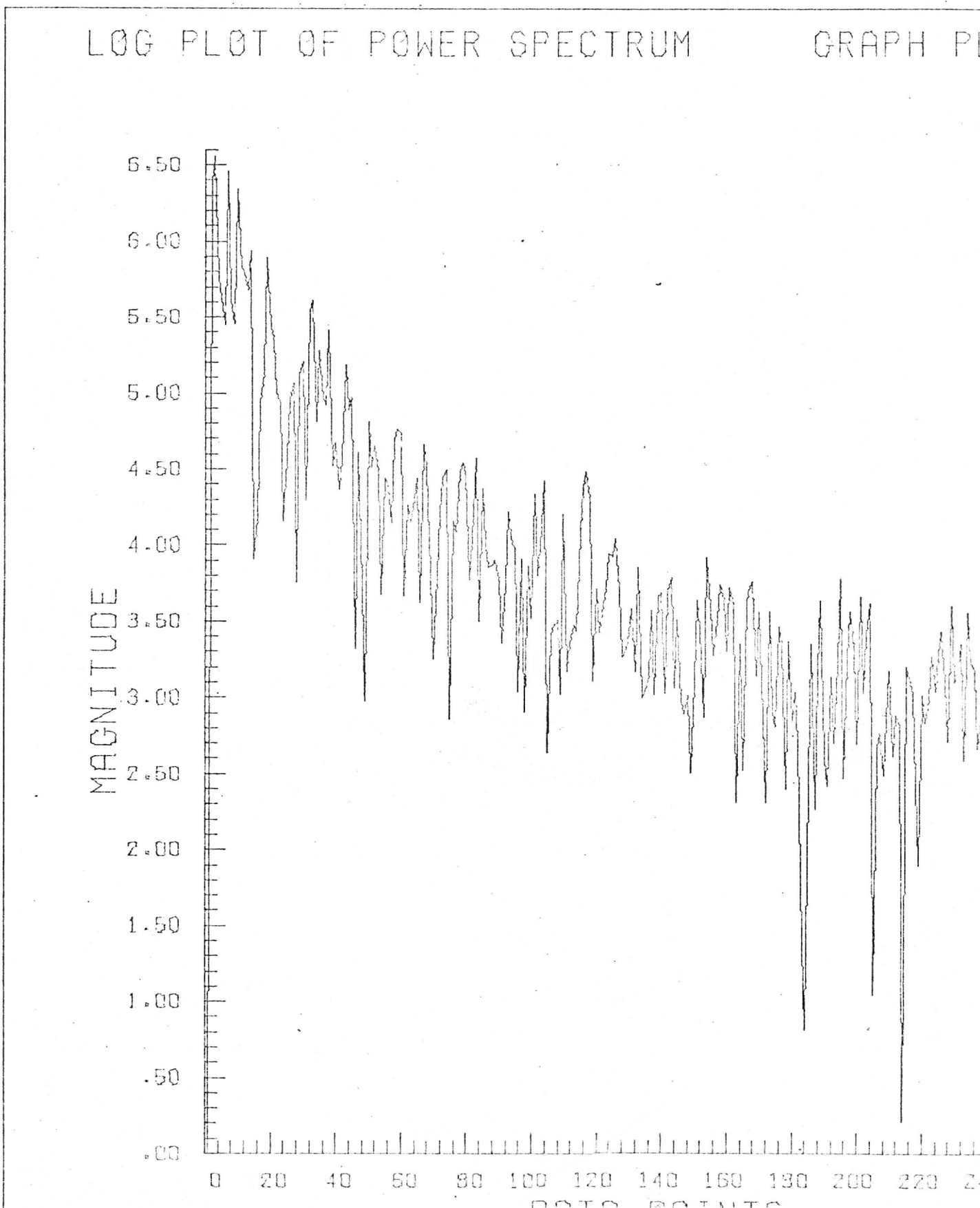

Apollo 56-2-948, (rect.)
Locator: Tape 17, File 3
Records: 800 - 804 Date: 2/1/73
Elements: 10 - 521
Plot: Log Avg. Power Spectrum

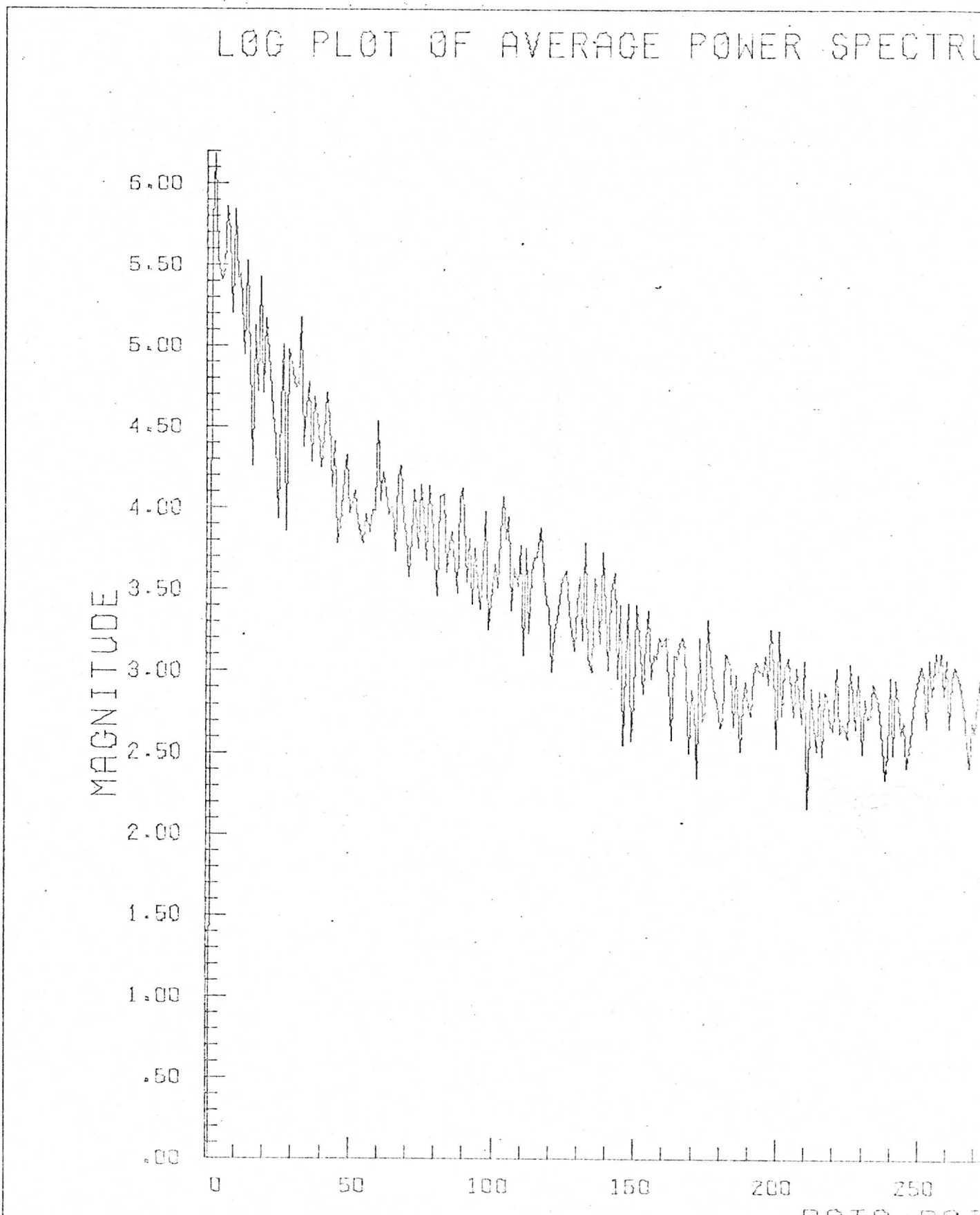

Apollo 56-2-948, (rect.)
Locator: Tape 17, File 3
Records: 800 - 804 Date: 2/1/73
Elements: 10 - 521
Plot: Avg. Autocorrelation

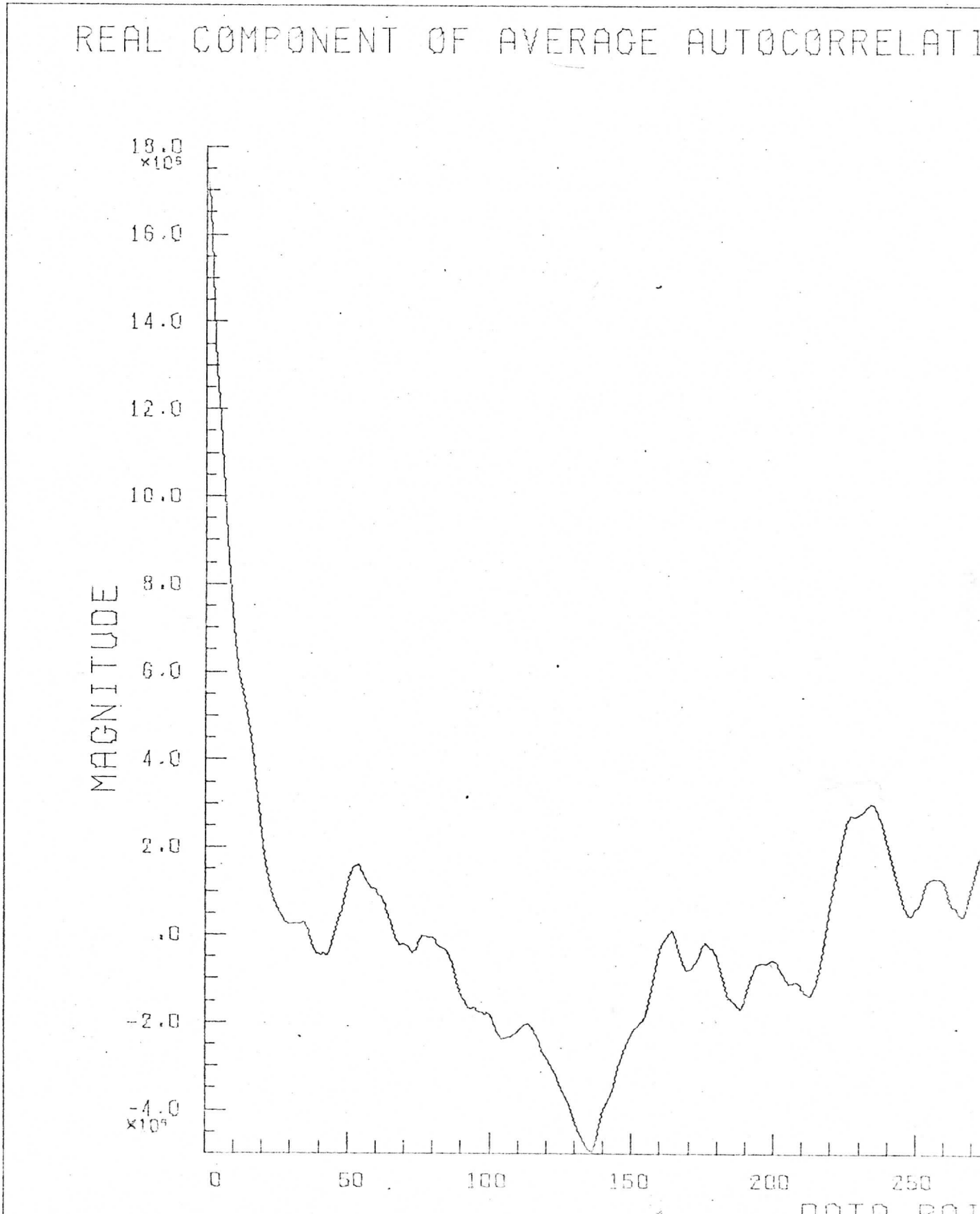

Apollo 56-2-1064, (rect.)
Locator: Tape 17, File 4
Records: 130 - 134 Date: 2/1/73
Elements: 510 - 1021
Plot: Log Power Spectrum, First Line

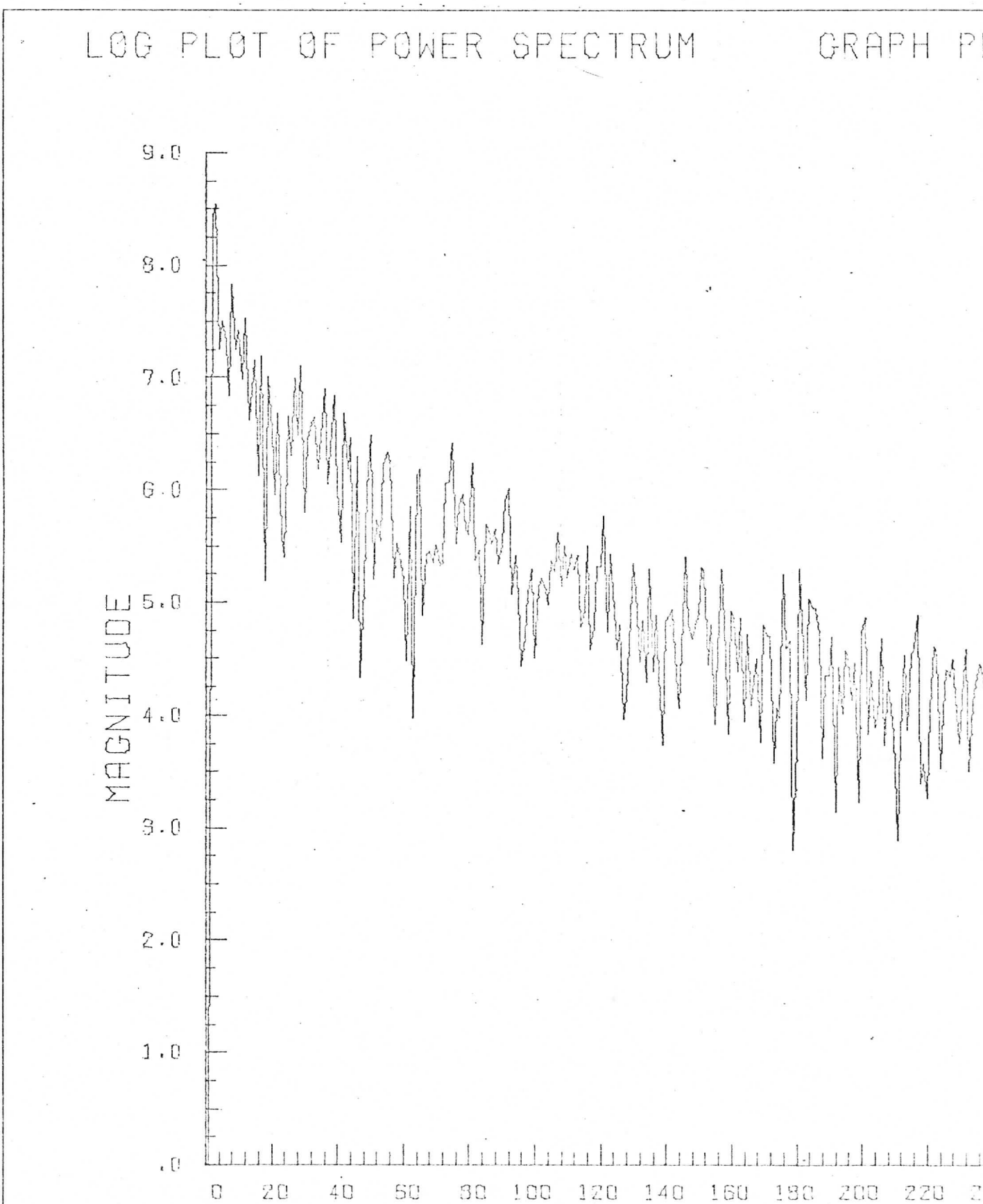

Apollo 56-2-1064, (rect.)
Locator: Tape 17, File 4
Records: 130 - 134 Date: 2/1/73
Elements: 510 - 1021
Plot: Autocorrelation, First Line

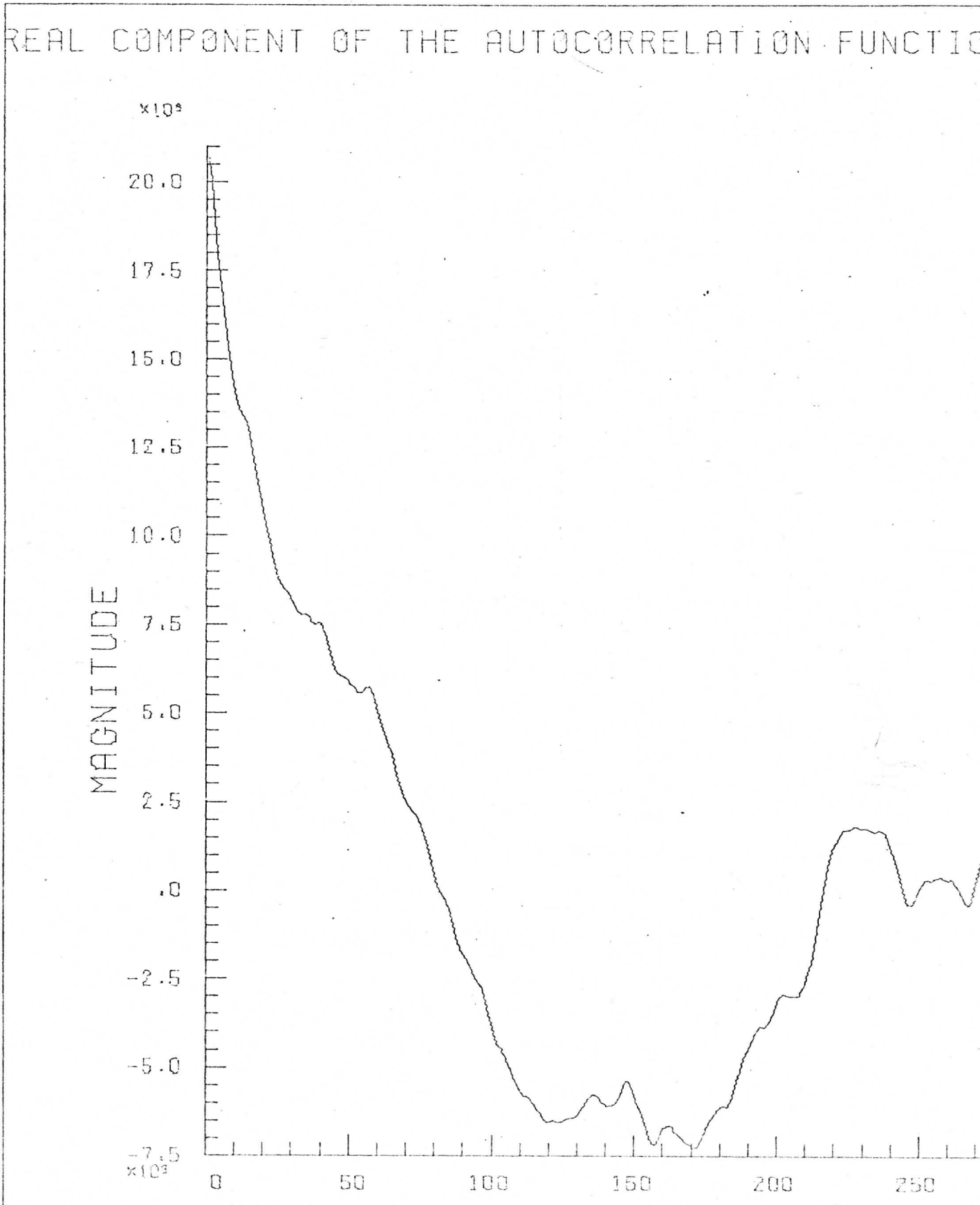

Apollo 56-2-1064, (rect.)
Locator: Tape 17, File 4
Records: 130 - 134 Date: 2/1/73
Elements: 510 - 1021
Plot: Log Power Spectrum, Fifth Line

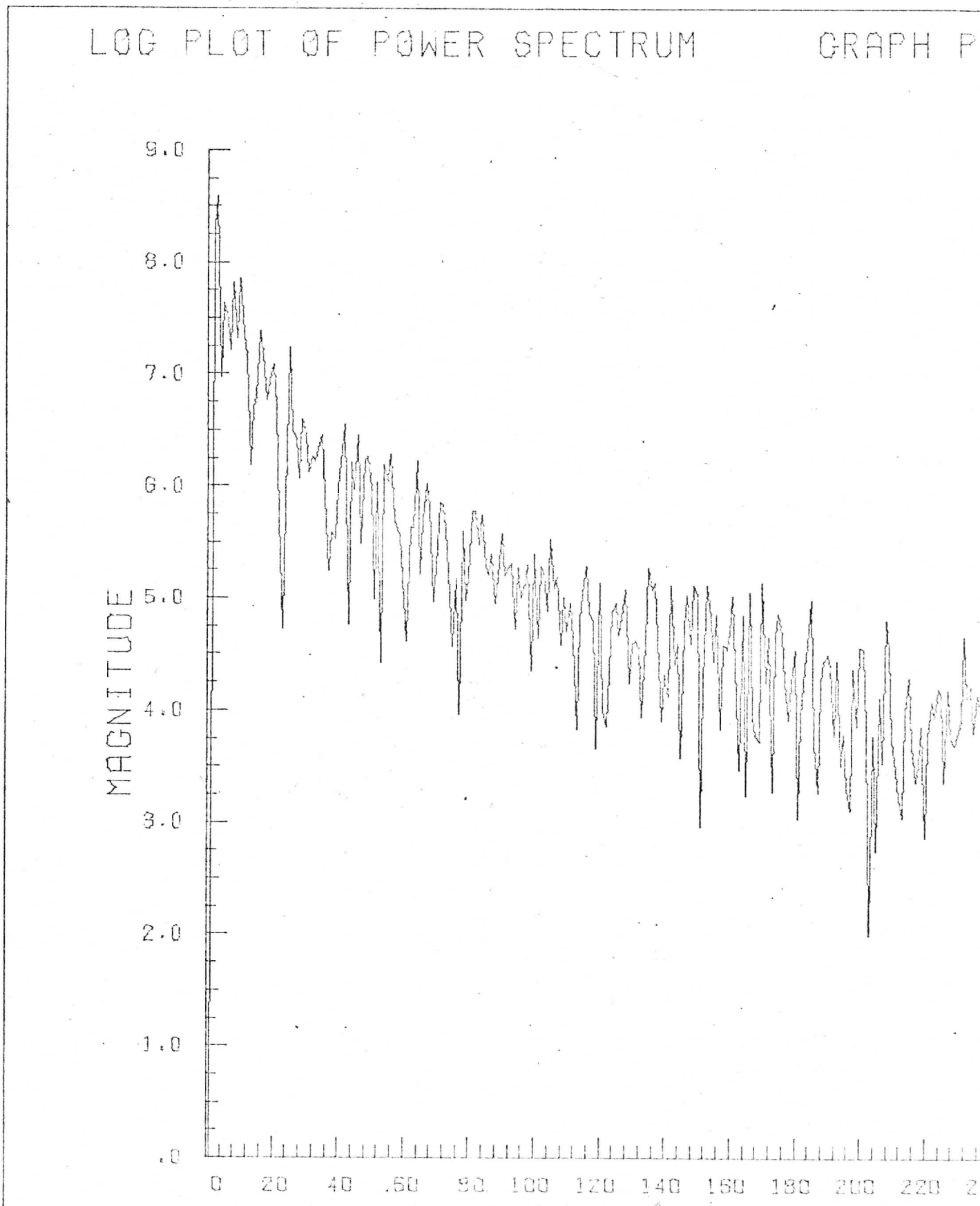

Apollo 56-2-1064, (rect.)
Locator: Tape 17, File 4
Records: 130 - 134 Date: 2/1/73
Elements: 510 - 1021
Plot: Log Avg. Power Spectrum

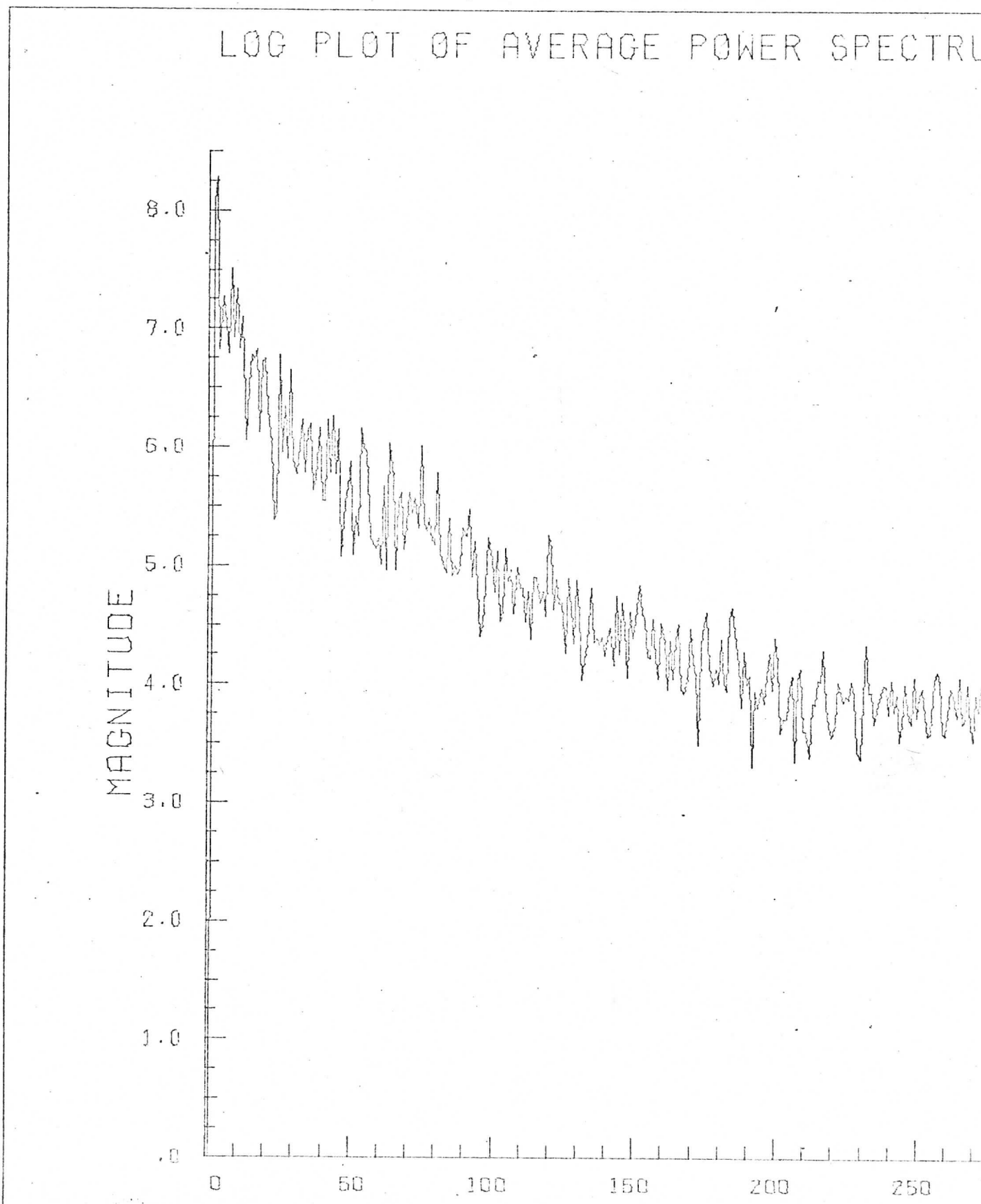

Apollo 56-2-1064, (rect.)
Locator: Tape 17, File 4
Records: 130 - 134 Date: 2/1/73
Elements: 510 - 1021
Plot: Avg. Autocorrelation

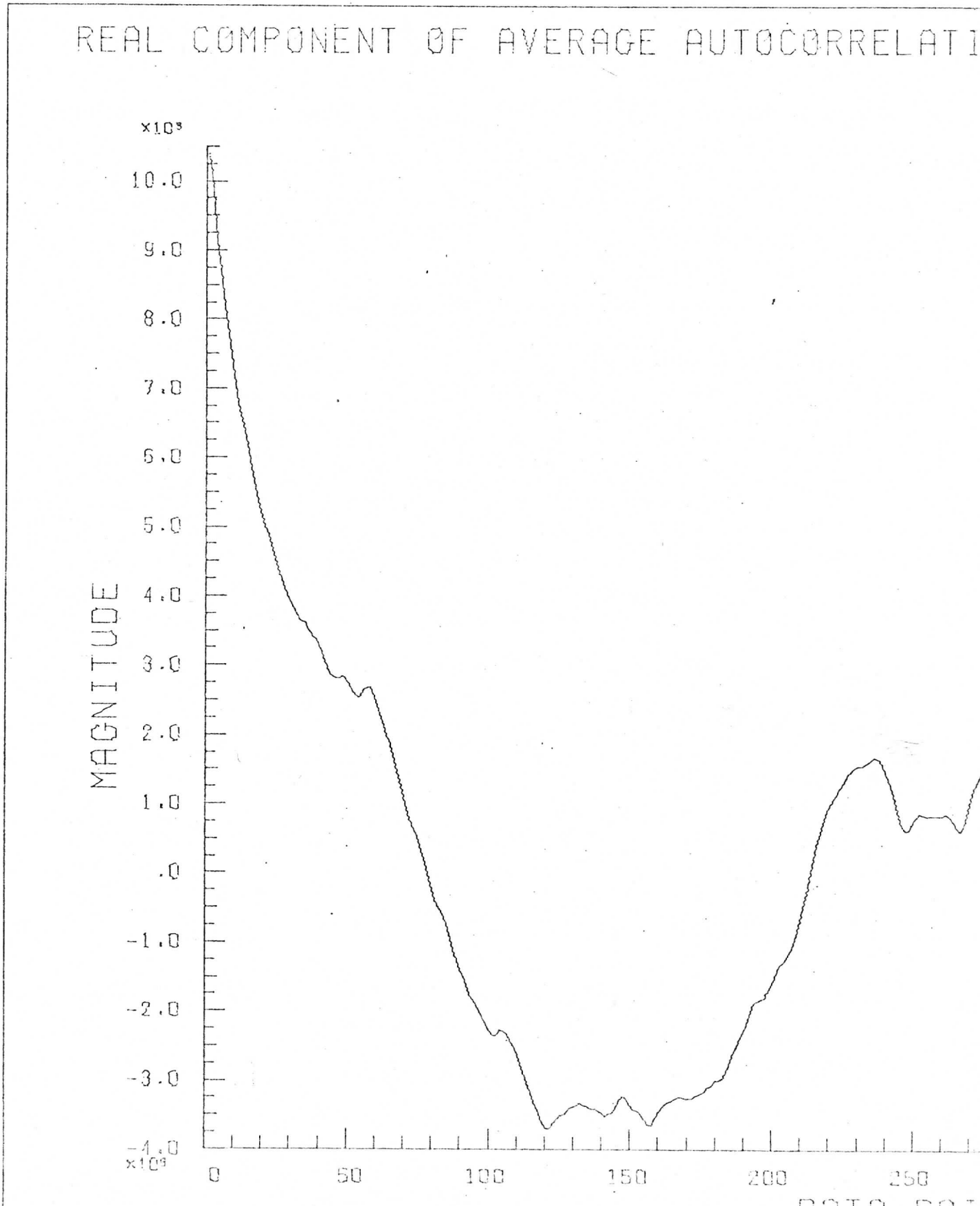

Apollo 56-2-1429, (rect.)
Locator: Tape 17, File 5
Records: 250 - 254 Date: 2/1/73
Elements: 510 - 1021
Plot: Log Power Spectrum, First Line

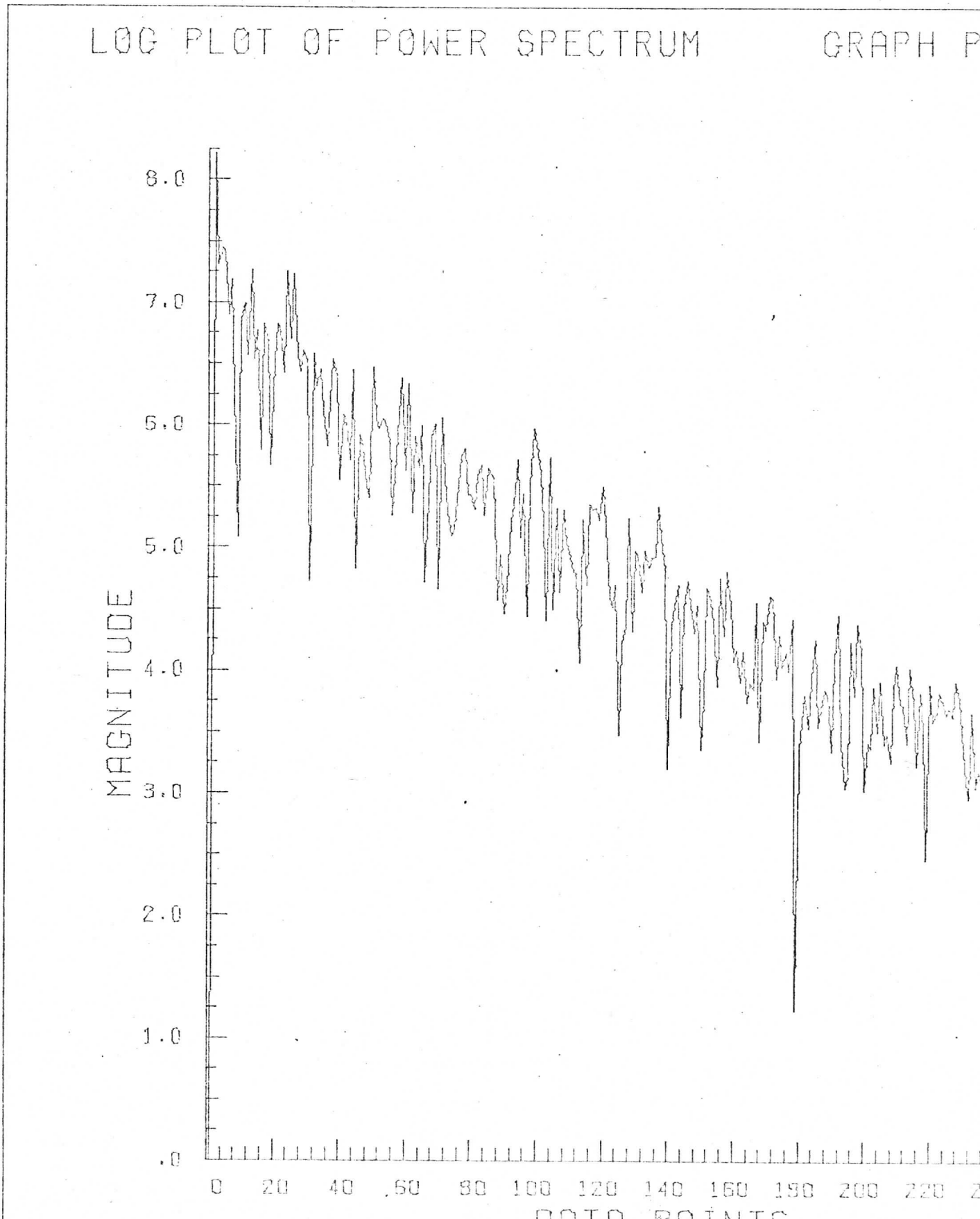

Apollo 56-2-1429, (rect.)
Locator: Tape 17, File 5
Records: 250 - 254 Date: 2/1/73
Elements: 510 - 1021
Plot: Autocorrelation, First Line

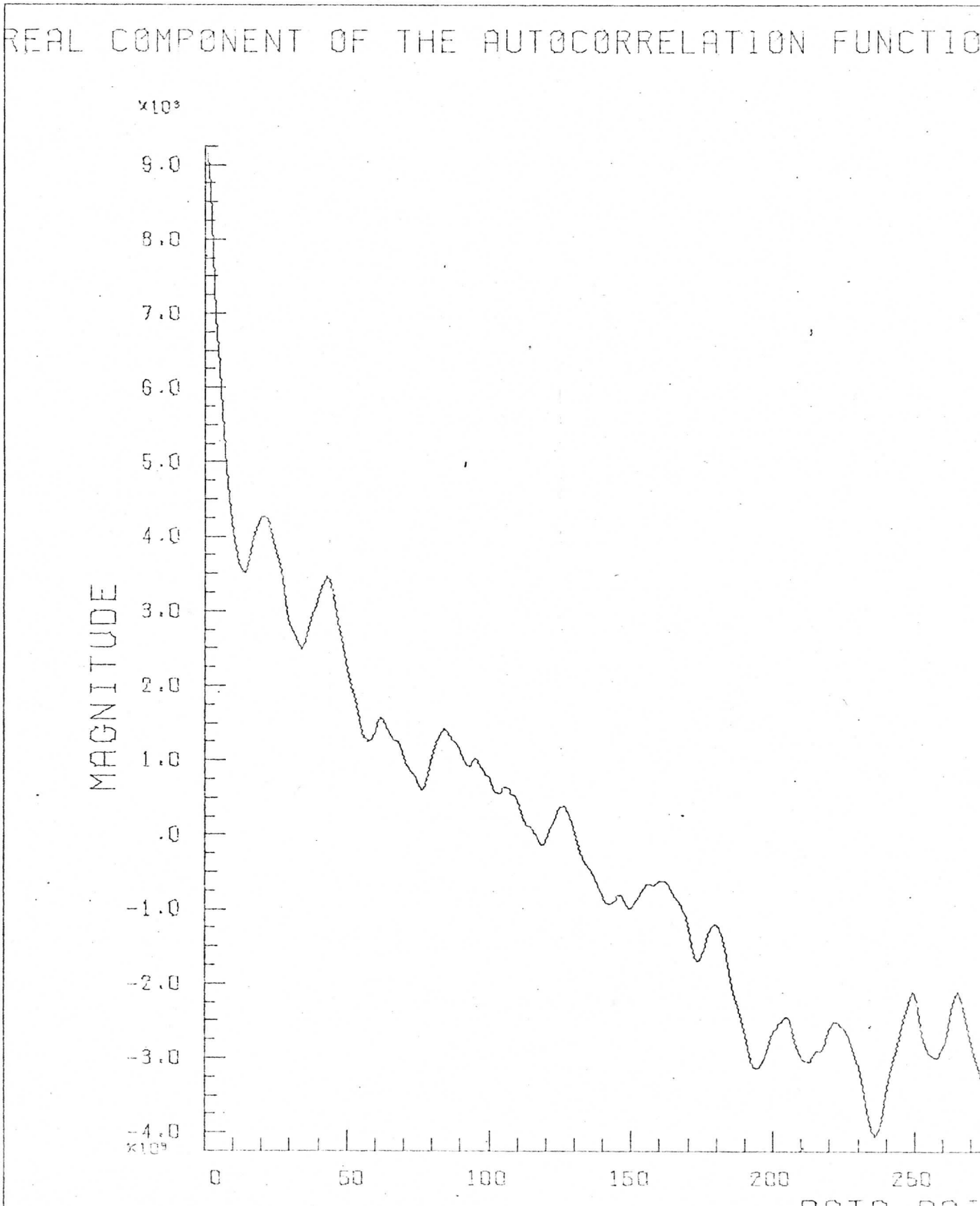

Apollo 56-2-1429, (rect.)
Locator: Tape 17, File 5
Records: 250 - 254 Date: 2/1/73
Elements: 510 - 1021
Plot: Log Power Spectrum, Fifth Line

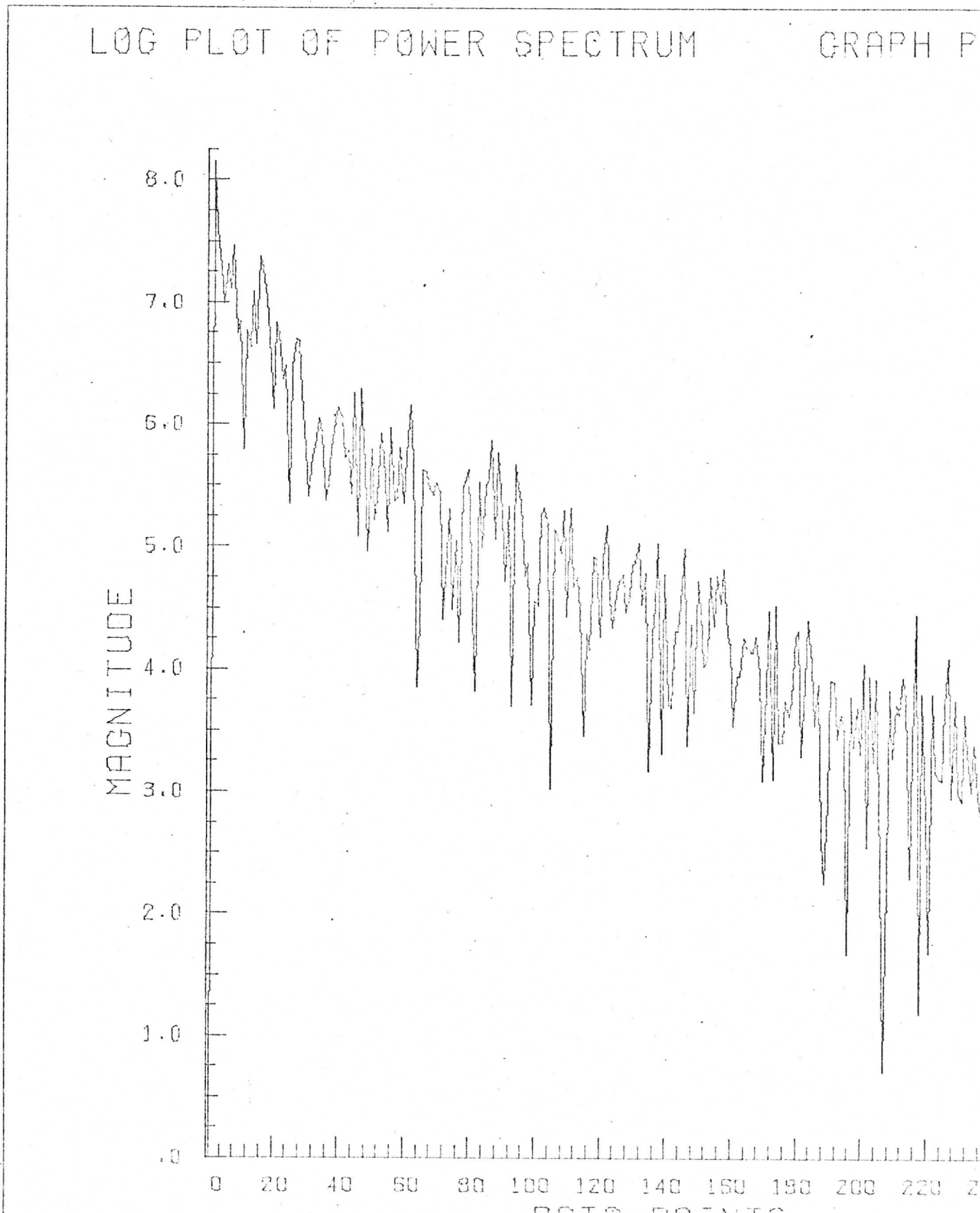

Apollo 56-2-1429, (rect.)
Locator: Tape 17, File 5
Records: 250 - 254 Date: 2/1/73
Elements: 510 - 1021
Plot: Log Avg. Power Spectrum

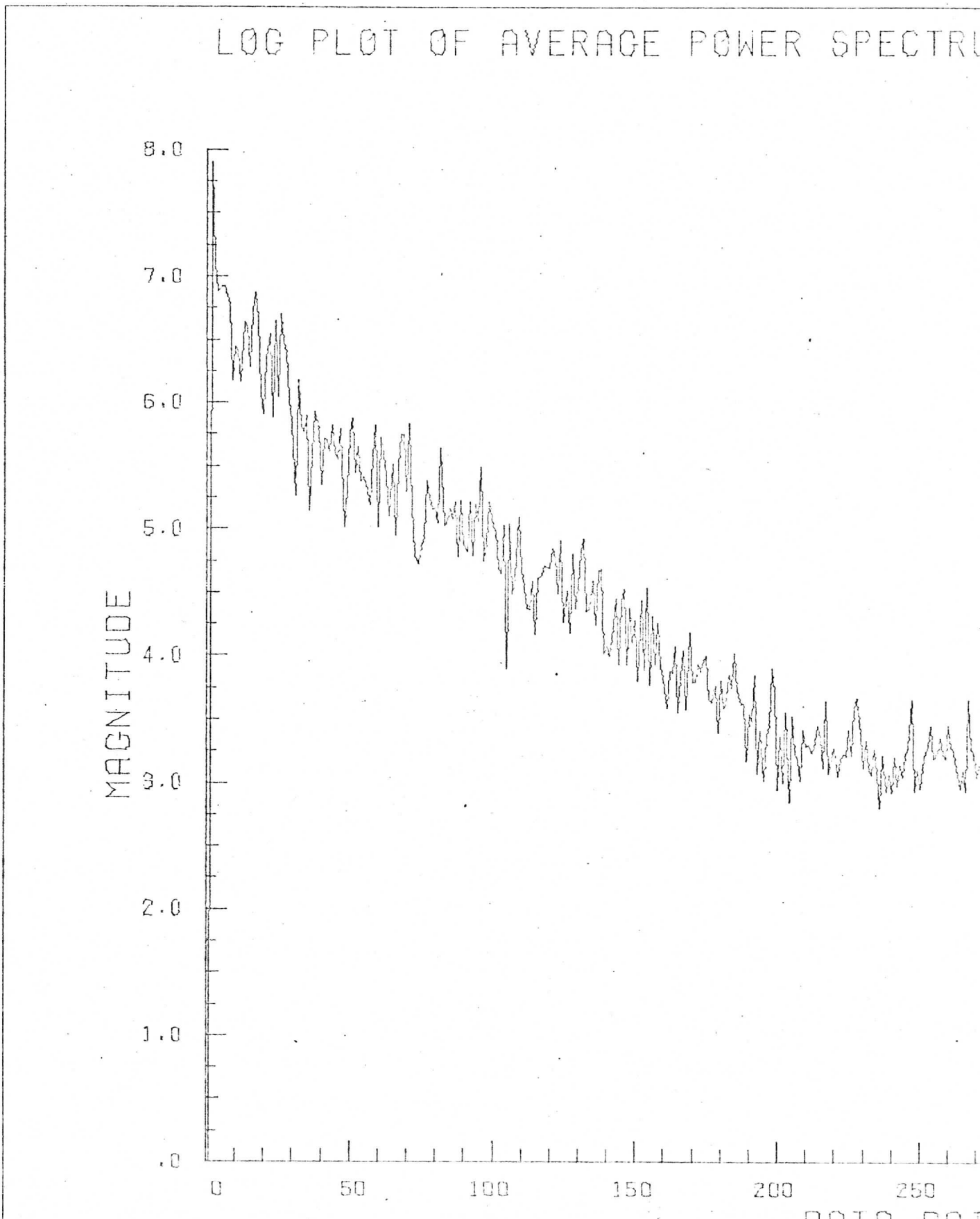

Apollo 56-2-1429, (rect.)
Locator: Tape 17, File 5
Records: 250 - 254 Date: 2/1/73
Elements: 510 - 1021
Plot: Avg. Autocorrelation

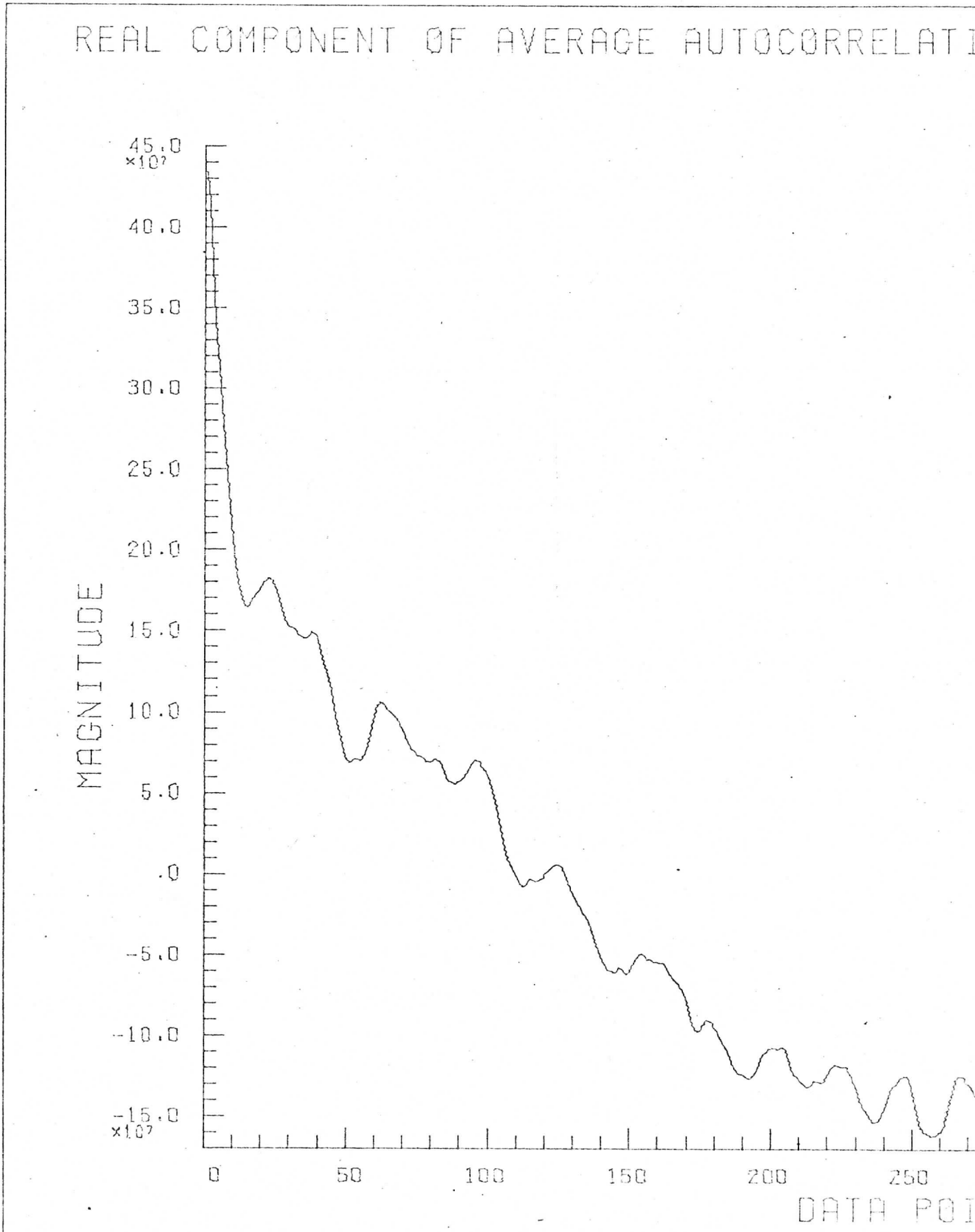

Apollo 56-2-1429, (rect.)
Locator: Tape 17, File 5
Records: 700 - 704 Date: 2/1/73
Elements: 510 - 1021
Plot: Log Power Spectrum, First Line

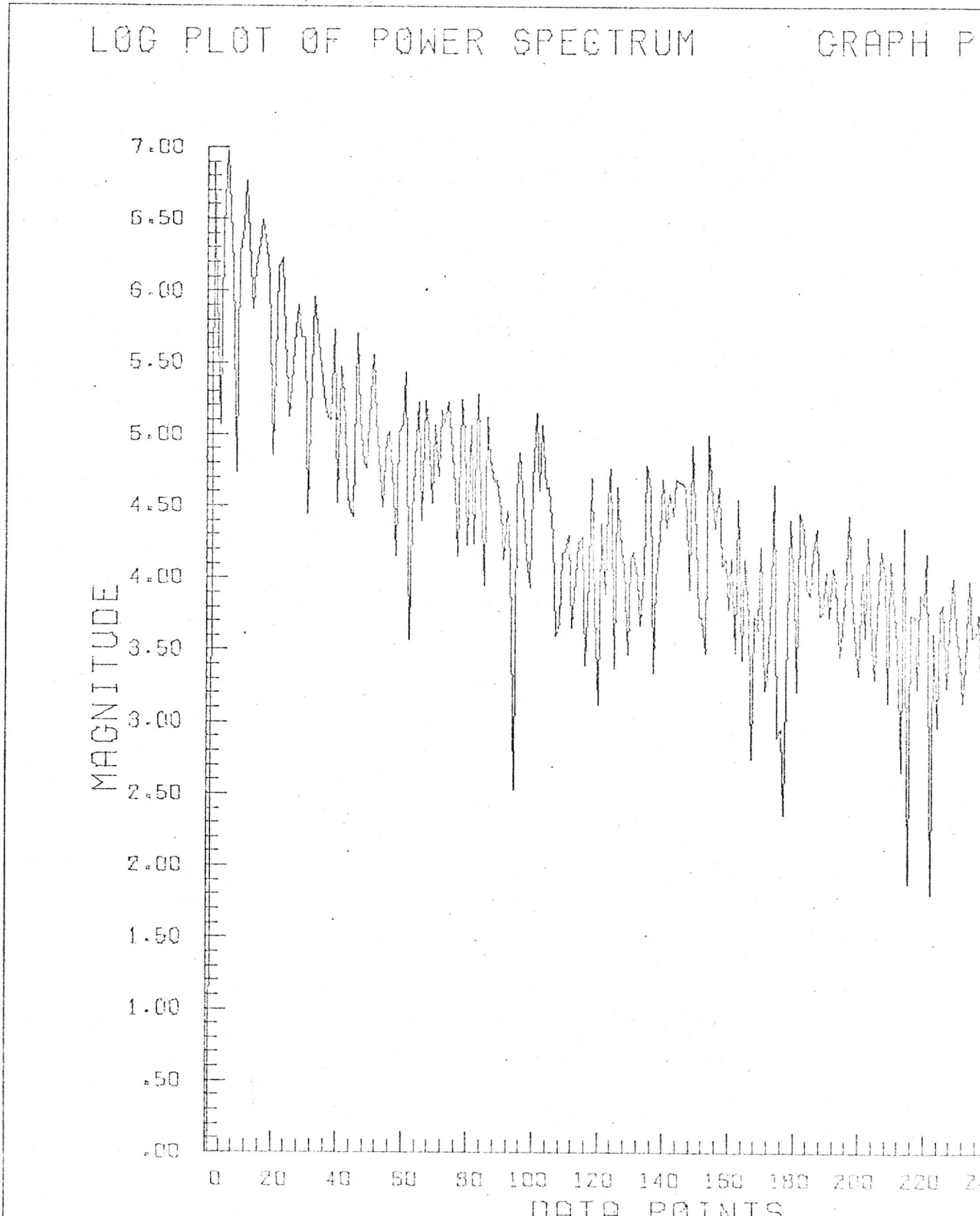

Apollo 56-2-1429, (rect.)
Locator: Tape 17, File 5
Records: 700 - 704 Date: 2/1/73
Elements: 510 - 1021
Plot: Autocorrelation, First Line

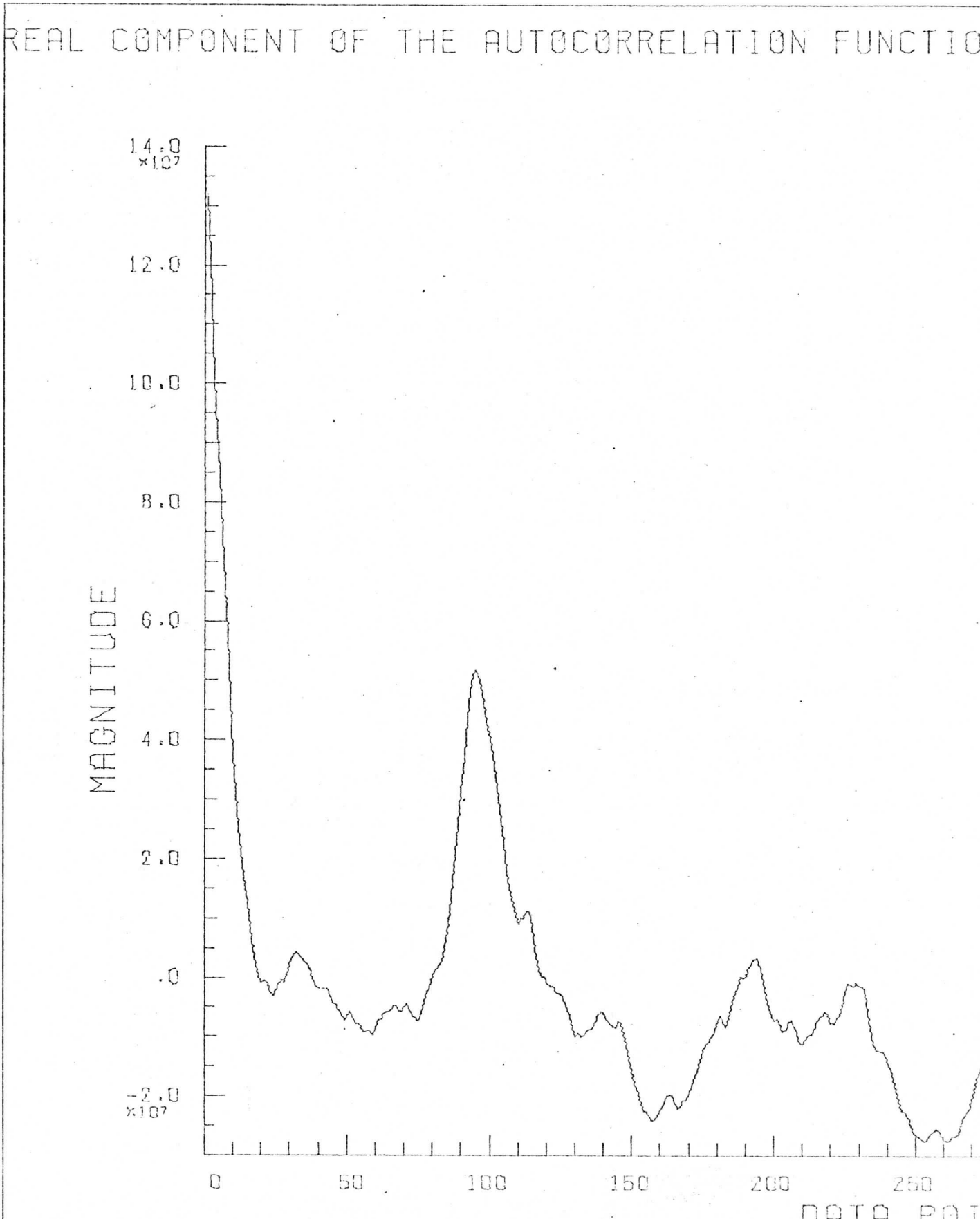

Apollo 56-2-1429, (rect.)
Locator: Tape 17, File 5
Records: 700 - 704 Date: 2/1/73
Elements: 510 - 1021
Plot: Log Power Spectrum, Fifth Line

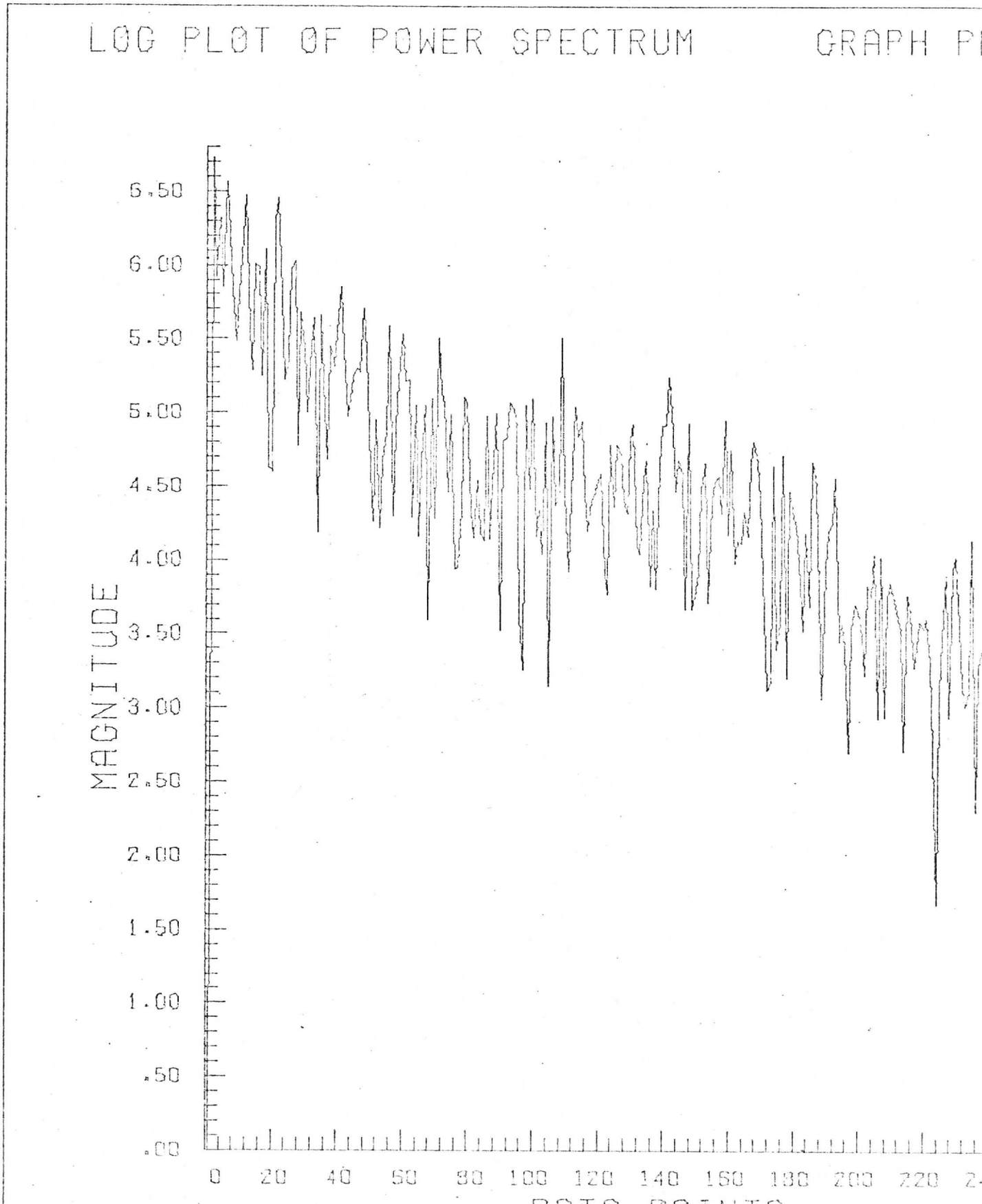

Apollo 56-2-1429, (rect.)
Locator: Tape 17, File 5
Records: 700 - 704 Date: 2/1/73
Elements: 510 - 1021
Plot: Log Avg. Power Spectrum

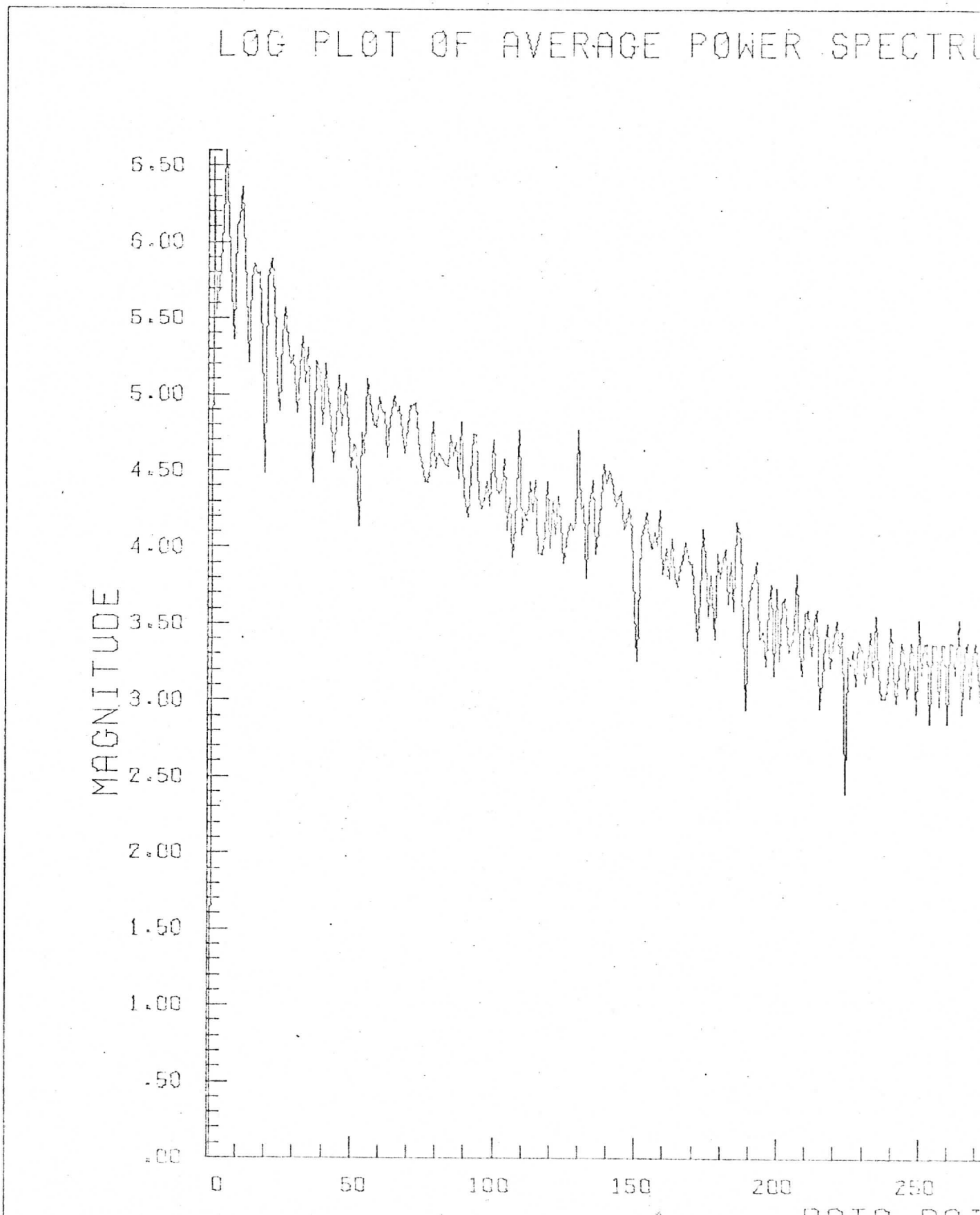

Apollo 56-2-1429, (rect.)
Locator: Tape 17, File 5
Records: 700 - 704 Date: 2/1/73
Elements: 510 - 1021
Plot: Avg. Autocorrelation

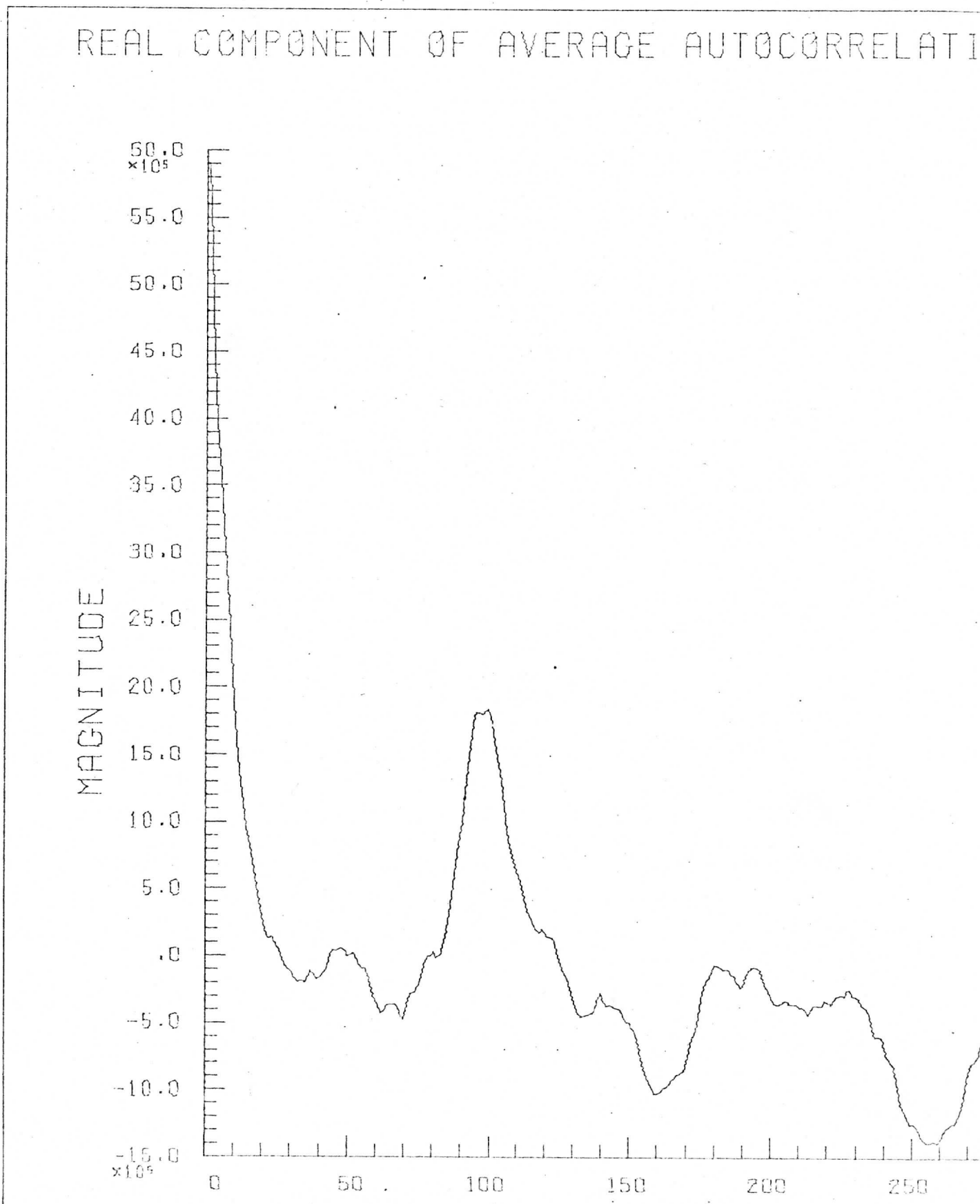

Apollo 56-2-1468, (rect.)
Locator: Tape 18, File 3
Records: 650 - 654 Date: 2/2/73
Elements: 510 - 1021
Plot: Log Power Spectrum, First Line

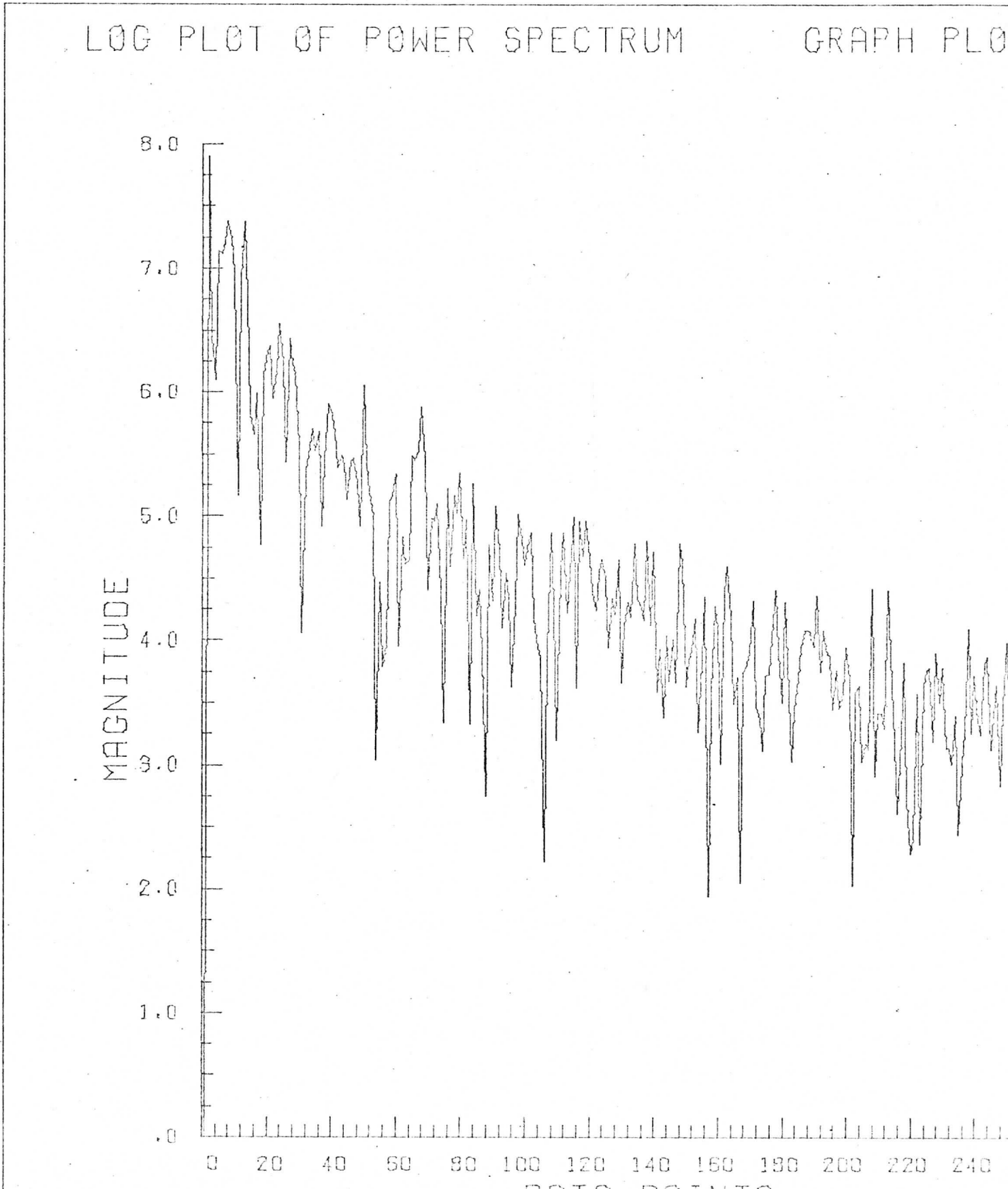

Apollo 56-2-1468, (rect.)
Locator: Tape 18, File 3
Records: 650 - 654 Date: 2/2/73
Elements: 510 - 1021
Plot: Autocorrelation, First Line

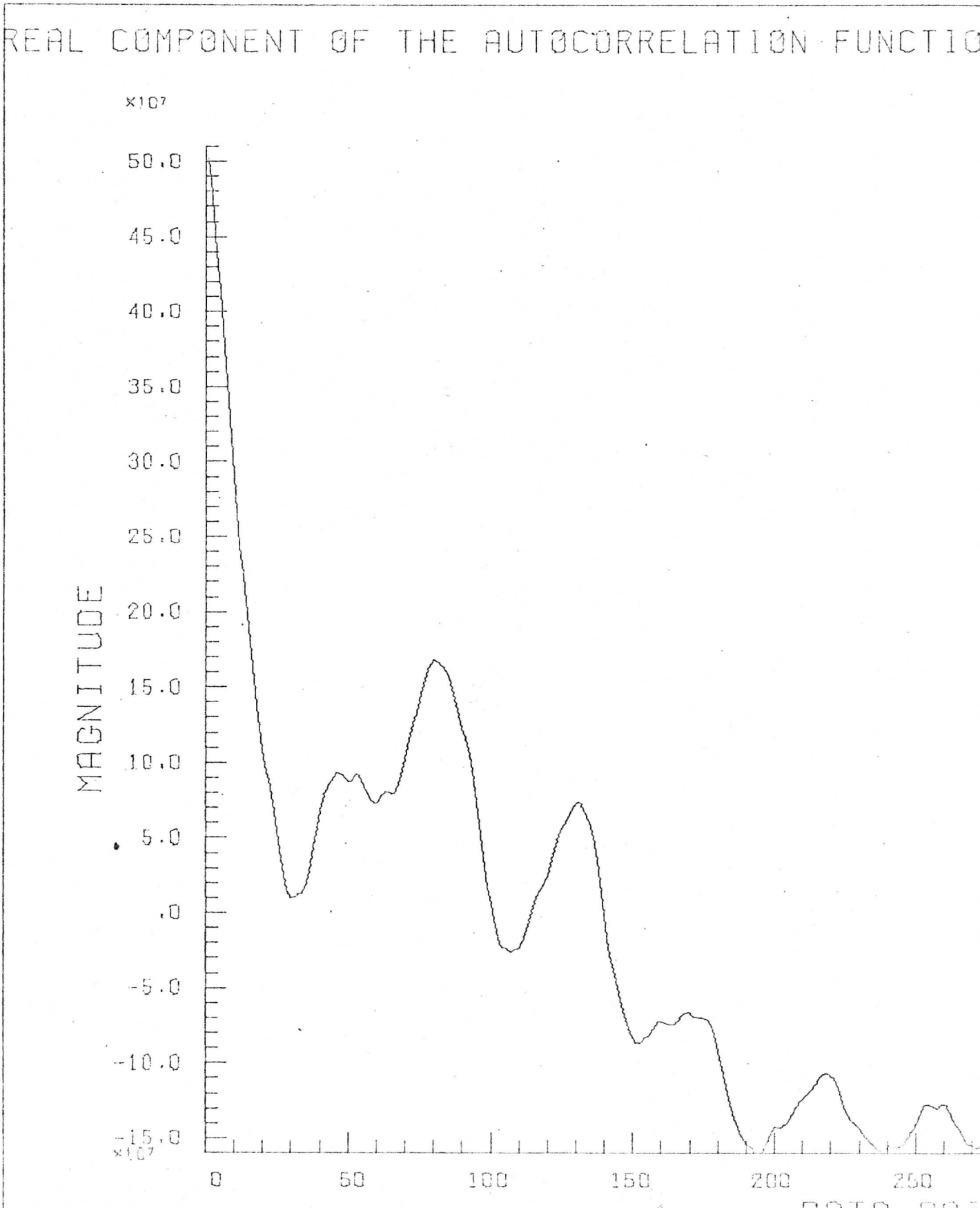

Apollo 56-2-1468, (rect.)
Locator: Tape 18, File 3
Records: 650 - 654 Date: 2/2/73
Elements: 510 - 1021
Plot: Log Power Spectrum, Fifth Line

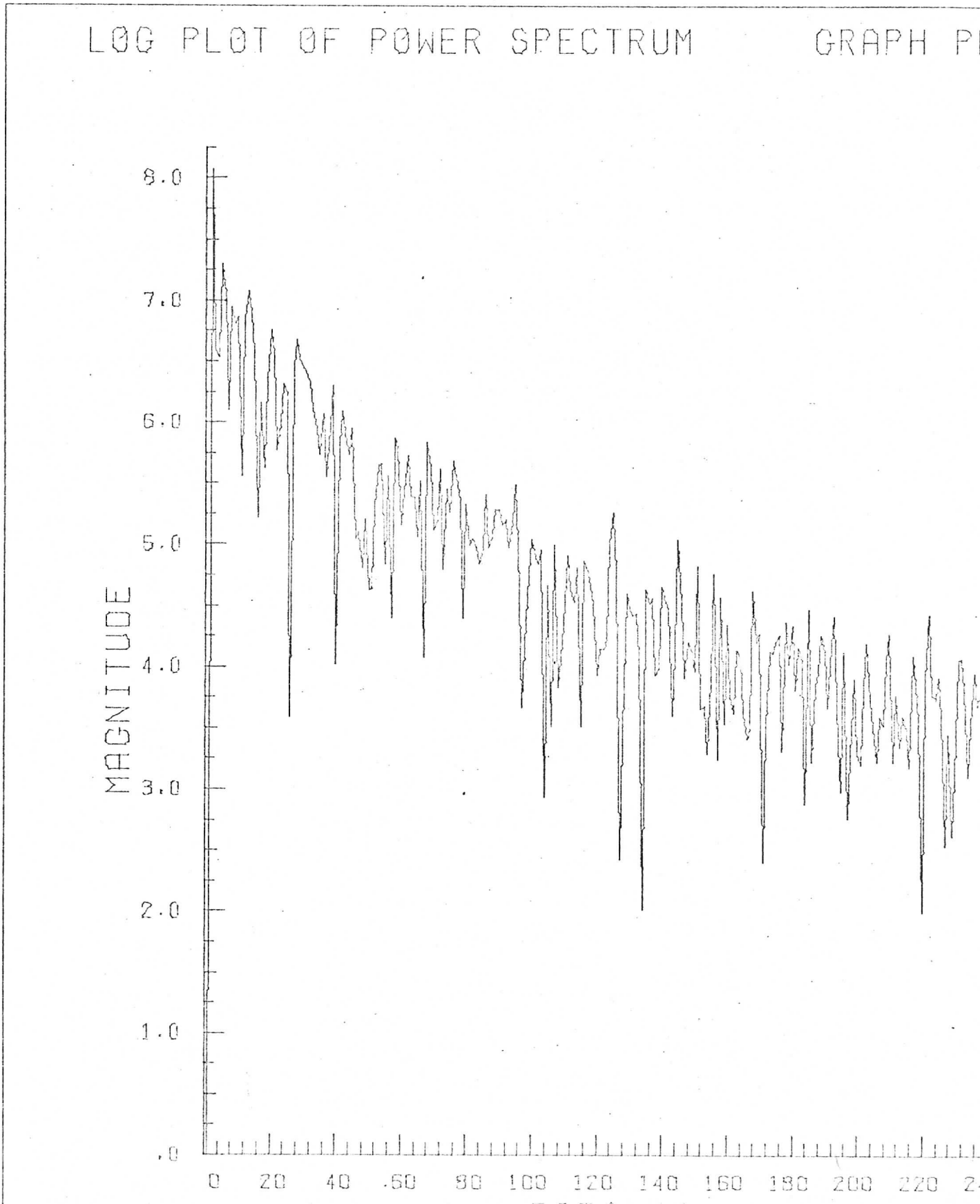

Apollo 56-2-1468, (rect.)
Locator: Tape 18, File 3
Records: 650 - 654 Date: 2/2/73
Elements: 510 - 1021
Plot: Log Avg. Power Spectrum

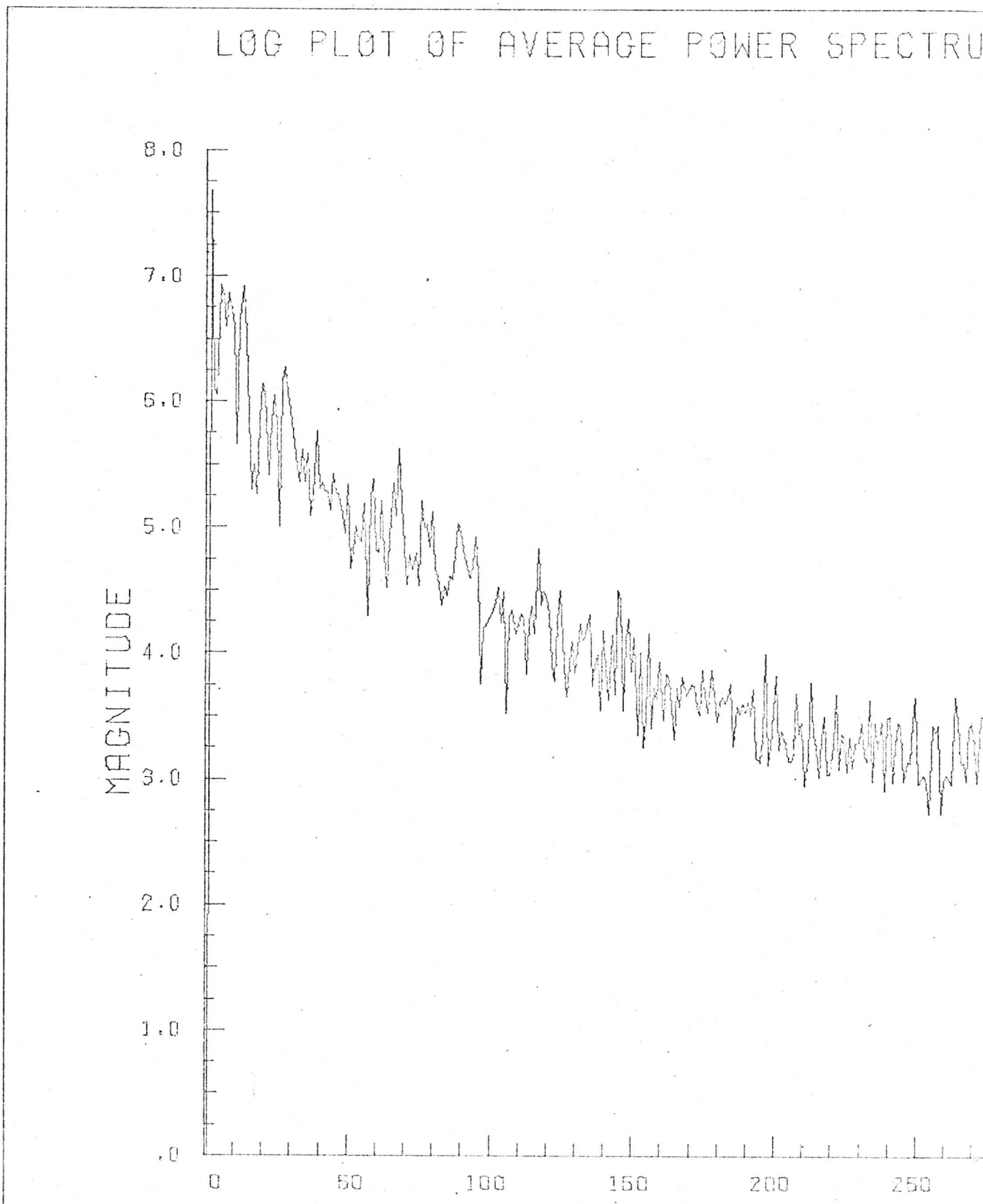

Apollo 56-2-1468, (rect.)
Locator: Tape 18, File 3
Records: 650 - 654 Date: 2/2/73
Elements: 510 - 1021
Plot: Avg. Autocorrelation

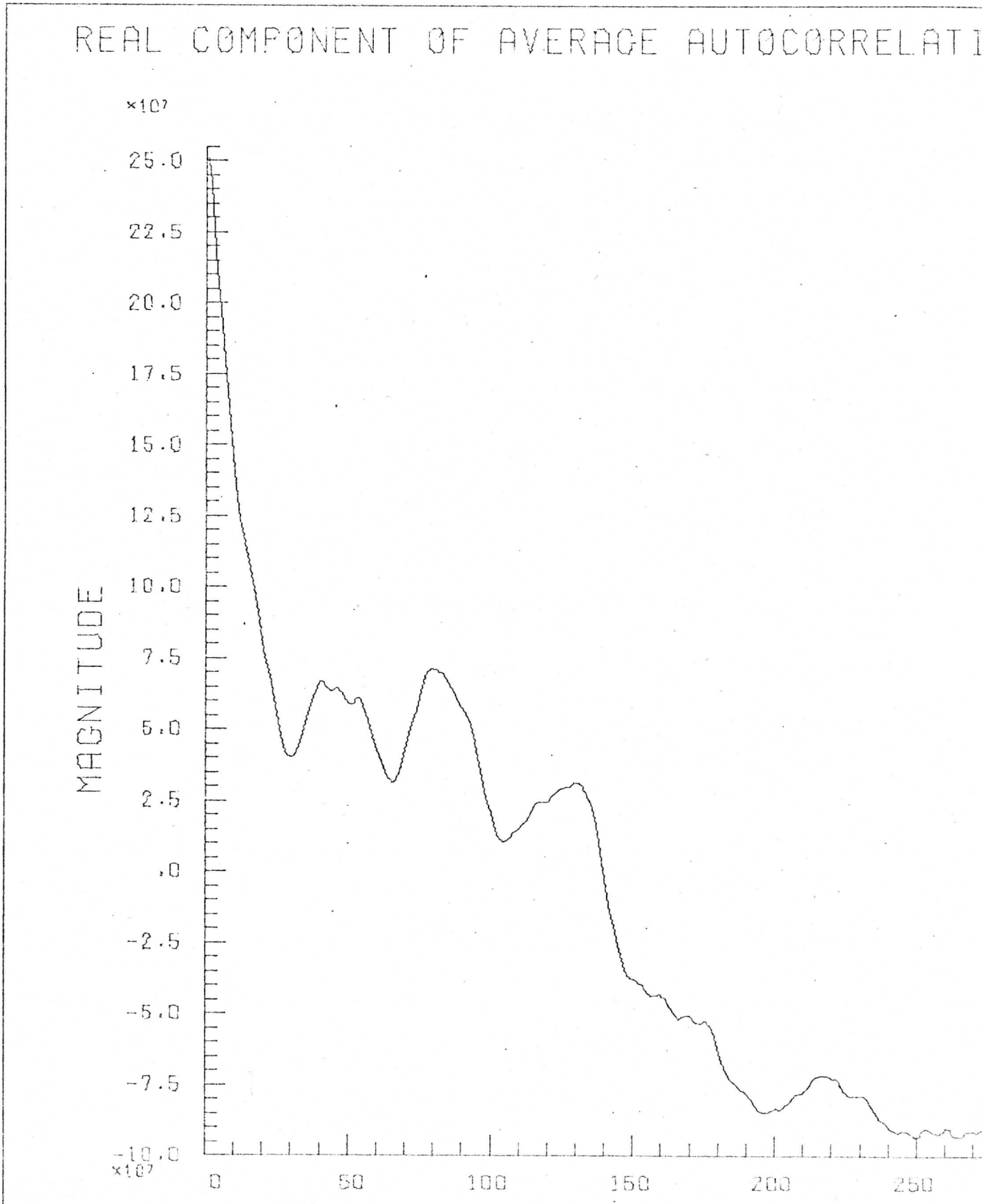

Apollo 56-2-1468, (rect.)
Locator: Tape 18, File 3
Records: 850 - 854 Date: 2/2/73
Elements: 10 - 521
Plot: Log Power Spectrum, First Line

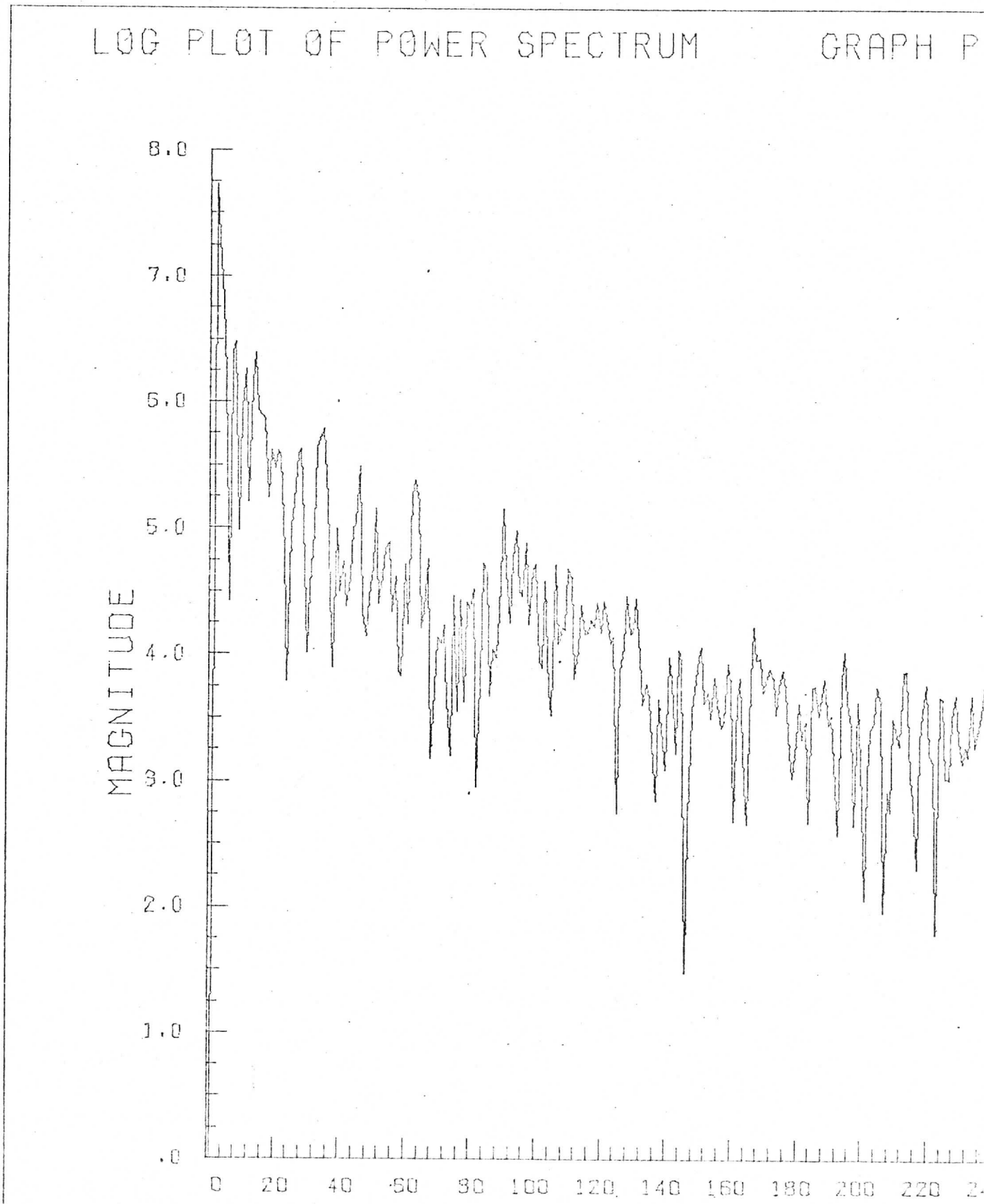

Apollo 56-2-1468, (rect.)
Locator: Tape 18, File 3
Records: 850 - 854 Date: 2/2/73
Elements: 10 - 521
Plot: Autocorrelation, First Line

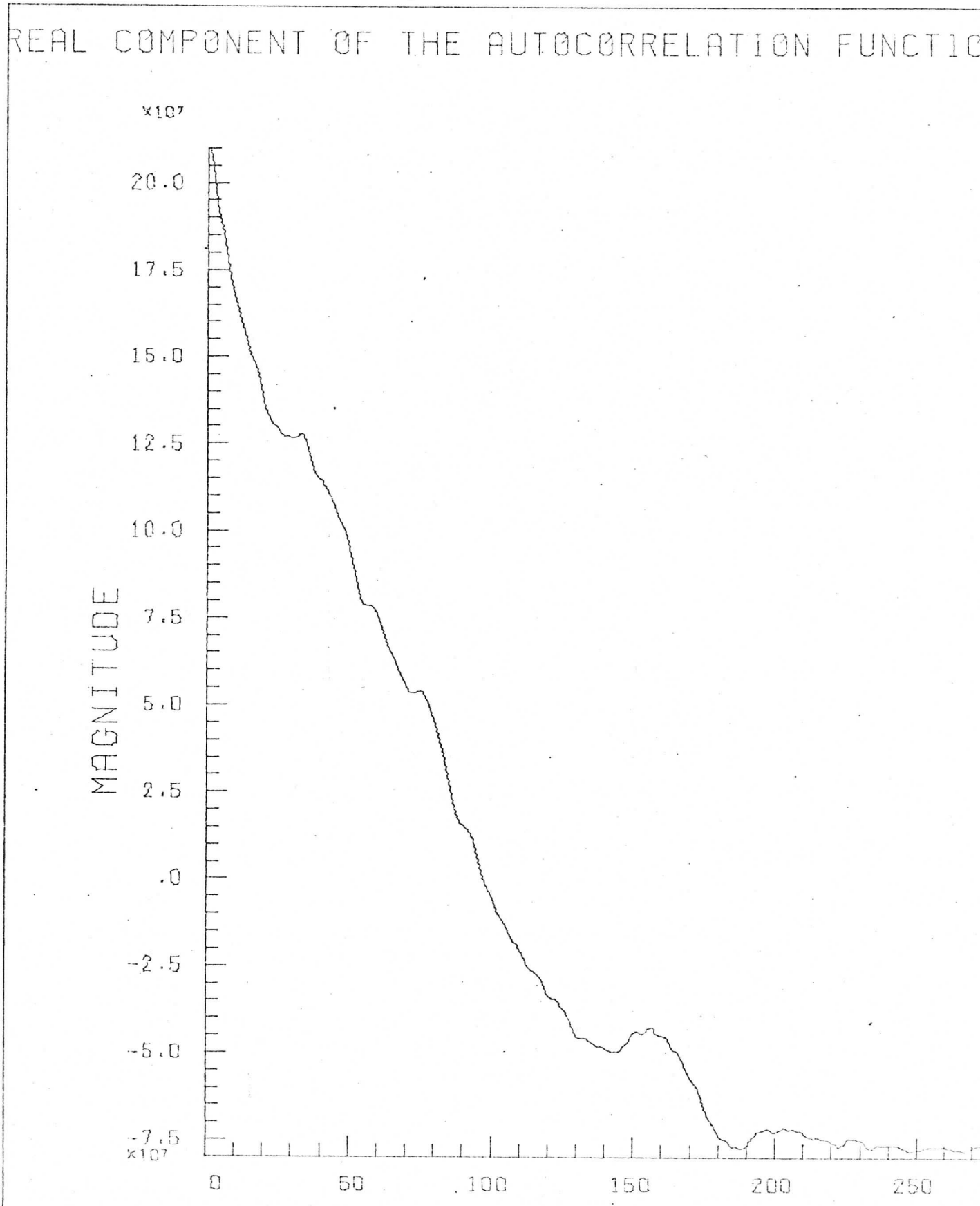

Apollo 56-2-1468, (rect.)
Locator: Tape 18, File 3
Records: 850 - 854 Date: 2/2/73
Elements: 10 - 521
Plot: Log Power Spectrum, Fifth Line

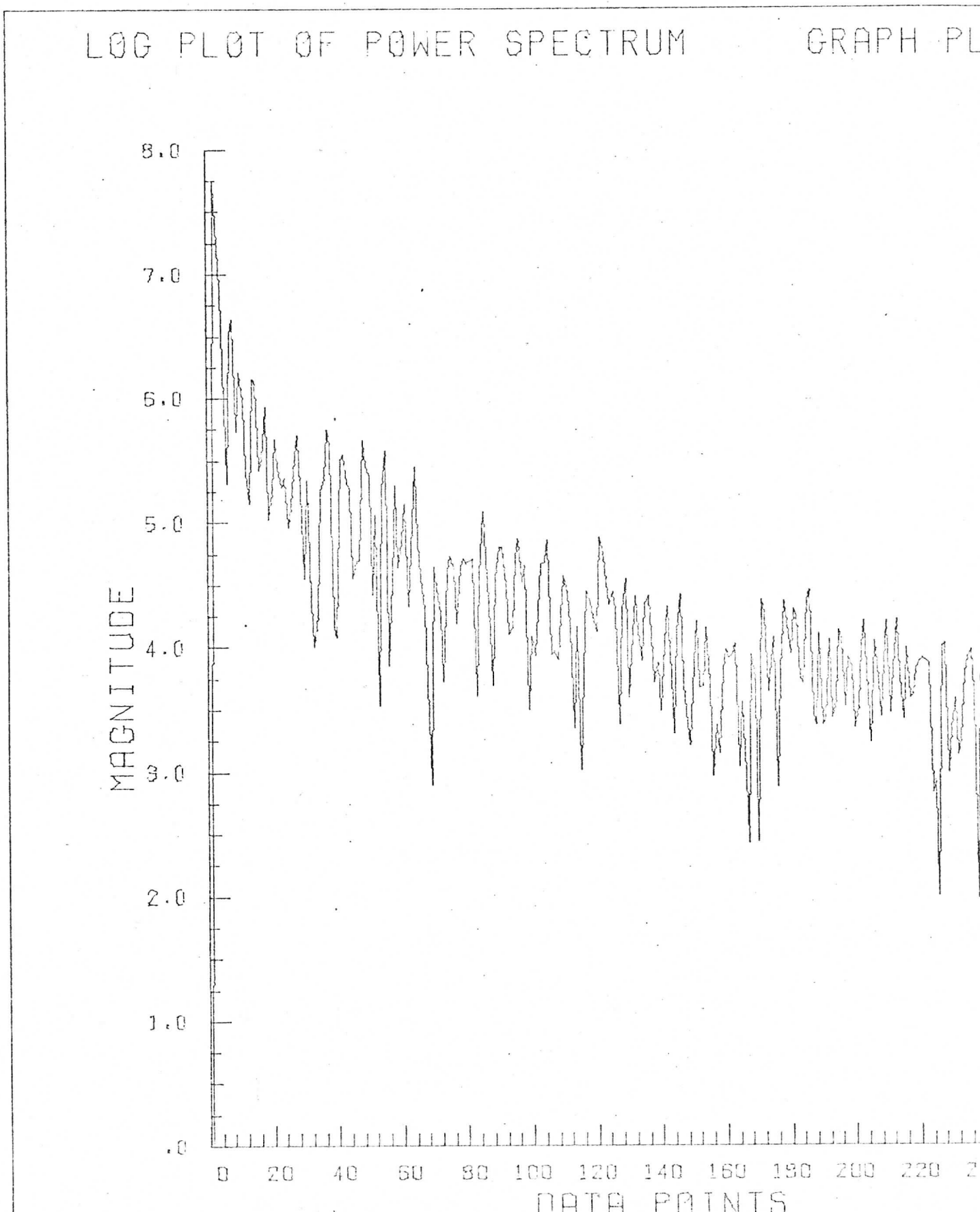

Apollo 56-2-1468, (rect.)
Locator: Tape 18, File 3
Records: 850 - 854 Date: 2/2/73
Elements: 10 - 521
Plot: Log Avg. Power Spectrum

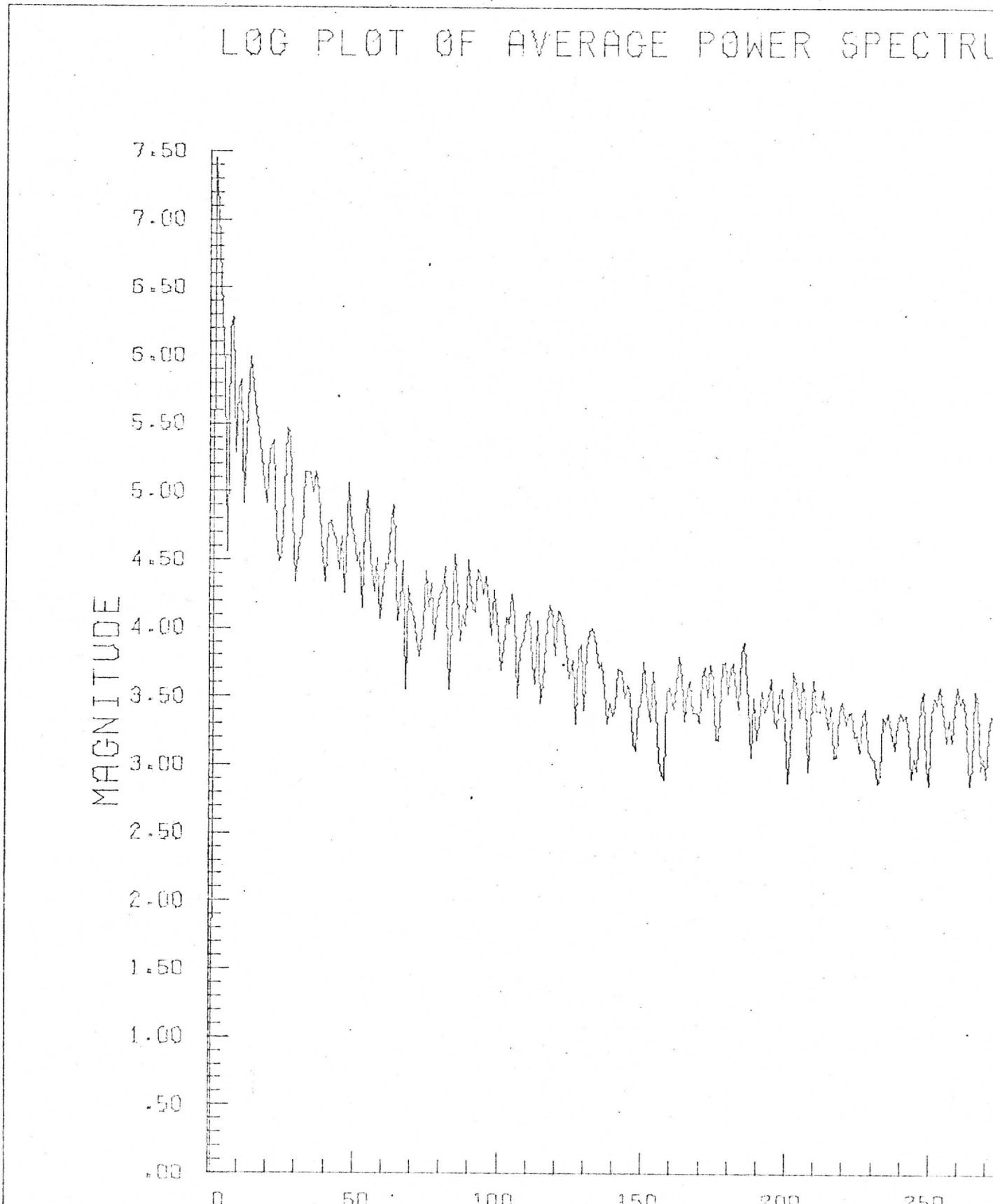

Apollo 56-2-1468, (rect.)
Locator: Tape 18, File 3
Records: 850 - 854 Date: 2/2/73
Elements: 10 - 521
Plot: Avg. Autocorrelation

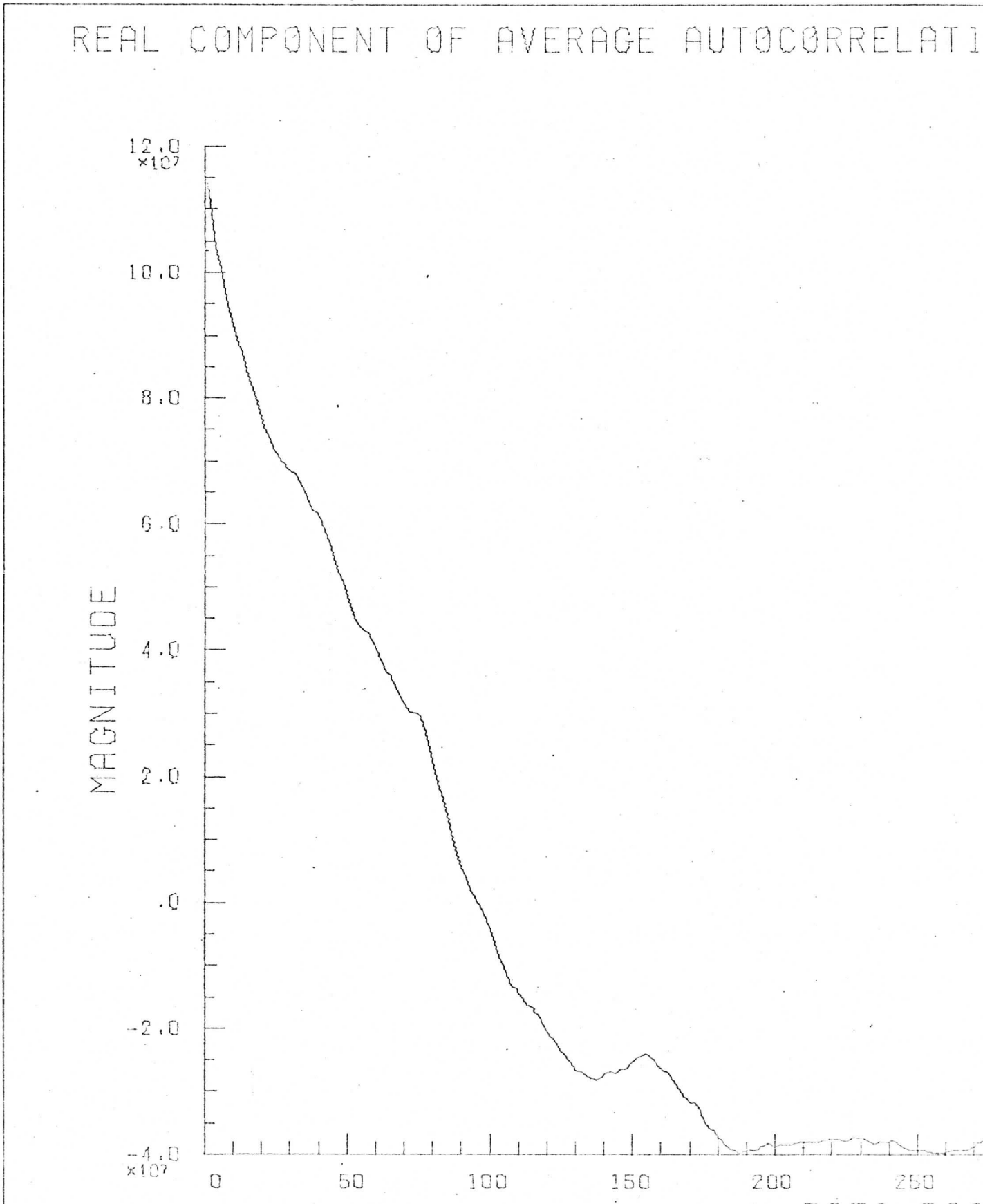

Apollo 56-2-1484 horizontal, (rect.)
Locator: Tape 18, File 5
Records: 350 - 354 Date: 2/2/73
Elements: 510 - 1021
Plot: Log Power Spectrum, First Line

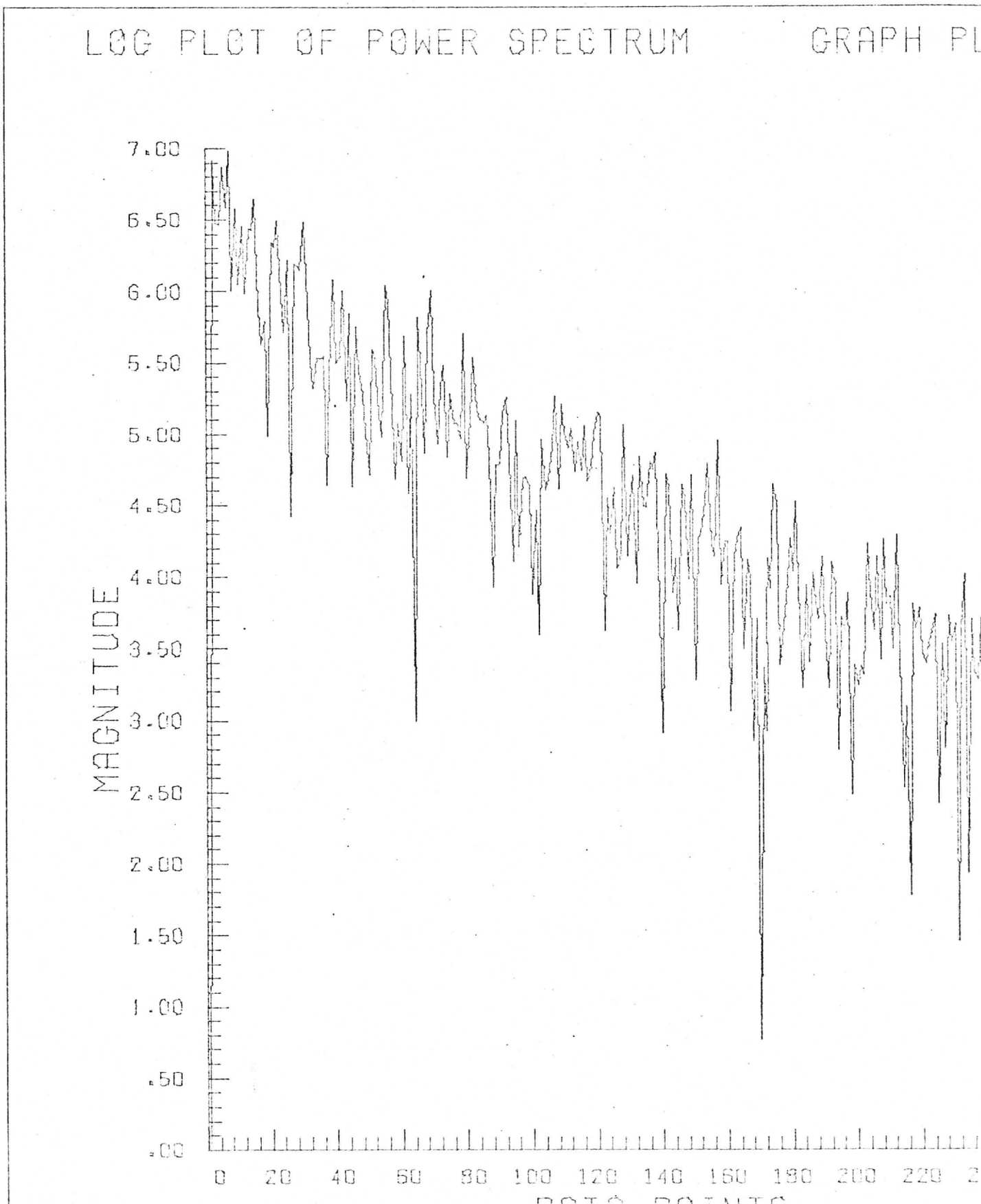

Apollo 56-2-1484 horizontal, (rect.)
Locator: Tape 18, File 5
Records: 350 - 354 Date: 2/2/73
Elements: 510 - 1021
Plot: Autocorrelation, First Line

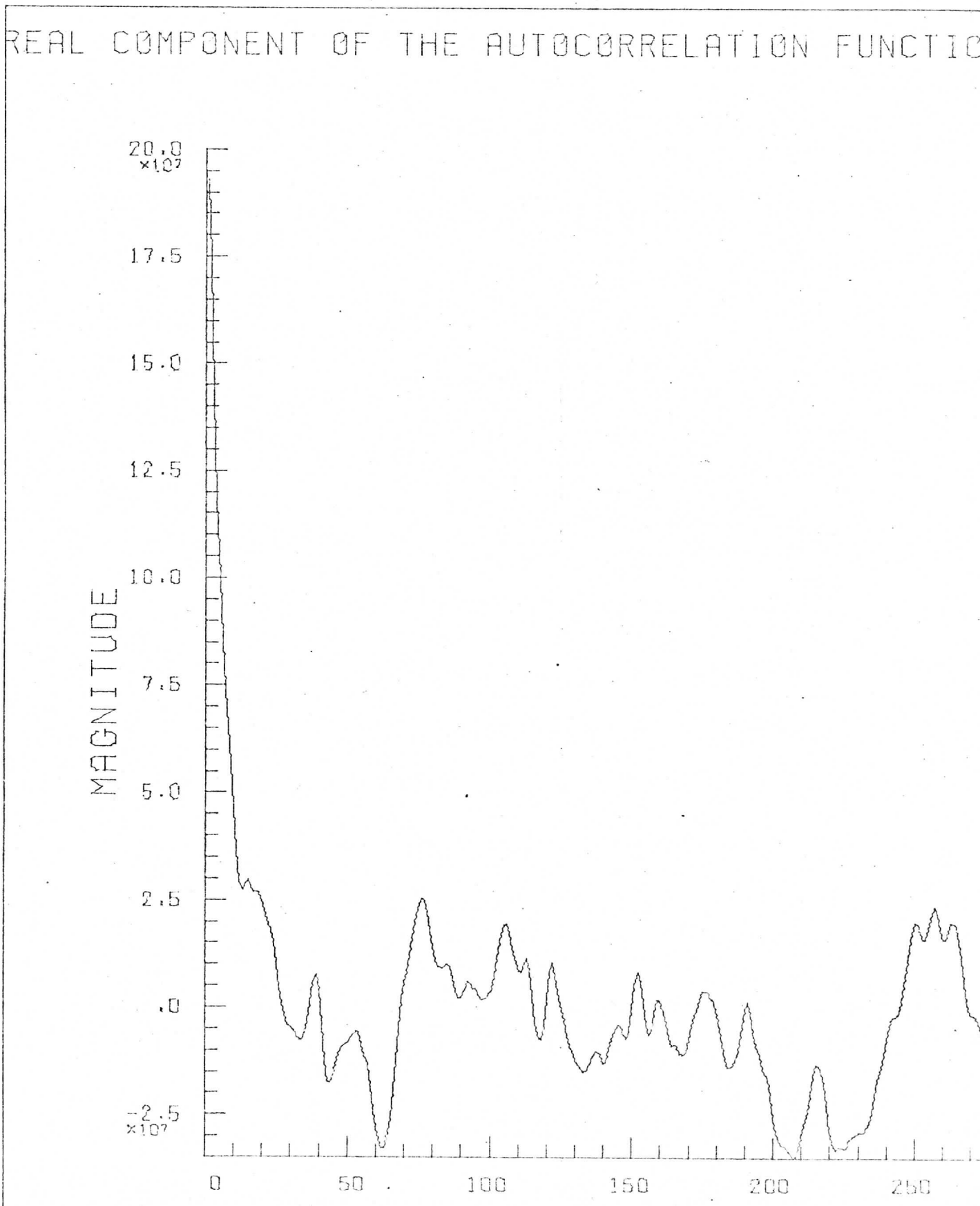

Apollo 56-2-1484 horizontal, (rect.)
Locator: Tape 18, File 5
Records: 350 - 354 Date: 2/2/73
Elements: 510 - 1021
Plot: Log Power Spectrum, Fifth Line

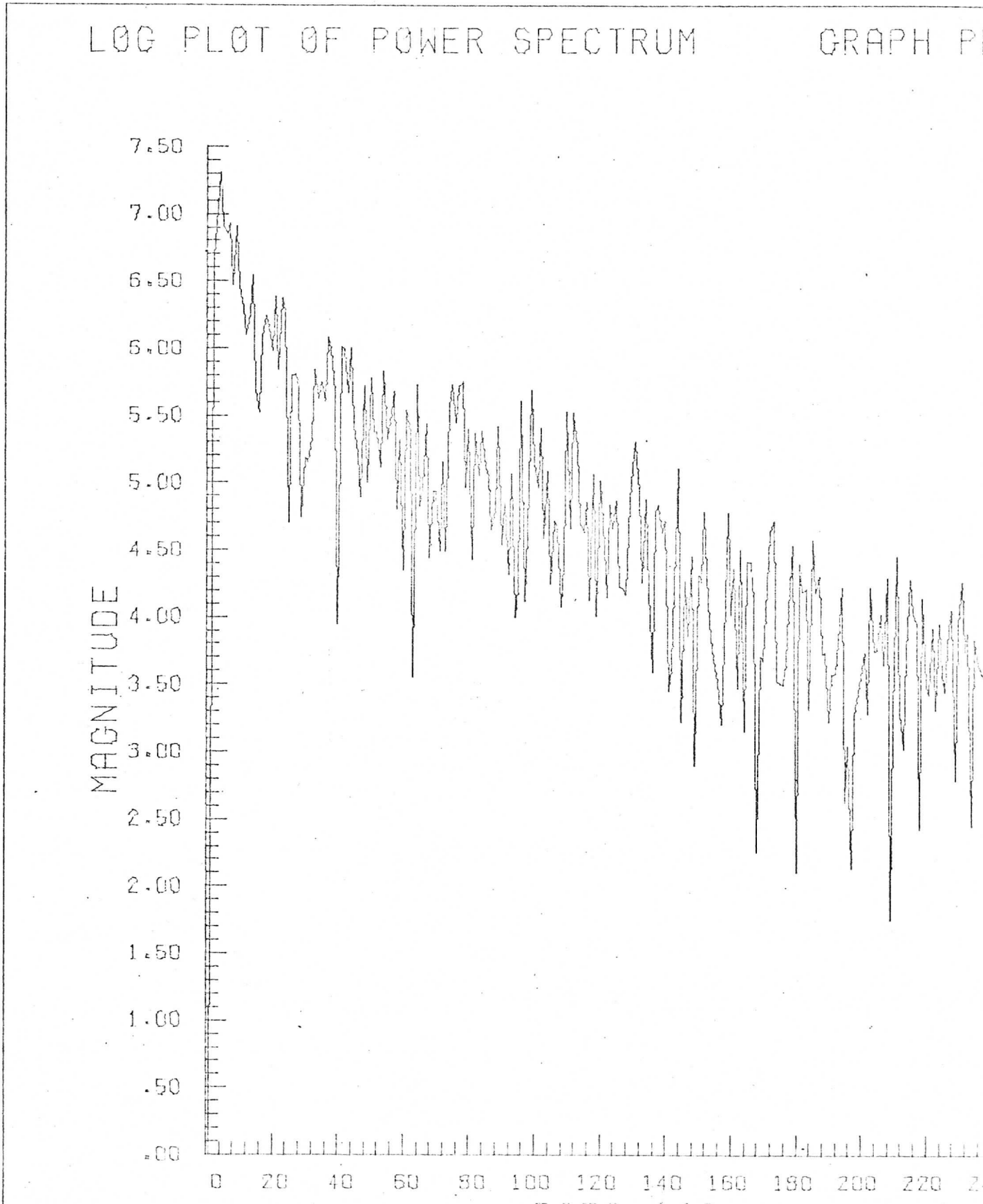

Apollo 56-2-1484 horizontal, (rect.)
Locator: Tape 18, File 5
Records: 350 - 354 Date: 2/2/73
Elements: 510 - 1021
Plot: Log Avg. Power Spectrum

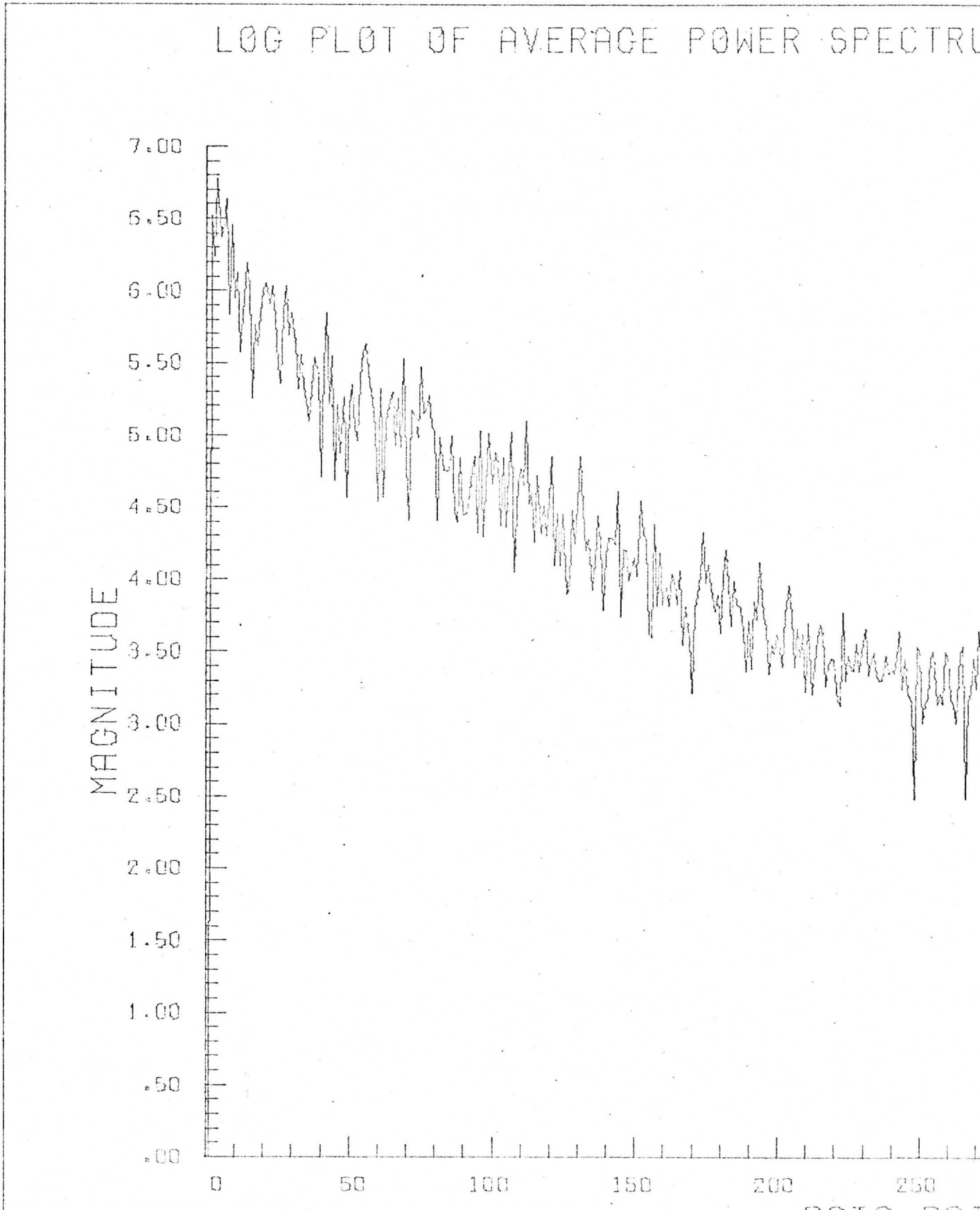

Apollo 56-2-1484 horizontal, (rect.)
Locator: Tape 18, File 5
Records: 350 - 354 Date: 2/2/73
Elements: 510 - 1021
Plot: Avg. Autocorrelation

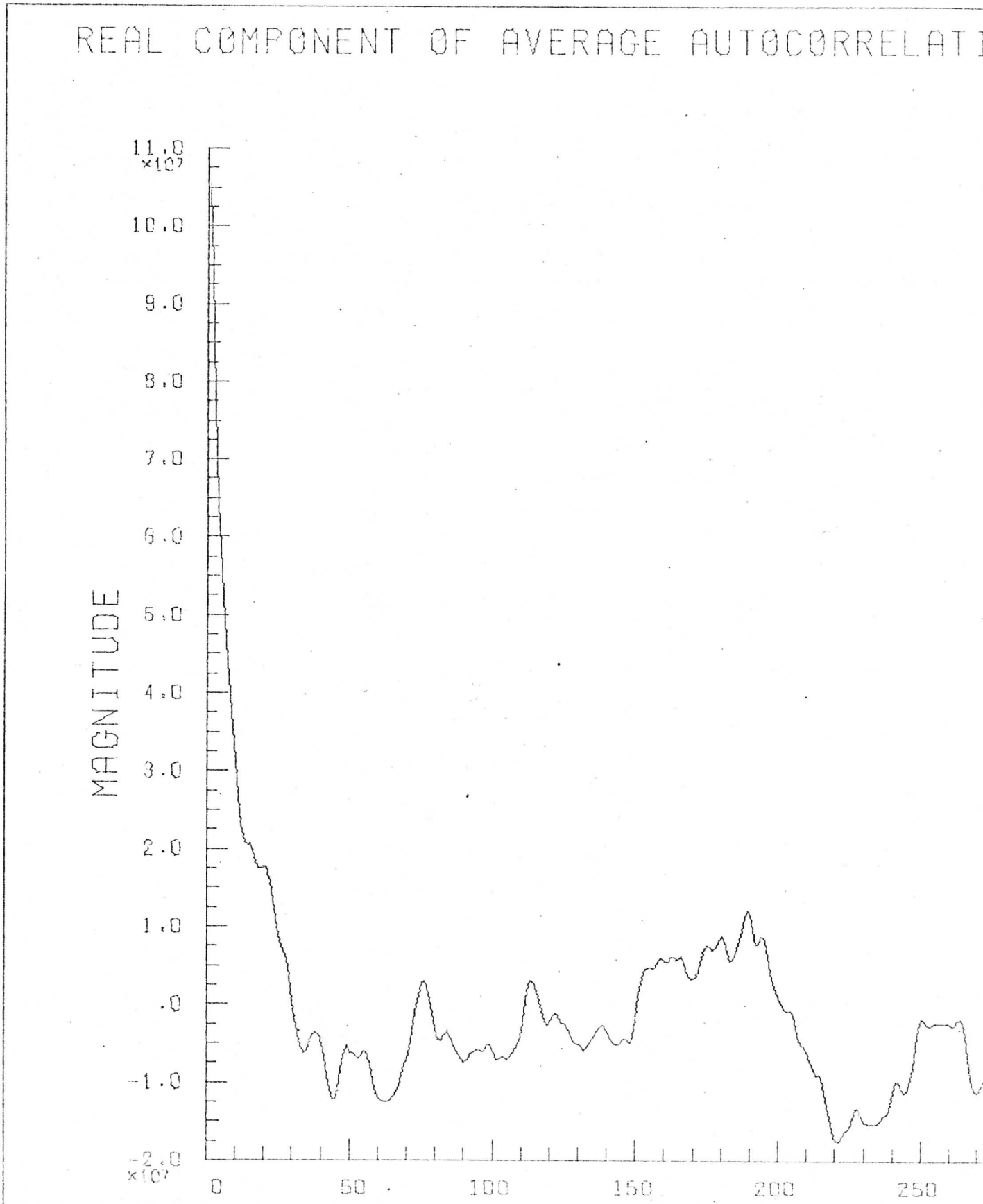

Apollo 56-2-1484 vertical, (rect.)
Locator: Tape 18, File 6
Records: 100 - 104 (from left)
Elements: 260 - 771 Date: 2/2/73
Plot: Log Power Spectrum, First Line

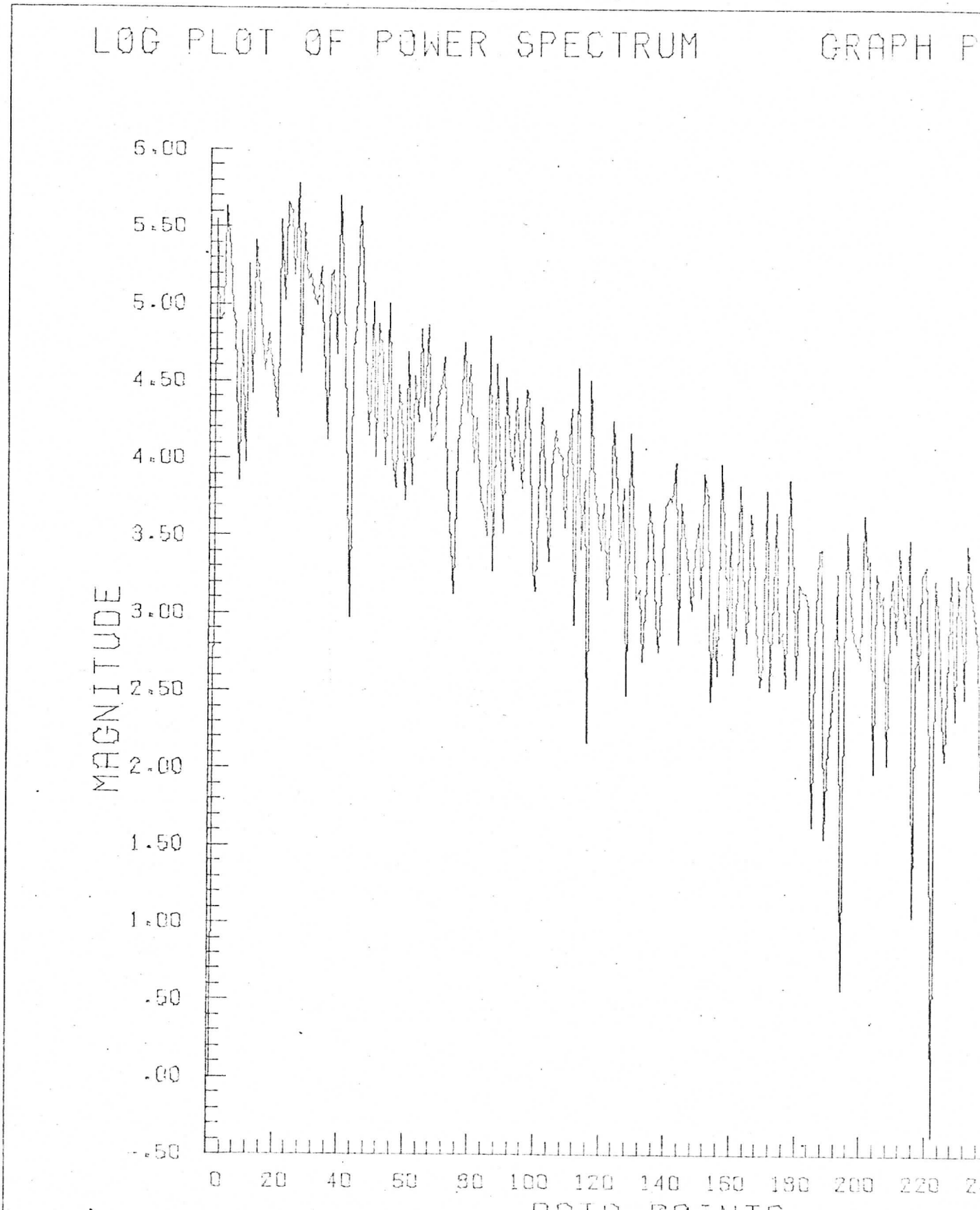

Apollo 56-2-1484 vertical, (rect.)
Locator: Tape 18, File 6
Records: 100 - 104 (from left)
Elements: 260 - 771 Date: 2/2/73
Plot: Autocorrelation, First Line

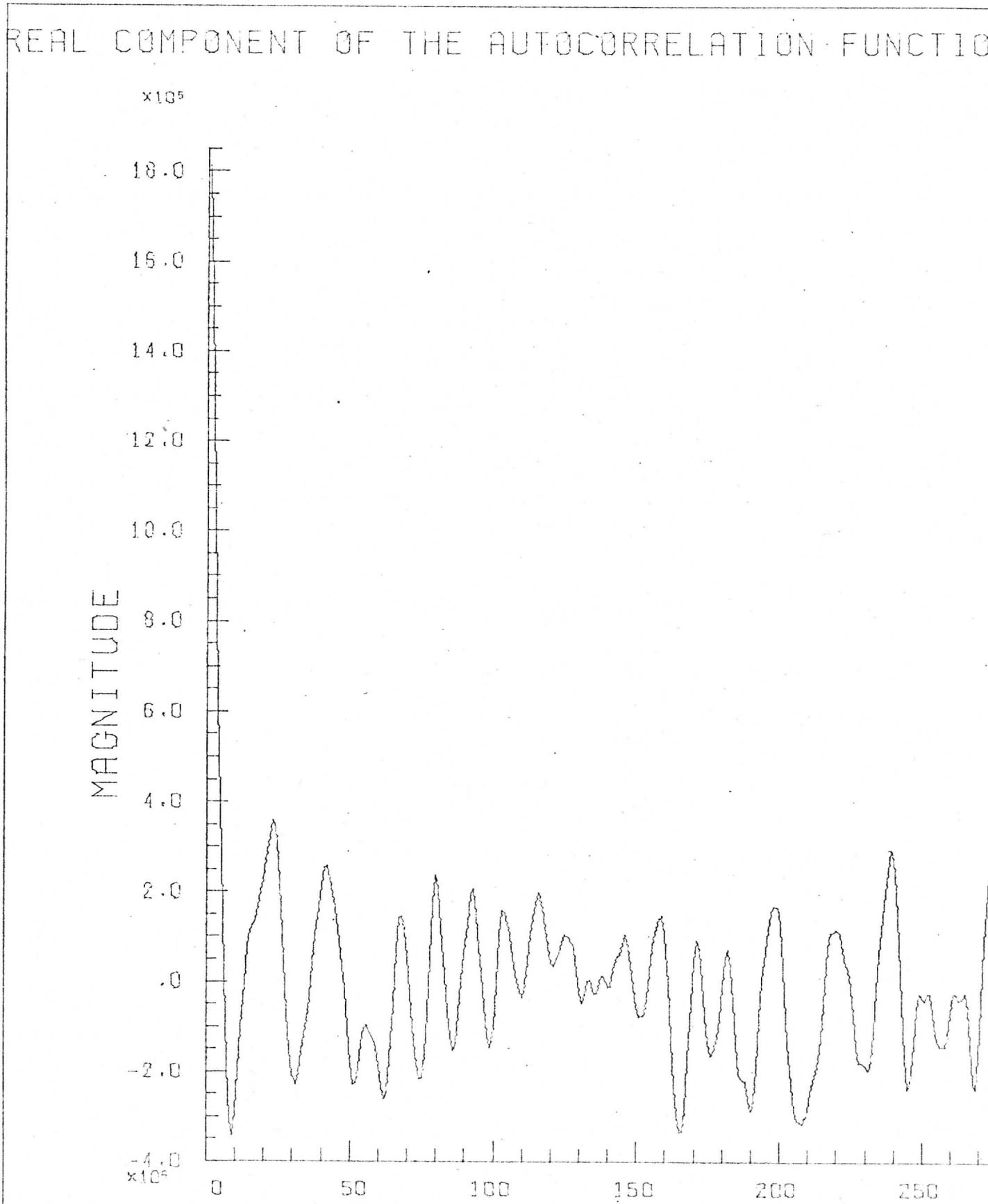

Apollo 56-2-1484 vertical, (rect.)
Locator: Tape 18, File 6
Records: 100 - 104 (from left)
Elements: 260 - 771 Date: 2/2/73
Plot: Log Power Spectrum, Fifth Line

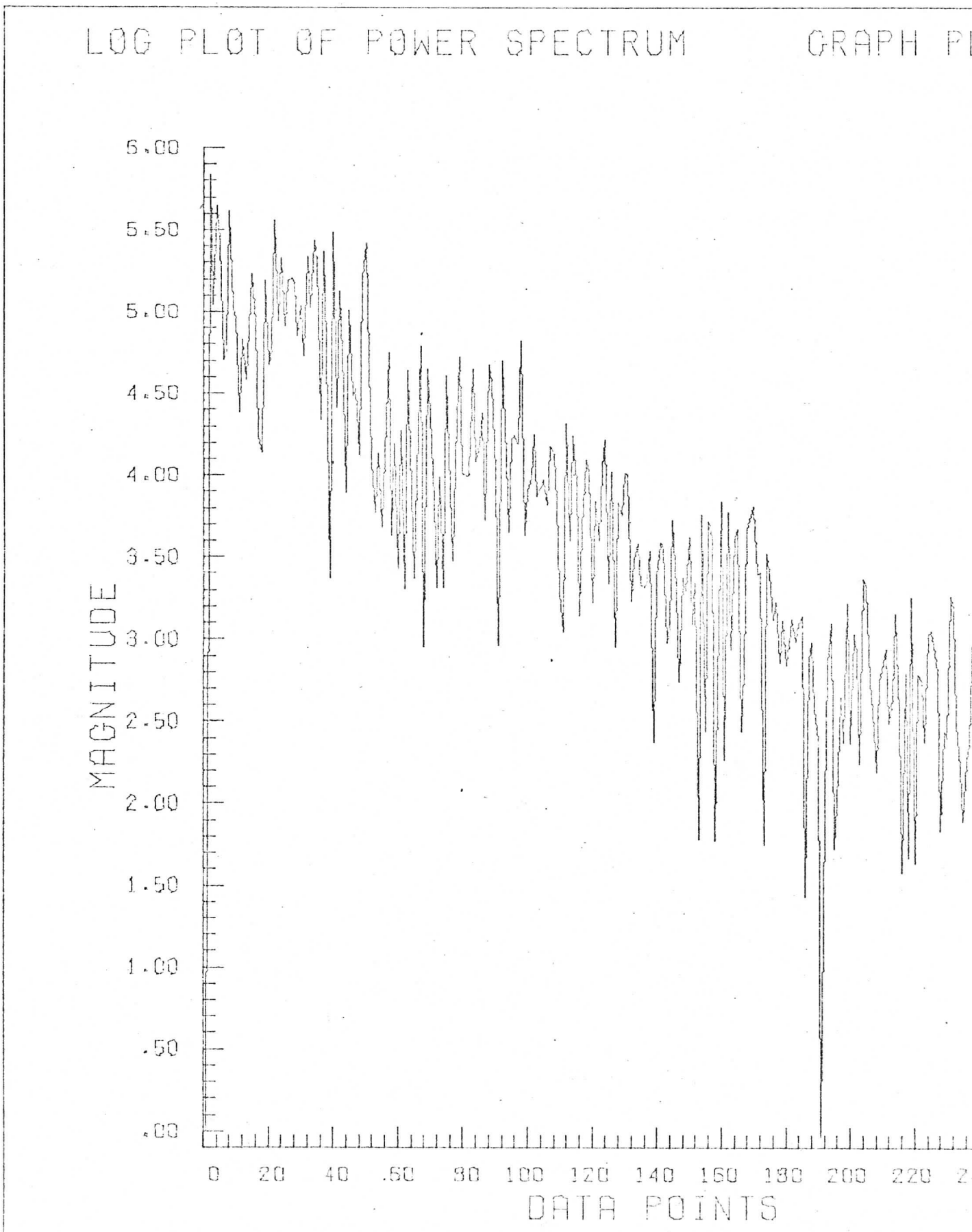

Apollo 56-2-1484 vertical, (rect.)
Locator: Tape 18, File 6
Records: 100 - 104 (from left)
Elements: 260 - 771 Date: 2/2/73
Plot: Log Avg. Power Spectrum

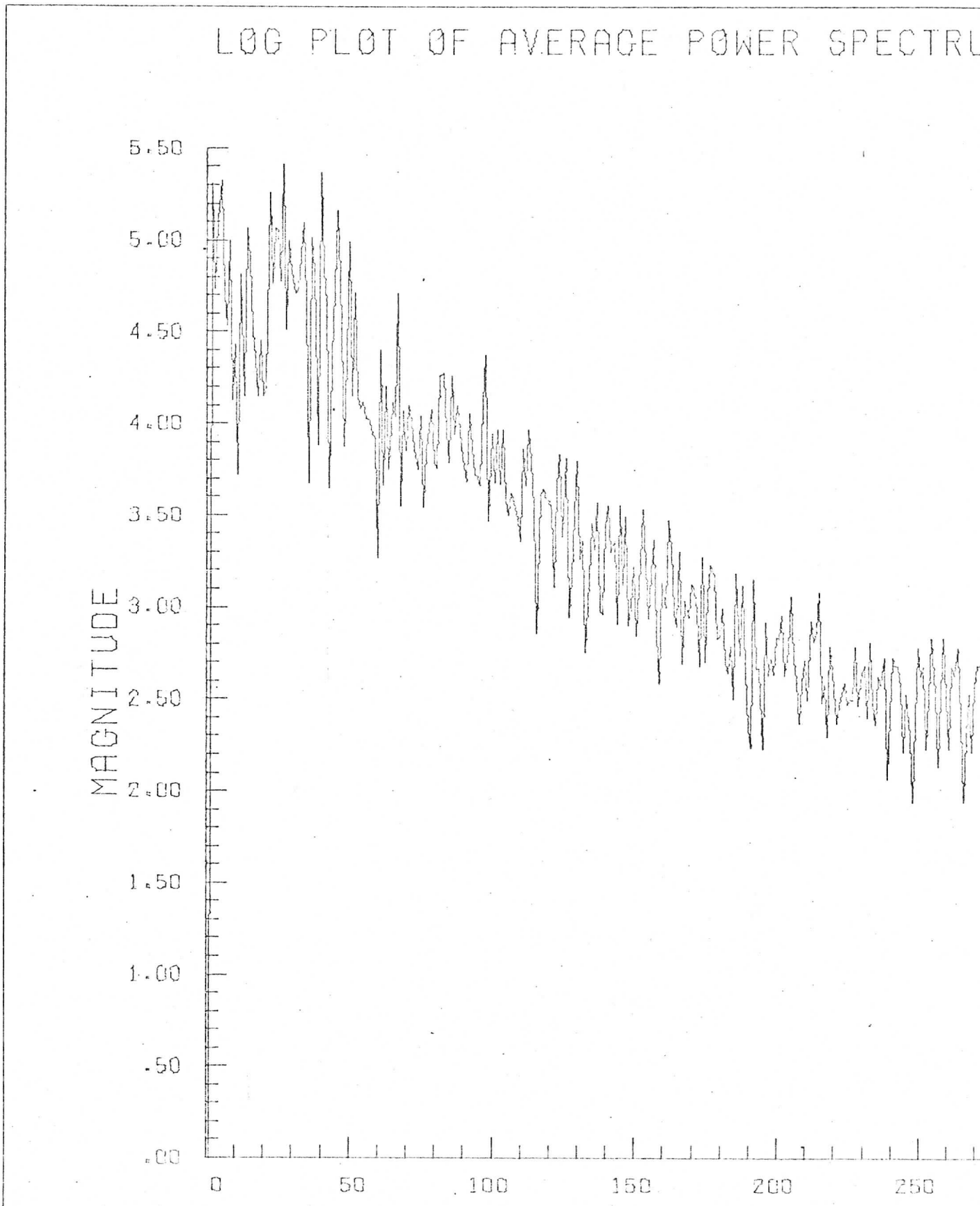

Apollo 56-2-1484 vertical, (rect.)
Locator: Tape 18, File 6
Records: 100 - 104 (from left)
Elements: 260 - 771 Date: 2/2/73
Plot: Avg. Autocorrelation

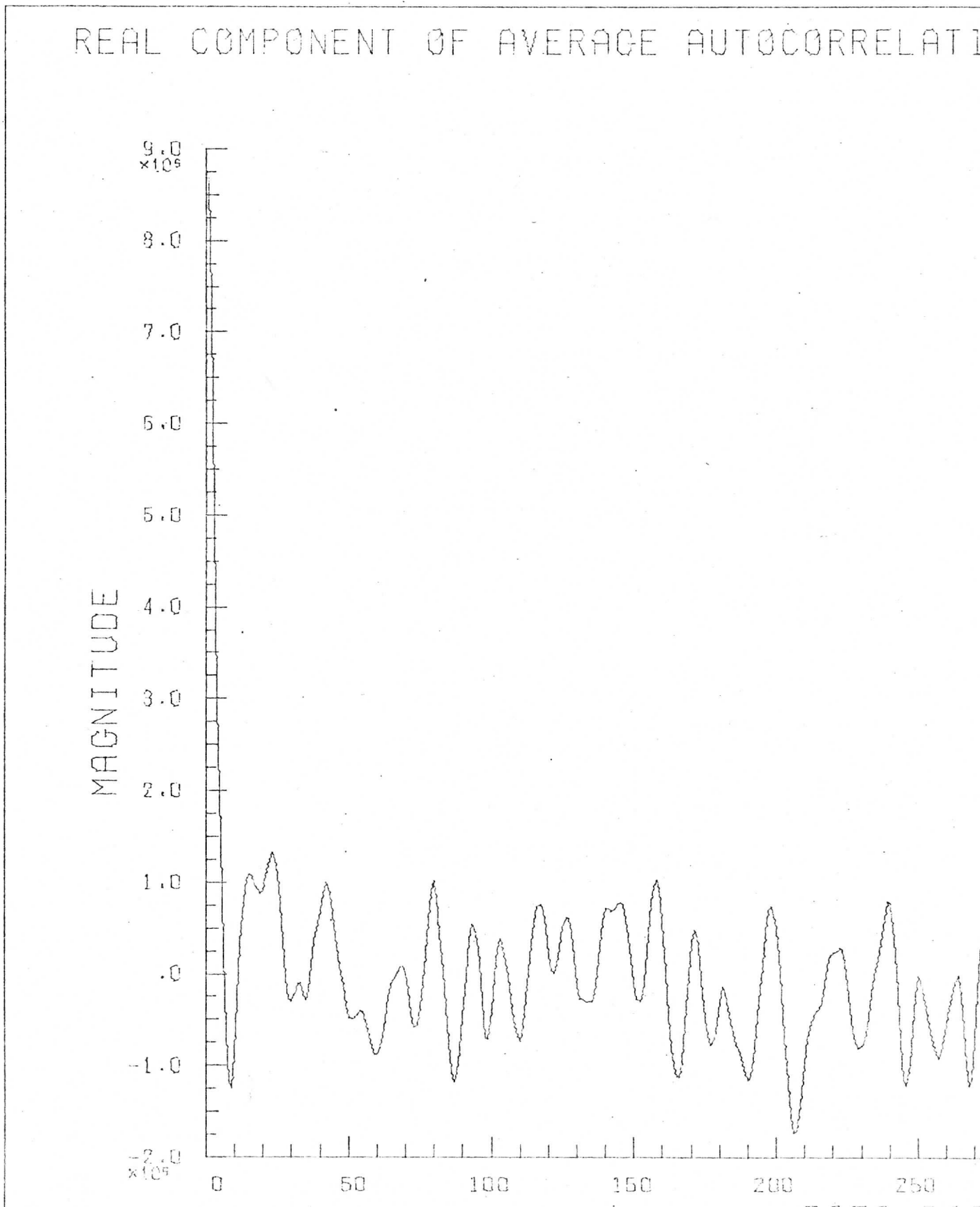

APPENDIX A

APERTURE EFFECTS

The Apollo 70 mm transparencies used for the power spectral analyses in this report were digitized using 1024 samples. Using 57 x 57 mm for the effective area of each transparency, the sampling area was restricted to 56 x 56 mm allowing 1/2 mm margin to avoid the effects of the abrupt edges of the picture. The scanning spot size used was 55 microns so that consecutive sample areas were approximately just adjacent to one another.

Assuming a circular scanning aperture, the impulse response of the scanning aperture of radius a is:

$$h(x) = \sqrt{a^2 - x^2} \qquad |x| < a \qquad \text{(A-1)}$$

$$= 0 \qquad \text{elsewhere}$$

The transfer function is then:

$$H(\omega) = \mathfrak{F}\{h(x)\} = \pi a^2 \frac{J_1(a\omega)}{(a\omega)} \qquad \text{(A-2)}$$

where $J_1(\omega)$ is the Bessel function of the first kind of order 1 and argument ω. Normalizing, we get that the weighting introduced into the power spectral plots is:

$$\frac{|H(\omega)|^2}{|H(0)|^2} = \left[\frac{2J_1(a\omega)}{(a\omega)}\right]^2 \qquad \text{(A-3)}$$

A graph of Eq. A-3 appears in Figure A.1. Note that the vertical scale is logarithmic to agree with the power spectral plots.

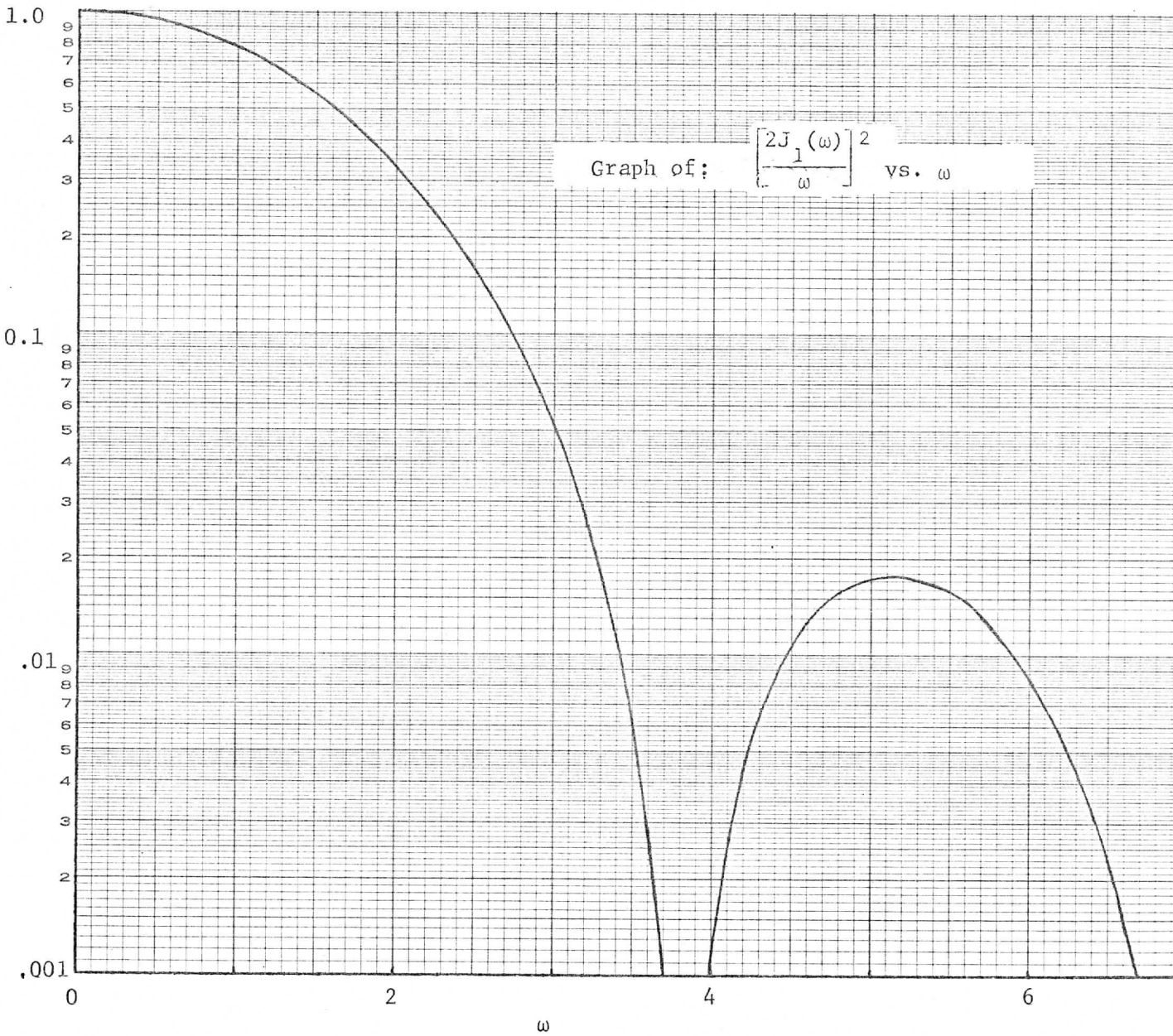

Figure A.1. Power Spectral Weighting of a Circular Scanning Aperture of Unit Radius.

The first zero of Eq. A-3 occurs for: $(a\omega_c) = 3.83$; for a spot diameter of 55 microns this gives:

$$f_c = \frac{3.83}{2\pi(.0275)} = 22.2 \text{ cycles/mm (15.4 cycles/n.mi.)}.$$

At the sampling rate used, 1024 samples = 56 mm, or the highest resolvable frequency is (from the sampling theorem):

$$f_{max} = \frac{512}{56} = 9.15 \text{ cycles/mm.}$$

Therefore the highest spatial frequency in these spectral plots corresponds to:

$$3.83 \frac{9.15}{22.2} = 1.58$$

on the graph in Figure A.1. This is about the -3dB point on the transfer function and because we are interested in what goes on at about one-sixth to one-third the maximum frequency, the effect of the scanning aperture on the spectral plots was judged to be a second-order effect. This is verified in Table A.1 where it is noted that the aperture weighting function is down less than 10% at a SMS subpoint frequency of 500 kHz.

TABLE A.1

Effects of Aperture Weighting in DicoMed Picture Sampling of Apollo VI.

Data Pts. (512 samples)	Spatial Frequency cycles/mm.	Spatial Frequency cycles/n.mi.	$a\omega$	$\left[\frac{2J_1(a\omega)}{(a\omega)}\right]^2$	SMS Freq. (MHz) @Subpt.
0	0	0	0	1.00	0
50	1.79	1.24	0.309	0.973	0.25
100	3.58	2.47	0.617	0.910	0.50
150	5.37	3.70	0.926	0.803	0.75
200	7.16	4.94	1.23	0.678	1.00
250	8.94	6.17	1.54	0.535	1.25

The effects of SMS scanning apertures were considered from both the diffraction-limited and the aberration-limited cases. The radius of the VISSR aperture is: $r_1 = 20.32$ cm. Choosing $\lambda = 0.707$ μm (Computer Sciences Corp. 1972) and a minimum satellite-to-earth distance of: $R_1 = 3.58 \times 10^4$ km, this easily satisfies the Fraunhofer criterion:

$$R_1 >> \frac{\pi r_1^2}{\lambda} = \frac{\pi(0.203)^2}{0.707 \times 10^6} = 183 \text{ km.} \qquad \text{(A-4)}$$

The actual VISSR aperture is annular and bounded by two concentric circles of radii r_1 and εr_1, where $\varepsilon = 0.400$. The normalized Fraunhofer diffraction pattern is (Born and Wolf, 1965):

$$\frac{2}{1-\varepsilon^2}\left[\frac{J_1(kr_1\alpha)}{(kr_1\alpha)} - \varepsilon^2 \frac{J_1(k\varepsilon r_1\alpha)}{(k\varepsilon r_1\alpha)}\right] \qquad \text{(A-5)}$$

where $k = 2\pi/\lambda$ and α is the angle from the center of the pattern in radians. It is not necessary to evaluate this result numerically, as will be evident below.

The voltage signal out of the photomultiplier is proportional to the magnitude squared of Eq. A-5. The Fourier transform of this magnitude squared voltage is the autocorrelation function or optical transfer function (OTF) of the aperture, scaled by $\lambda R_1 f$ (Goodman, 1968). The magnitude-squared of this autocorrelation function is the weighting function for the diffraction-limited case.

A well-known property of the autocorrelation function of a spatially-limited function is that it is spatially limited to twice the interval. Therefore the maximum or "cut-off" frequency of the diffraction-limited system is:

$$\lambda R f_{max} = 2r_1$$

or

$$f_{max} = \frac{2r_1}{\lambda R} = \frac{2(0.203)}{(0.707 \times 10^{-6})(1.936 \times 10^{4})} = 29.6 \text{ cycles/n.mi.}$$

This is almost twice the effective spread of the DicoMed scanner discussed above and is quite negligible. This, of course, represents the best possible case.

An opposite extreme is to admit enough aberrations to yield a uniform-intensity blur circle of diameter such that consecutive samples are adjacent but not overlapping. Any worse situation will yield samples which are no longer entirely independent. For the SMS parameters, this diameter is 0.405 n.mi. at the satellite subpoint. Assuming a circular pattern for convenience allows us to use the previous results for the circular scanning aperture. The spectral weighting is then given by the graph of Figure A.1. The interval to the first zero in the weighting is:

$$f_c = \frac{3.83}{2\pi\ (0.203)} = 3.01 \text{ cycles/n.mi}$$

(≃602 kHz at SMS subpt.)

This weighting pattern is no longer negligible. However, if the pre-aliasing filter is included and this filter has a steep "fall-off" characteristic, the aperture effect is still secondary. For example, the response of a fifth-order low-pass filter with a -3dB bandwidth at 250 kHz will be down -30dB at 500 kHz. In contrast, the above aperture weighting at 250 kHz (1.24 cycles/n.mi at the subpt.) is 0.513 while that at 500 kHz is 0.366--a decrease of -1.5 dB.

Our conclusion is that, while aperture effects do exist, they are, within the above assumptions, of second-order effect and the system performance is governed primarily by the pre-alias filtering. Actual test data on the system modulation transfer function (MTF) can be incorporated into our results at a later date as a refinement.

APPENDIX B

DETERMINATION OF THE POWER SPECTRAL DENSITY USING THE DISCRETE FOURIER TRANSFORM

In this appendix we will outline the procedure for determining the power spectral density function by an approximation technique which involves the Discrete Fourier Transform (DFT). We are interested in a process $\{z(x)\}$ which depends on a linear distance parameter x. Its power spectral density is defined as (Papoulis, 1965):

$$S_z(\omega) = \lim_{A\to\infty} \left\{ \frac{E[|Z_A(\omega)|^2]}{2A} \right\} \tag{B-1}$$

where:

$$Z_A(\omega) = \int_{-A}^{+A} z(x) e^{-j\omega x}\, dx. \tag{B-2}$$

Note that Eq. B-2 is the Fourier Transform of a segment of a sample function of the process $\{z(x)\}$ from -A to A. In effect we multiply the process by a "box-car function", i.e., a function with value 1 from -A to +A and zero elsewhere, and then take the transform of the resultant.

It is well known that the spectrum $Z_A(\omega)$ can be very closely approximated by the discrete version of Eq. B-2 (McGillem and Cooper, 1973):

$$Z(k\Omega) = \sum_{\ell=0}^{N-1} z(\ell \frac{2A}{N}) e^{-j(2\pi/N)\ell k} \qquad \Omega = 2\pi/2A. \tag{B-3}$$

We have divided the interval (-A,A) into N equal segments and assigned: $z(-A) = z(0 \frac{2A}{N})$. The nature of the approximation is revealed by noting:

$$Z_A(\omega)\Big|_{\omega=k\Omega} = (2A) Z(k\Omega). \tag{B-4}$$

The values of the DFT are proportional to the sampled version of the true spectral density $Z_A(\omega)$ at the N sample points.

We approximate the expectation operation of the transform by averaging M adjacent samples of the spectrum.

$$E[|Z_A(\omega)|^2]\Big|_{\omega=k\Omega} = \frac{1}{M}\sum_{i=1}^{M}|Z_i(k\Omega)|^2 \qquad \text{(B-5)}$$

The value of M is judiciously chosen so that the M sample spectra represent adjacent samples which are indistinguishable as far as the aperture of the optics in the satellite is concerned. We further assume that the value of A is sufficiently large so that the limit in Eq. B-1 can be approximated. Then, for a fixed A, we have:

$$S_z(\omega)\Big|_{\omega=k\Omega} = 2A\,\frac{1}{M}\sum_{i=1}^{M}|Z_i(k\Omega)|^2. \qquad \text{(B-6)}$$

Implicit in the use of the DFT is the assumption that the true spectrum is bandlimited. This assumption is sufficient to guarantee that the samples of z(x) fully represent the data. Hence after the power spectrum has been computed, the results must be examined to verify the bandlimited criterion.

As was noted earlier the data has in effect been multiplied by a rectangular window function. Viewing these effects in the frequency domain, it is seen that the restriction of the data to a finite length tends to smear or broaden the true spectrum. Hence spectral weighting functions called windows or tapering functions are often employed instead of the rectangular one (Otnes and Enochson, 1972). In the data domain the window functions suppress the abrupt discontinuities at the start and finish of the finite record length.

We include the following examples to demonstrate several points. Since Eq. B-3 and subsequent computations are implemented on a digital computer which must of necessity operate with finite word lengths to perform all of its functions, the first item of interest is the effect of round-off errors in the arithmetic operations of the machine. The second point is the sensitivity of Eq. B-3 to monochromatic signals, i.e., pure sine or cosine waves. Finally we are interested in the effects of different window functions. In the accompanying figures we will always be plotting:

$$\log |Z(k\Omega)|^2 \qquad k = 0, 1, \ldots, N-1$$

where: (B-7)

$$Z(k\Omega) = \sum_{\ell=0}^{N-1} w(\ell \frac{2A}{N}) (\cos \frac{2\pi}{N} f\ell) e^{-j(2\pi/N)\ell k}$$

$$N = 512.$$

There are four forms of the window function used here:

$$w_R(\ell \frac{2A}{N}) = 1 \qquad \text{Rectangular} \qquad \text{(B-8)}$$

$$w_{HN}(\ell \frac{2A}{N}) = 0.5(1 - \cos \frac{2\pi}{N} (\ell-1)) \qquad \text{Hanning} \qquad \text{(B-9)}$$

$$w_{HM}(\ell \frac{2A}{N}) = (0.54 - 0.46 \cos \frac{2\pi}{N} (\ell-1)) \qquad \text{Hamming} \qquad \text{(B-10)}$$

$$w_P(\ell \frac{2A}{N}) = \frac{1}{\pi}\left|\sin \pi\left[\frac{\ell-1-(N/2)}{N/2}\right]\right| + \left\{1 - \left|\frac{\ell-1-(N/2)}{N/2}\right|\right\} \cos \pi\left[\frac{\ell-1-(N/2)}{N/2}\right]$$

(Papoulis, 1973) (B-11)

We have selected eight test frequencies. Half of them represent functions which contain integer number of cycles in a sample of width 2A whereas the remaining half have fractional numbers of cycles in the range sample width. Because the plots are drawn to take

advantage of the maximum dynamic range of the plotter, there is no uniform scaling among the ordinates of the figures. Furthermore, it must be emphasized that the ordinate axis represents the logarithm of the values. The maximum value of each figure occurs at the point(s) nearest the frequency of the input signal. However, the magnitude of sidelobes and their widths differ depending on the type of window function. It is also possible to observe the round-off noise generated by the operations in the computer. This is most easily seen in the graphs of signals with an integer number of cycles present.

Cycles: 20.000
Window: Rectangular
Avg. Value: 0.00000
Date: 12/30/72-1

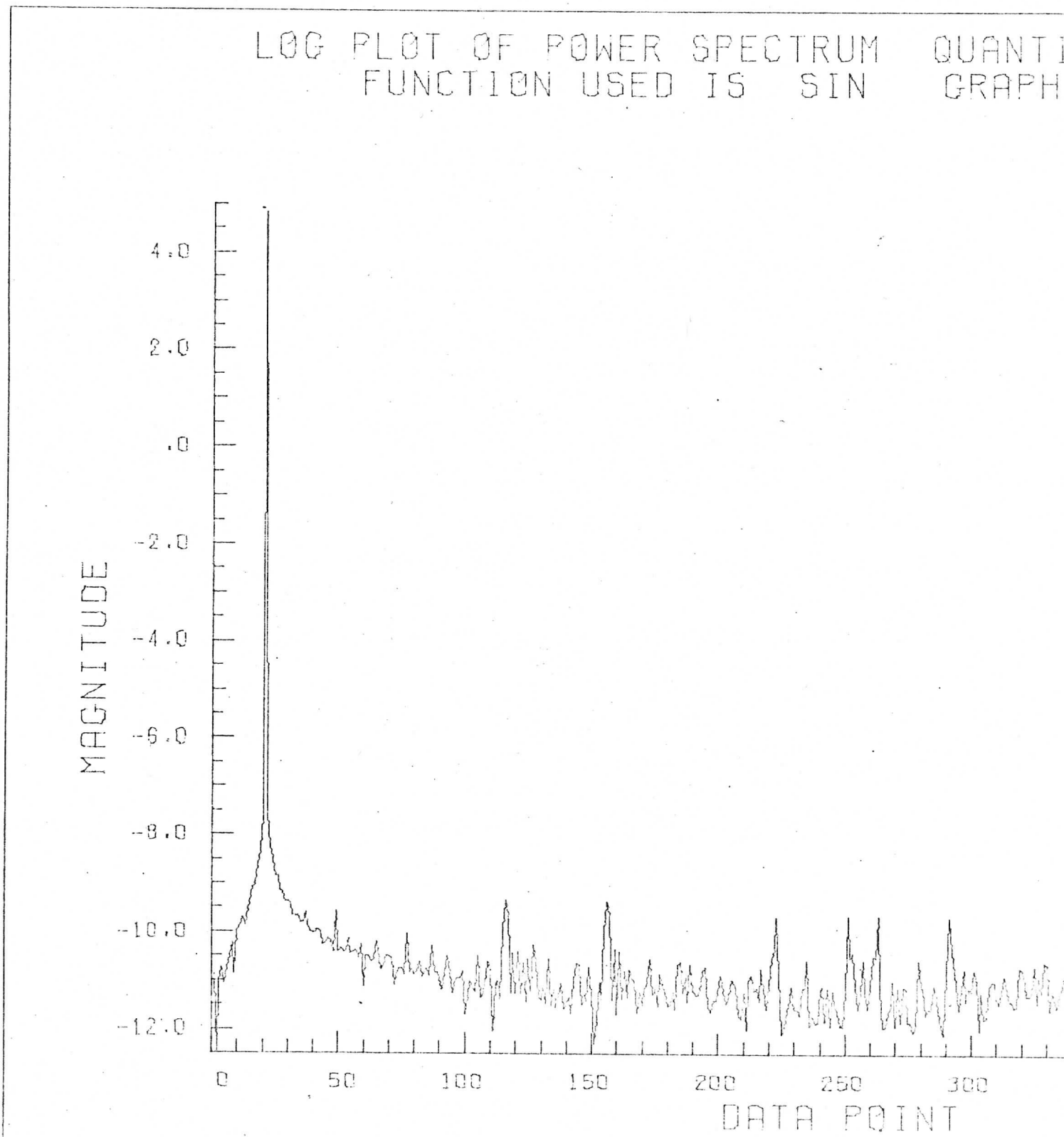

Cycles: 20.000
Window: Hanning
Avg. Value: 0.00000
Date: 12/30/72-2

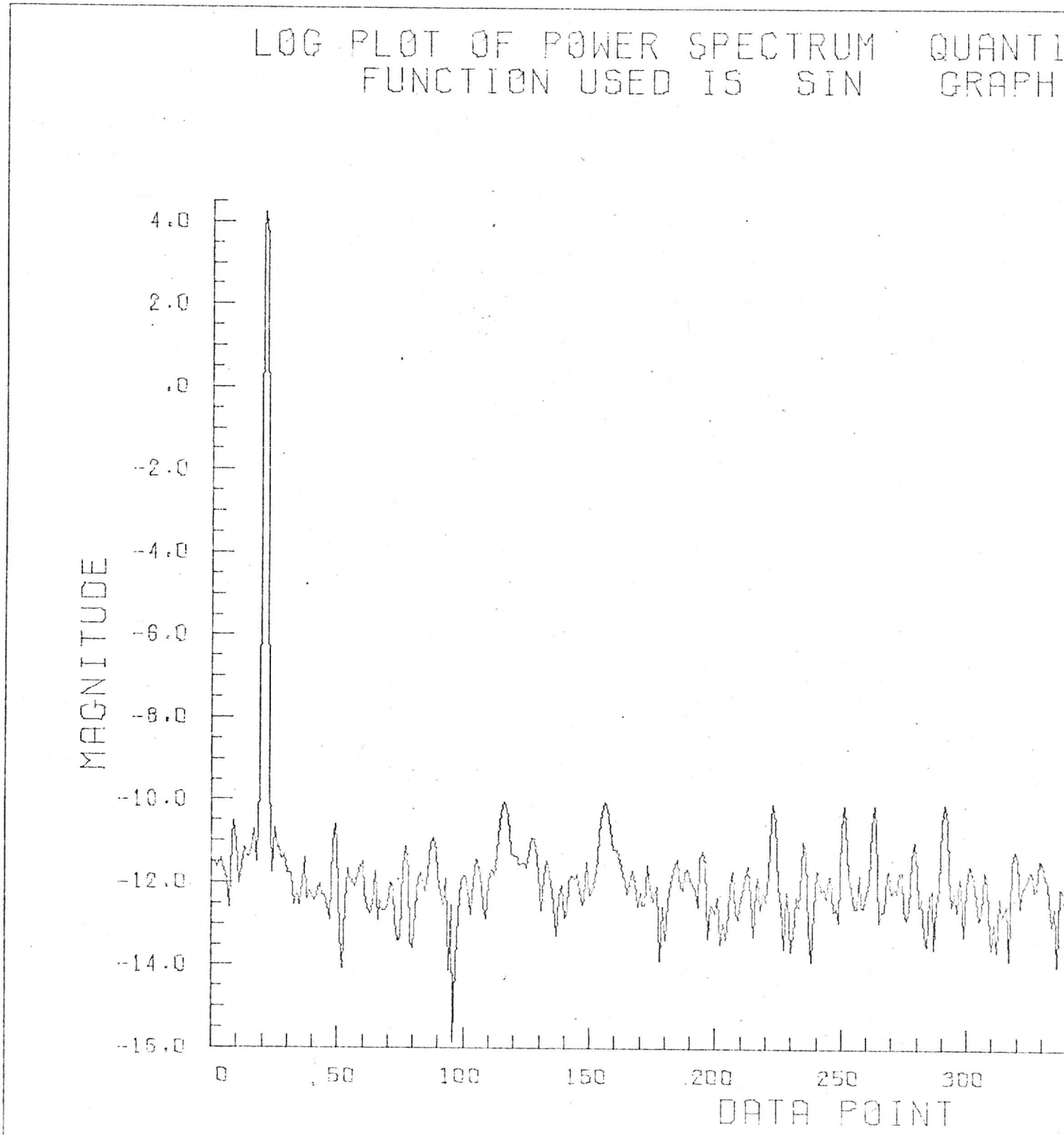

Cycles: 20.000
Window: Hamming
Avg. Value: 0.00000
Date: 12/30/72-3

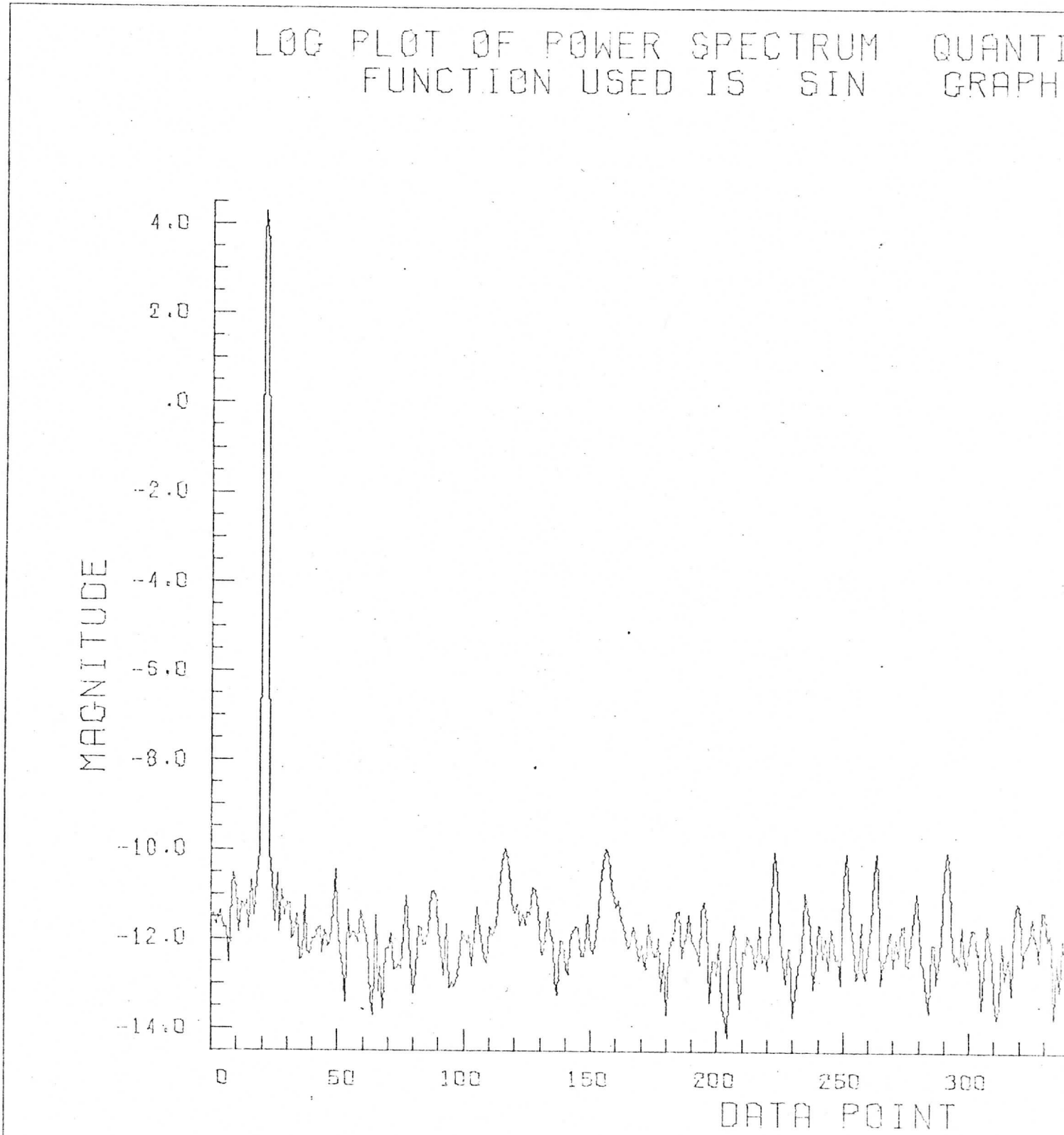

Cycles: 20.000
Window: Papoulis
Avg. Value: 0.0000
Date: 2/15/73-2

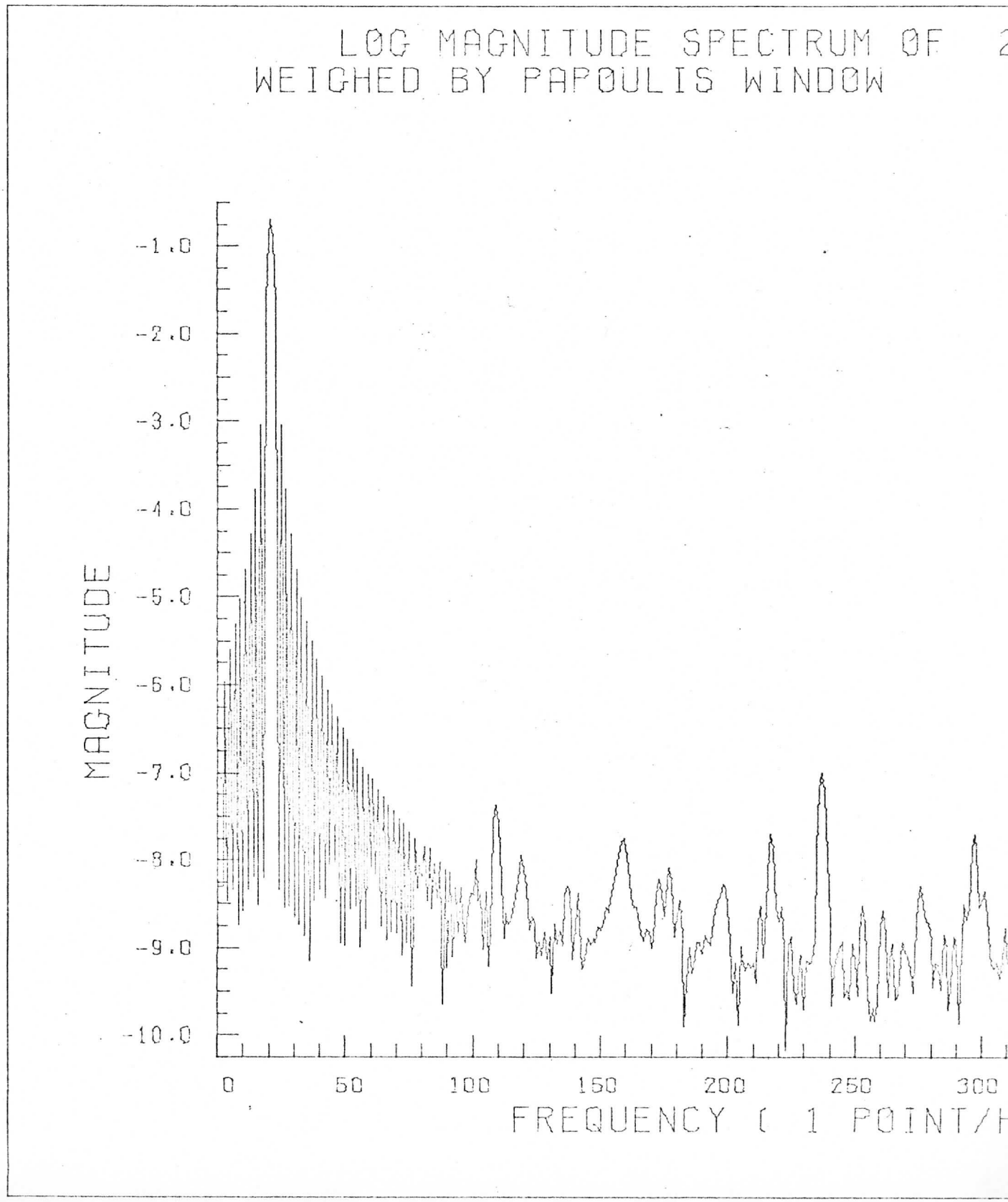

Cycles: 20.300
Window: Rectangular
Avg. Value: 0.00000
Date: 12/30/72-5

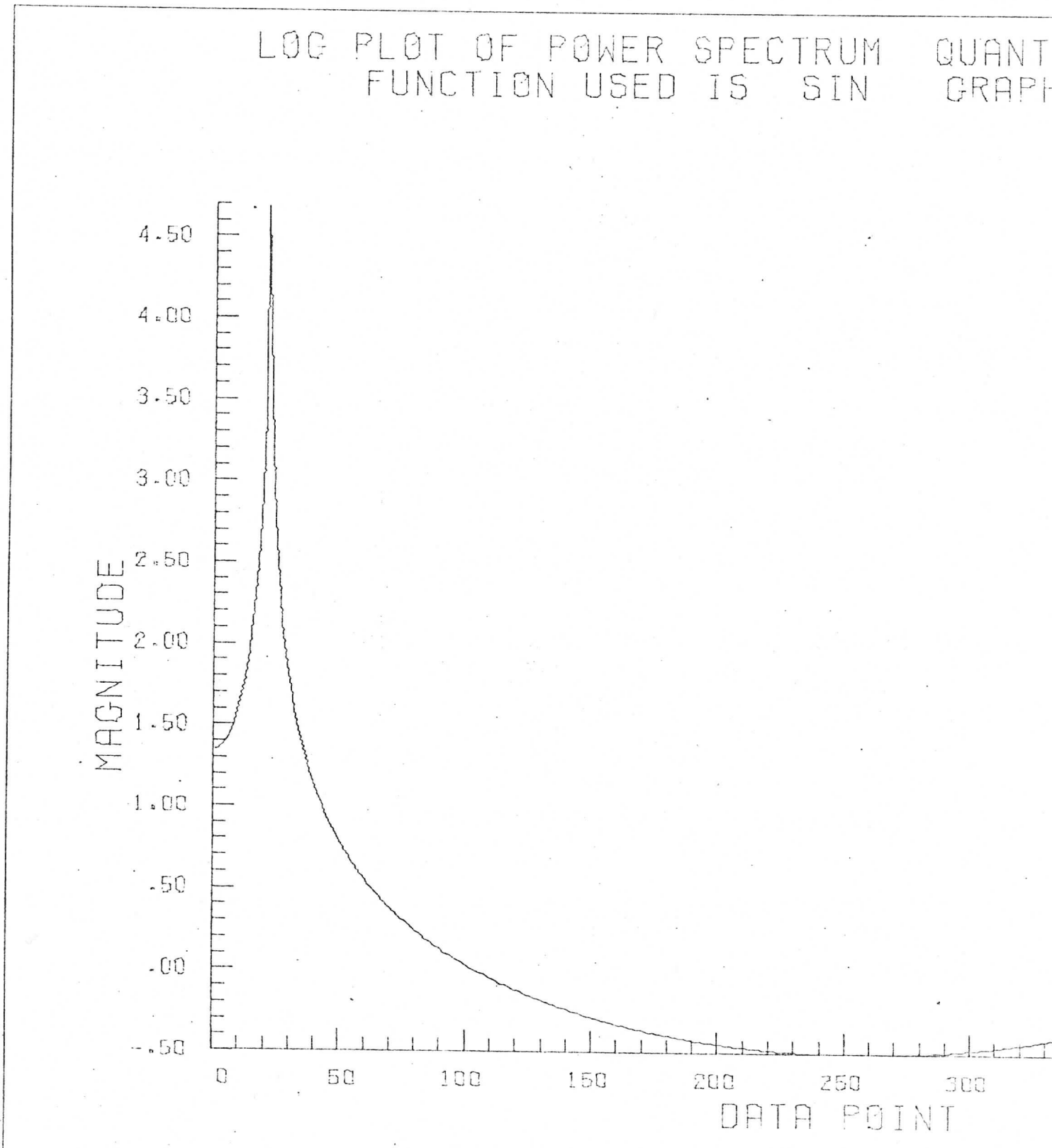

Cycles: 20.300
Window: Hanning
Avg. Value: 0.00000
Date: 12/30/72-6

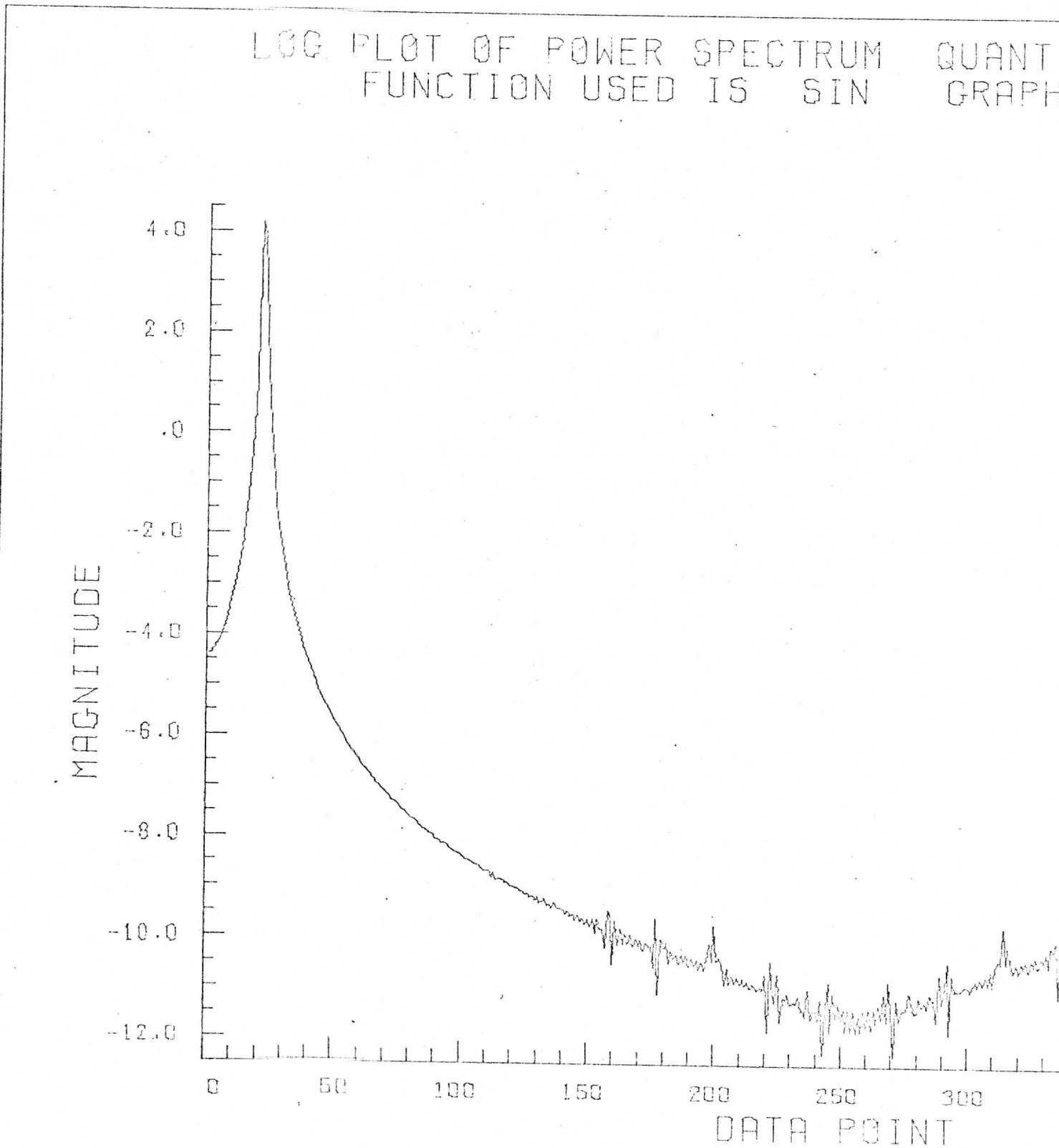

Cycles: 20.300
Window: Hamming
Avg. Value: 0.00000
Date: 12/30/72-7

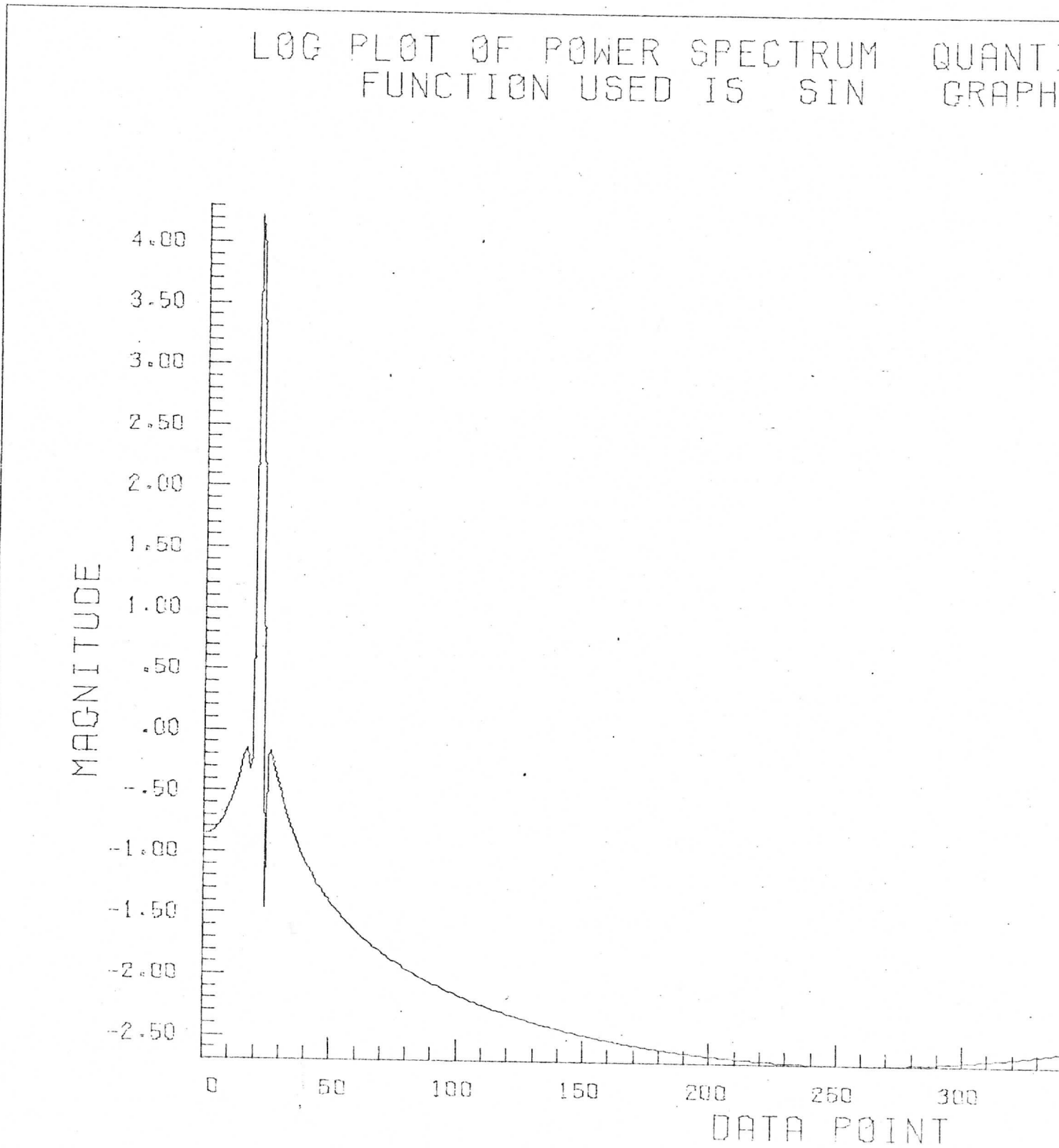

Cycles: 20.300
Window: Papoulis
Avg. Value: 0.0000
Date: 2/15/73-4

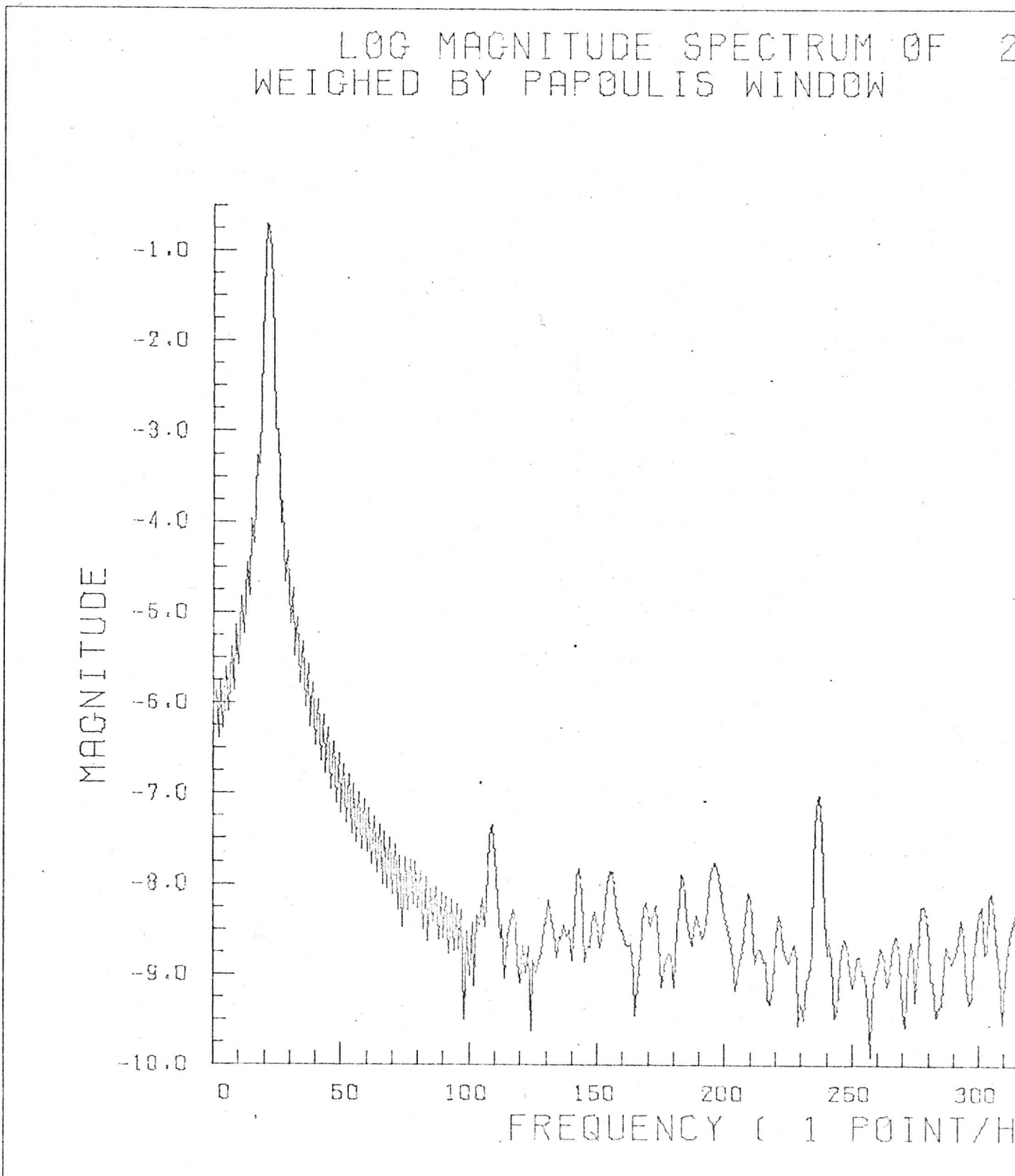

Cycles: 97.000
Window: Rectangular
Avg. Value: 0.01000
Date: 12/30/72-9

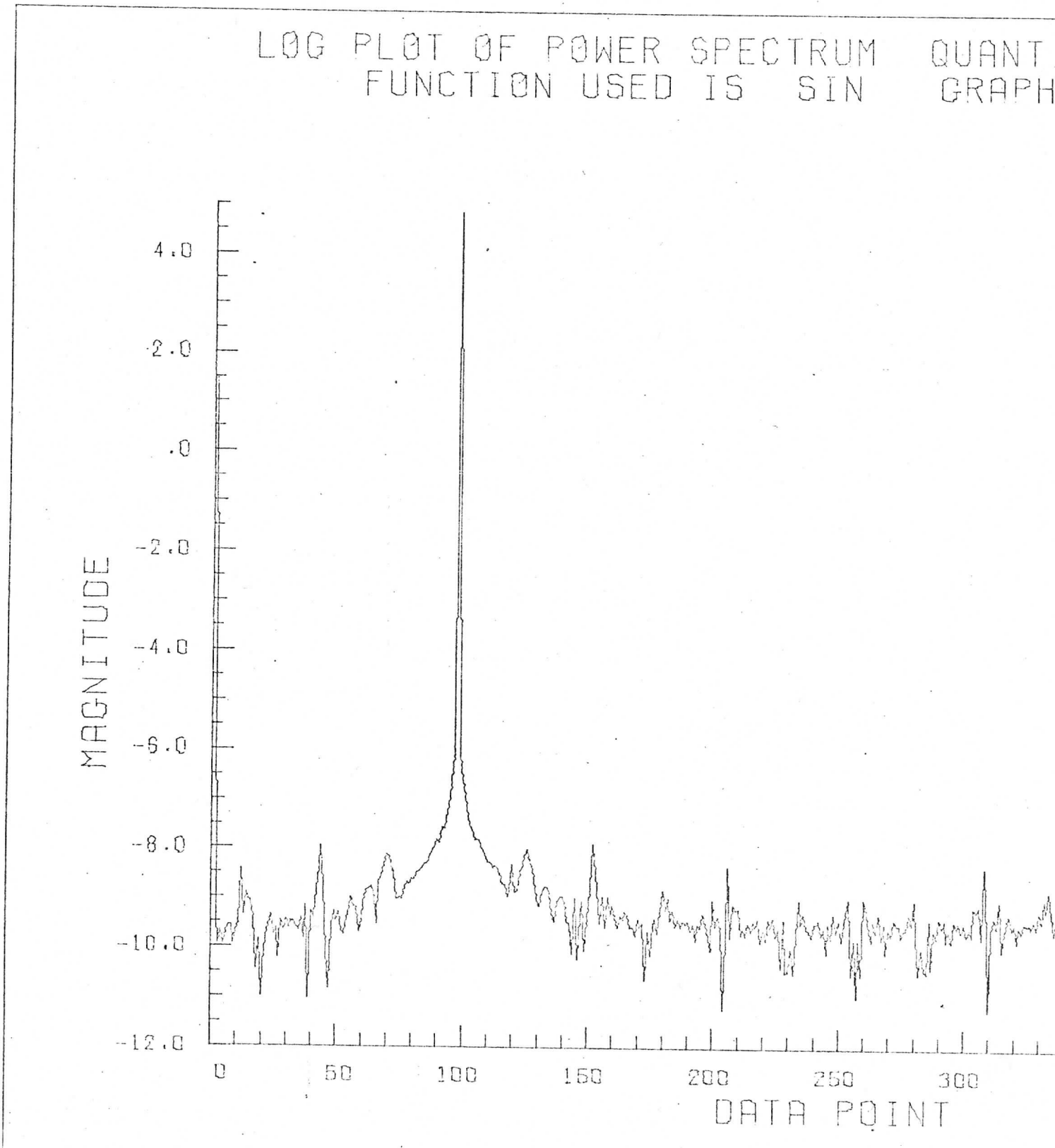

Cycles: 97.000
Window: Hanning
Avg. Value: 0.01000
Date: 12/30/72-10

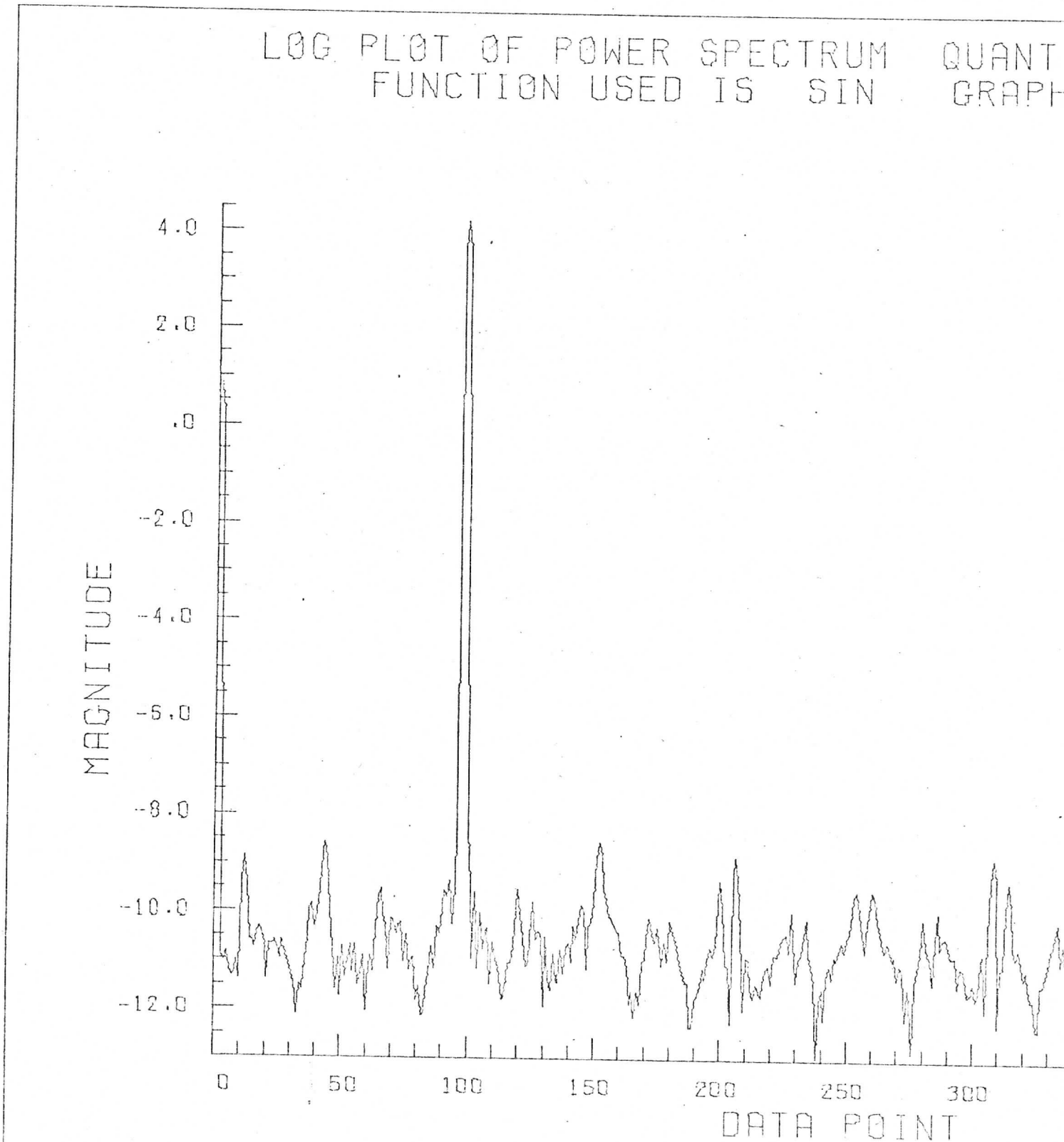

Cycles: 96.700
Window: Rectangular
Avg. Value: 0.01000
Date: 12/30/72-11

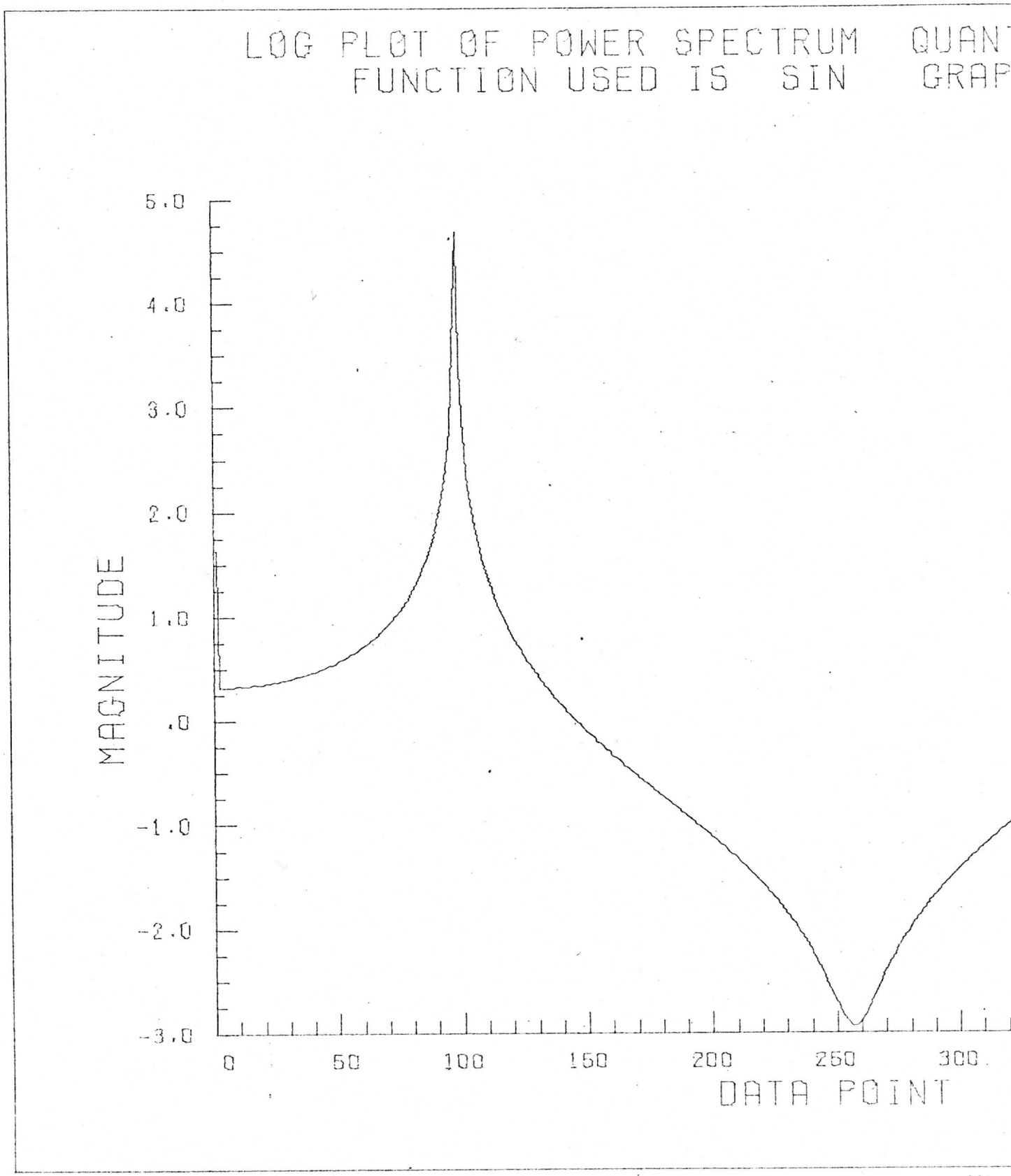

Cycles: 96.700
Window: Hanning
Avg. Value: 0.01000
Date: 12/30/72-12

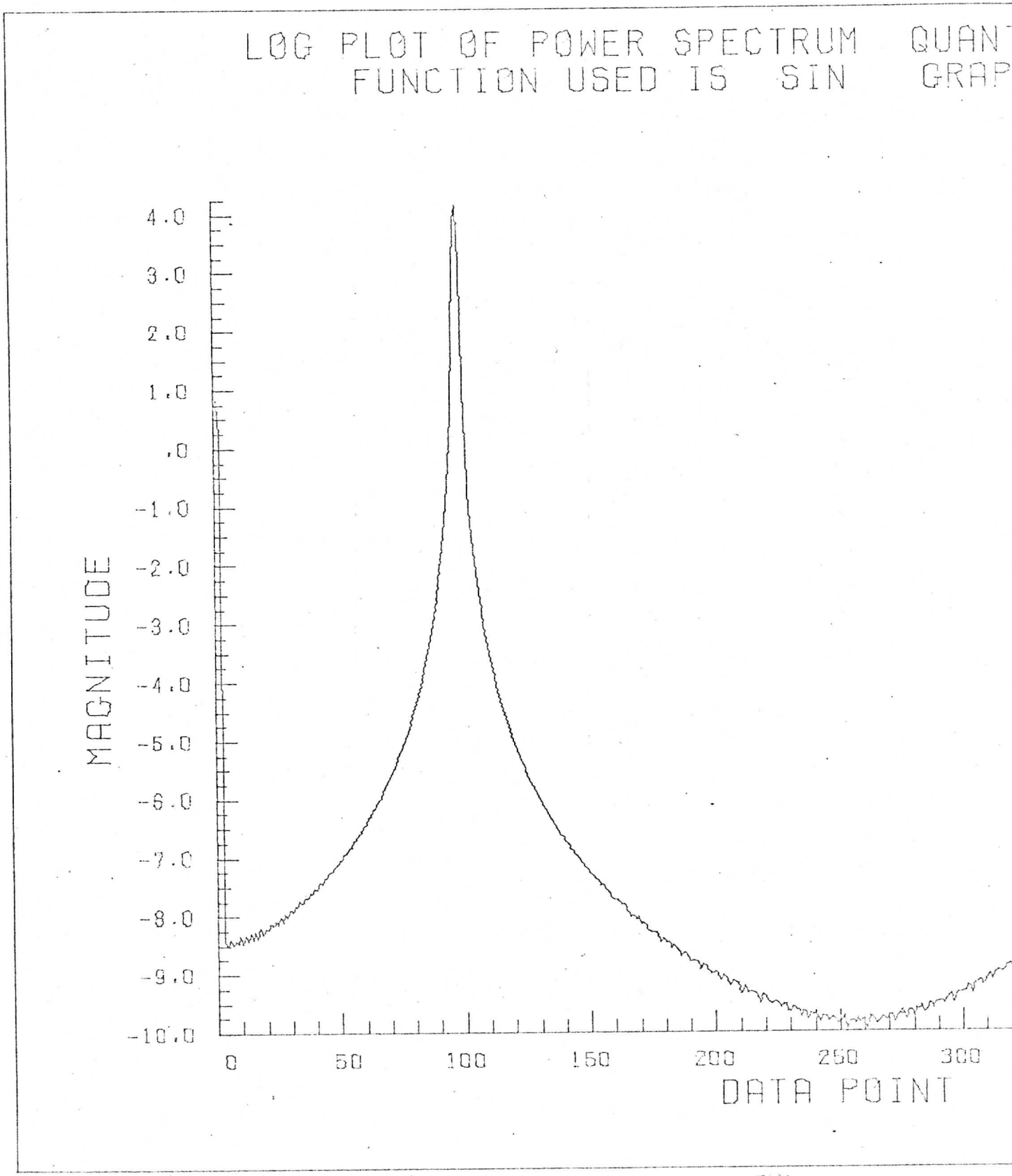

Cycles: 96.700
Window: Hamming
Avg. Value: 0.01000
Date: 12/30/72-13

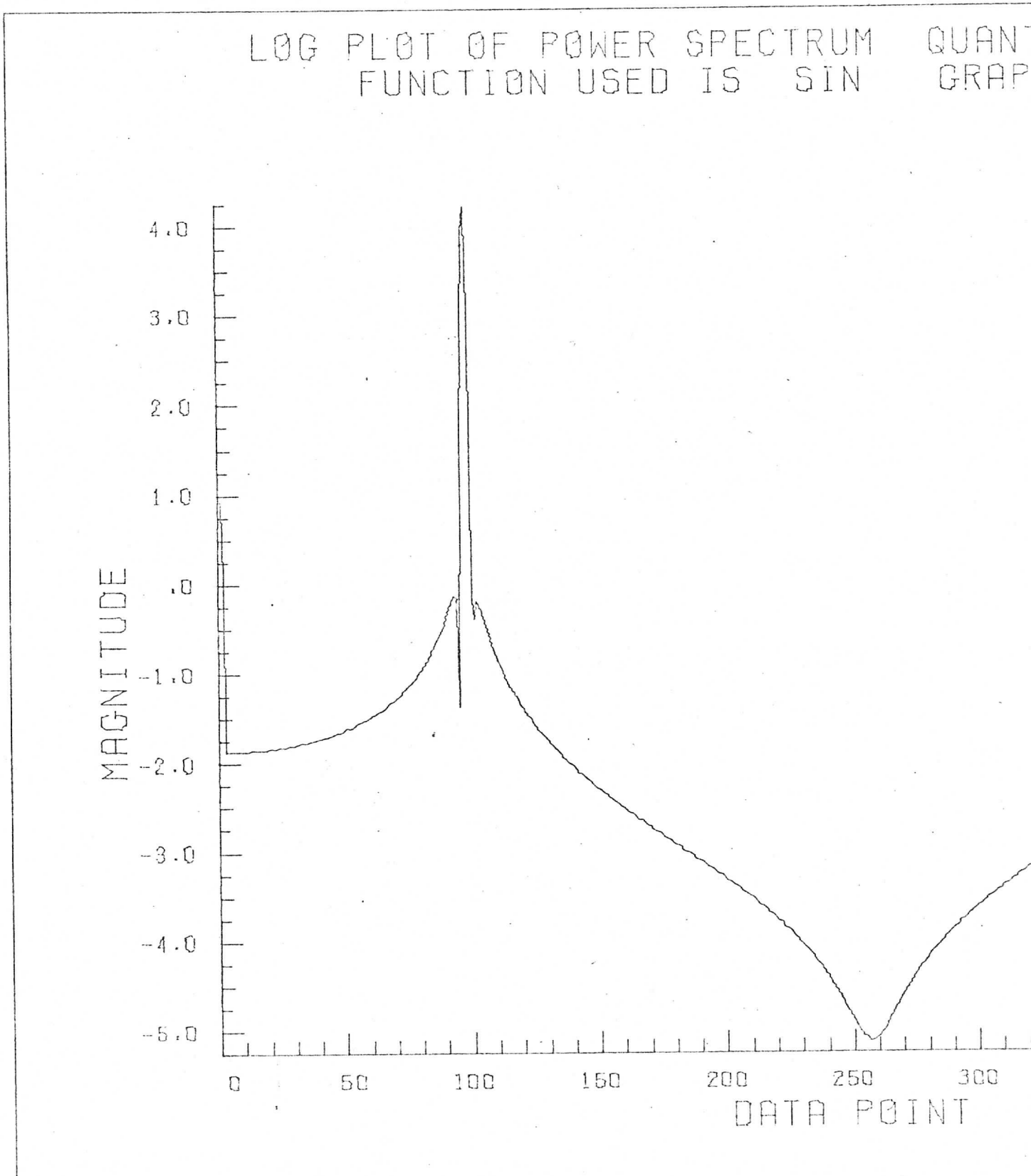

Cycles: 96.700
Window: Papoulis
Avg. Value: 0.0000
Date: 2/15/73-6

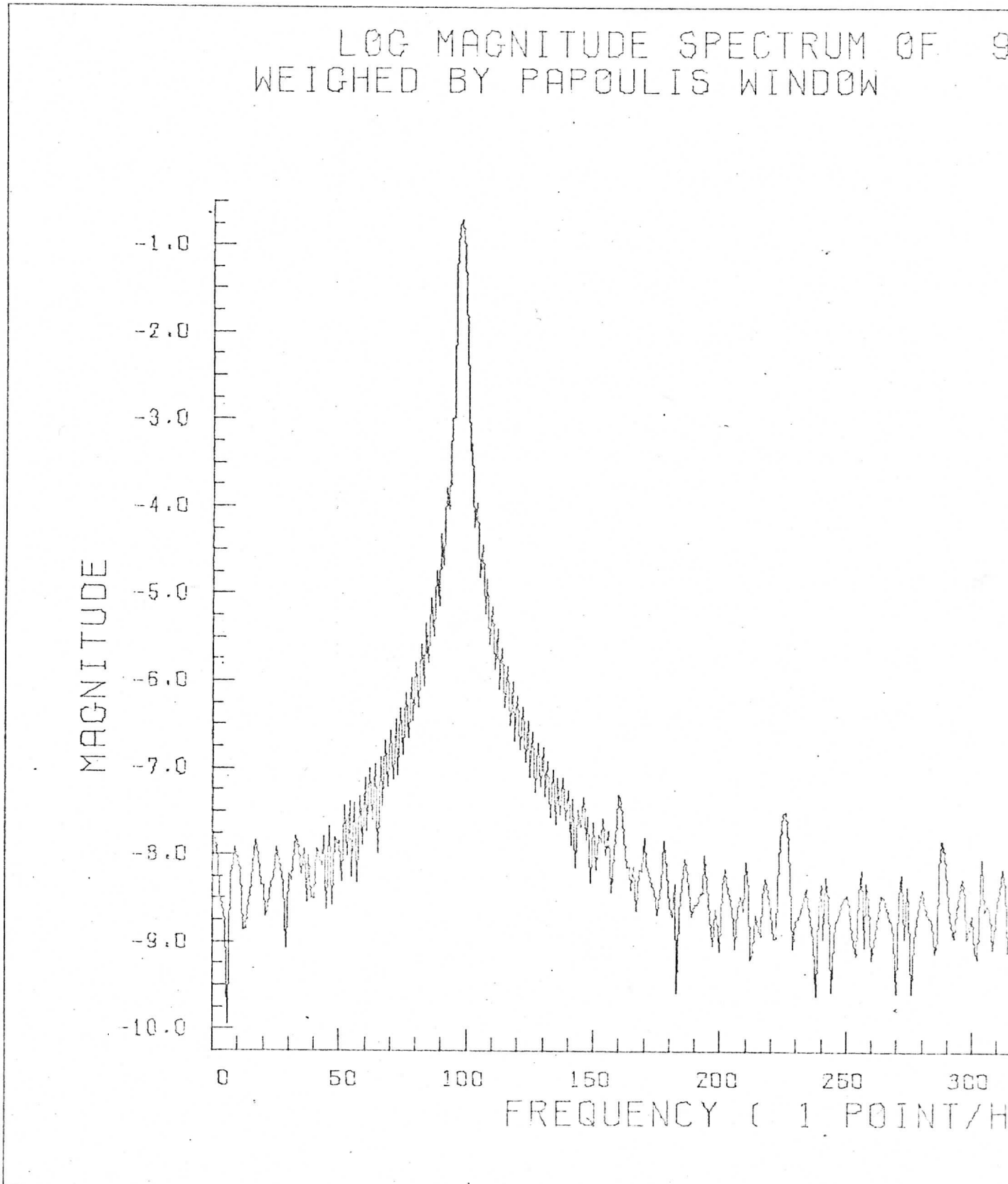

Cycles: 131.000
Window: Rectangular
Avg. Value: 0.10000
Date: 12/30/72-15

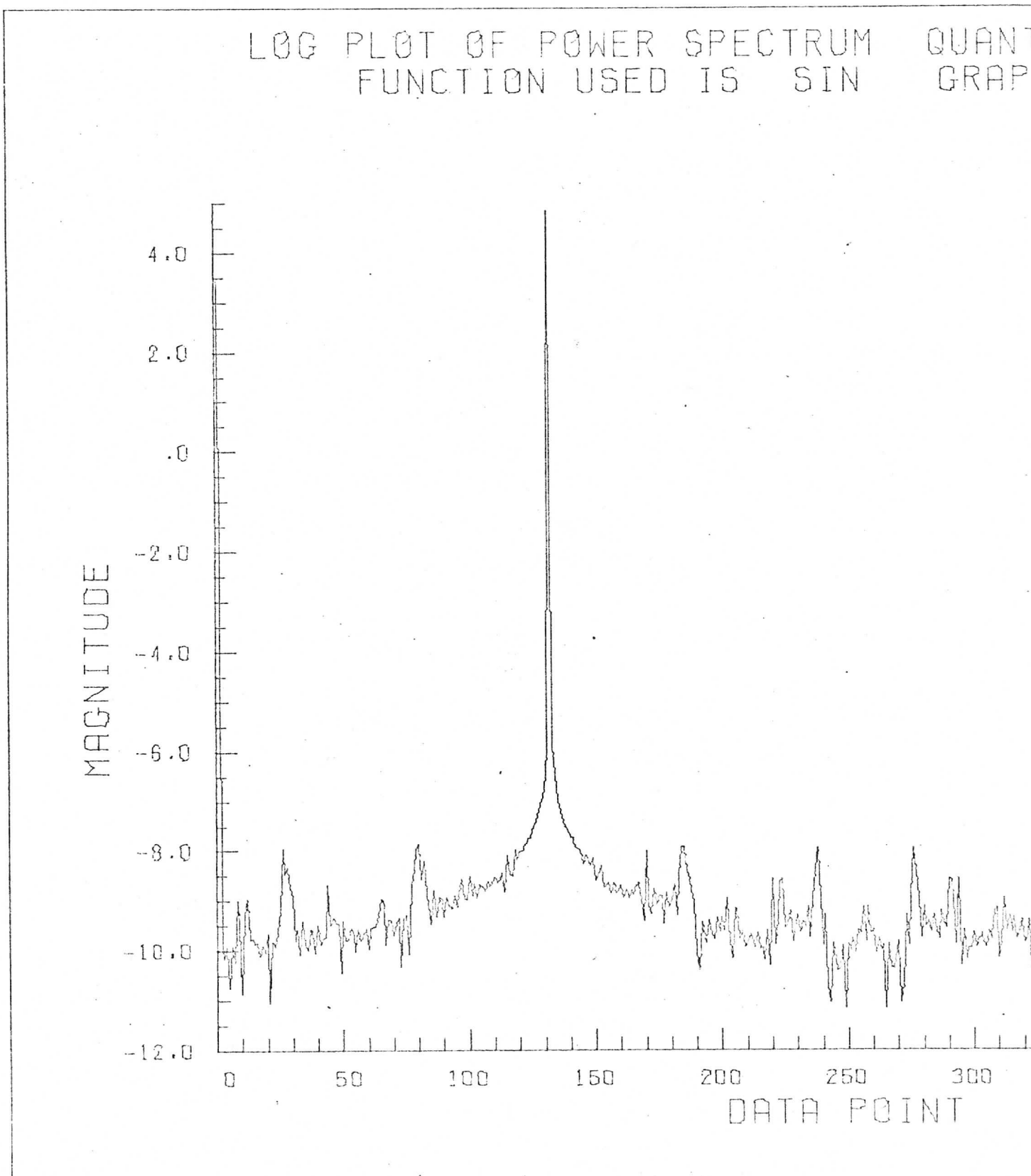

Cycles: 131.000
Window: Hanning
Avg. Value: 0.10000
Date: 12/30/72-16

LOG PLOT OF POWER SPECTRUM QUANT
FUNCTION USED IS SIN GRAPI

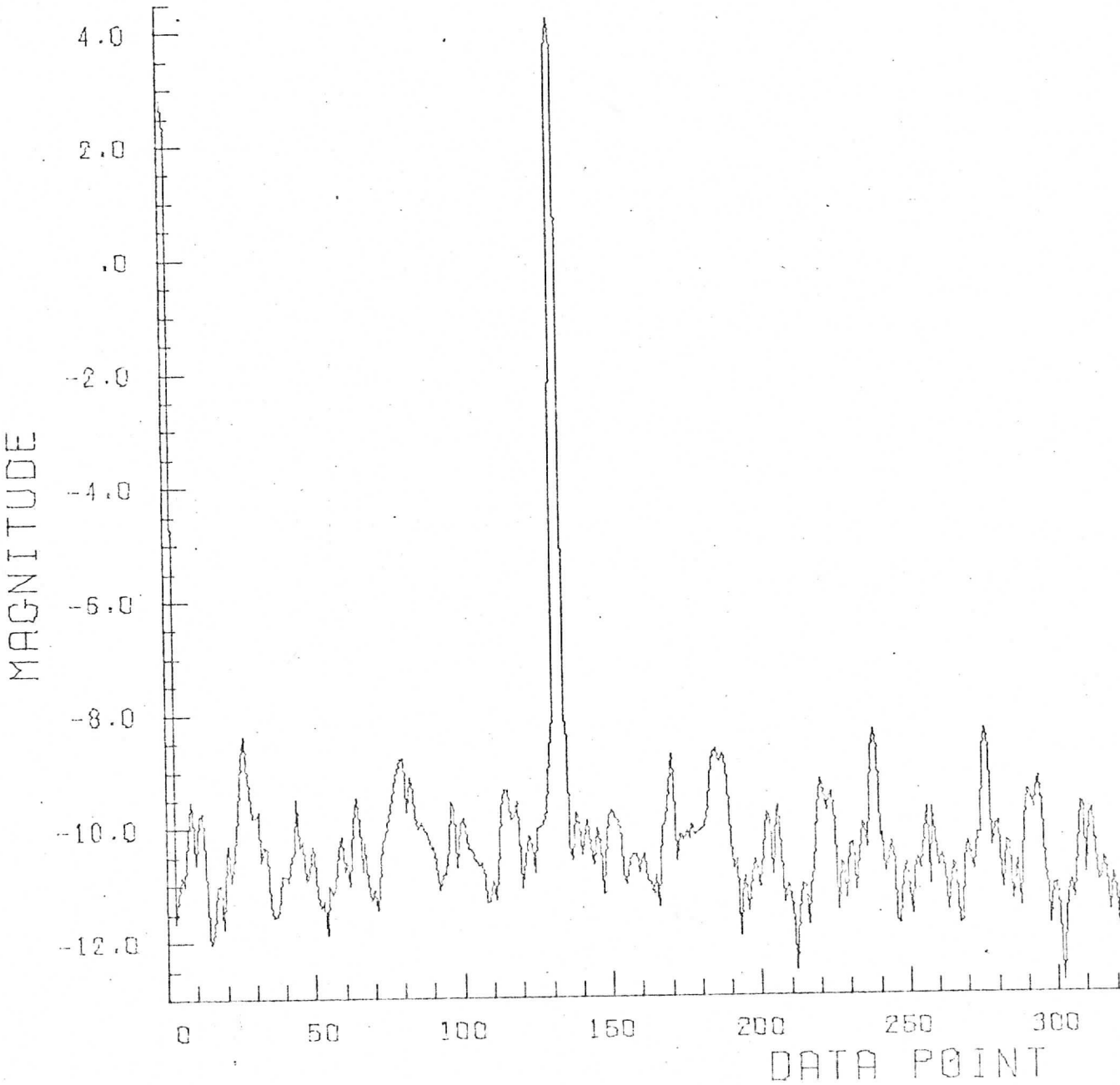

Cycles: 131.200
Window: Rectangular
Avg. Value: 0.10000
Date: 12/30/72-17

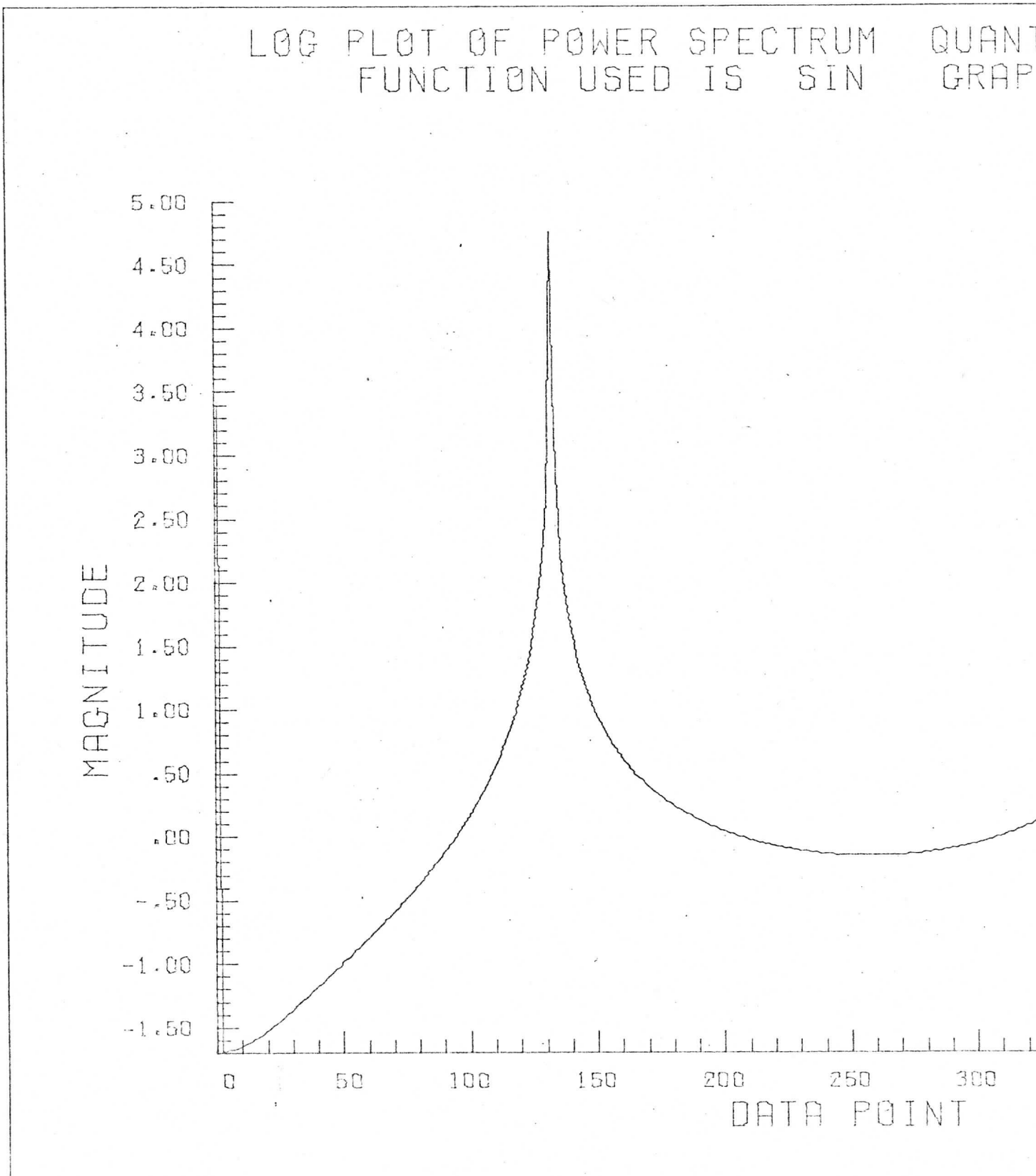

Cycles: 131.200
Window: Hanning
Avg. Value: 0.10000
Date: 12/30/72-18

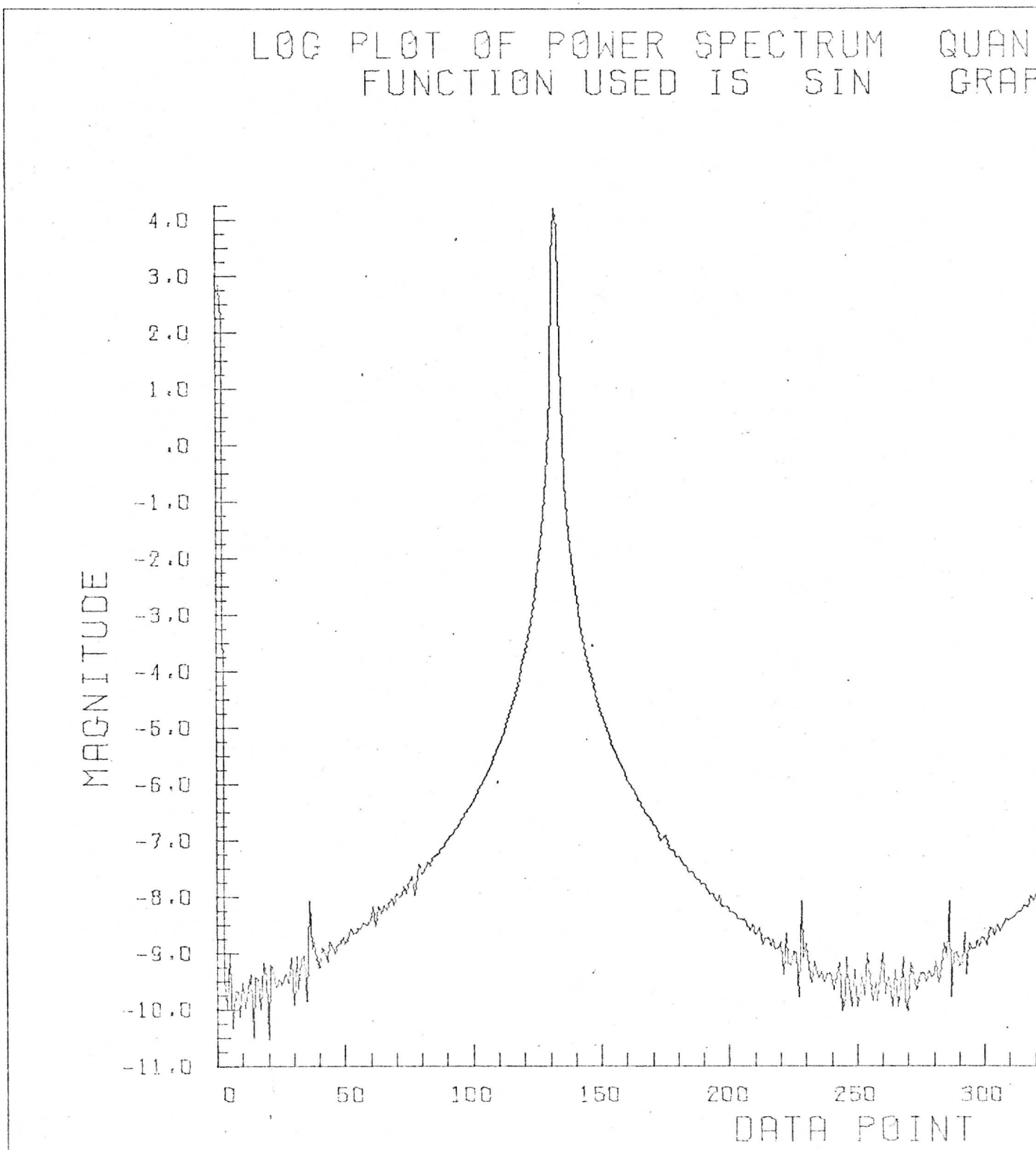

Cycles: 131.200
Window: Hamming
Avg. Value: 0.10000
Date: 12/30/72-19

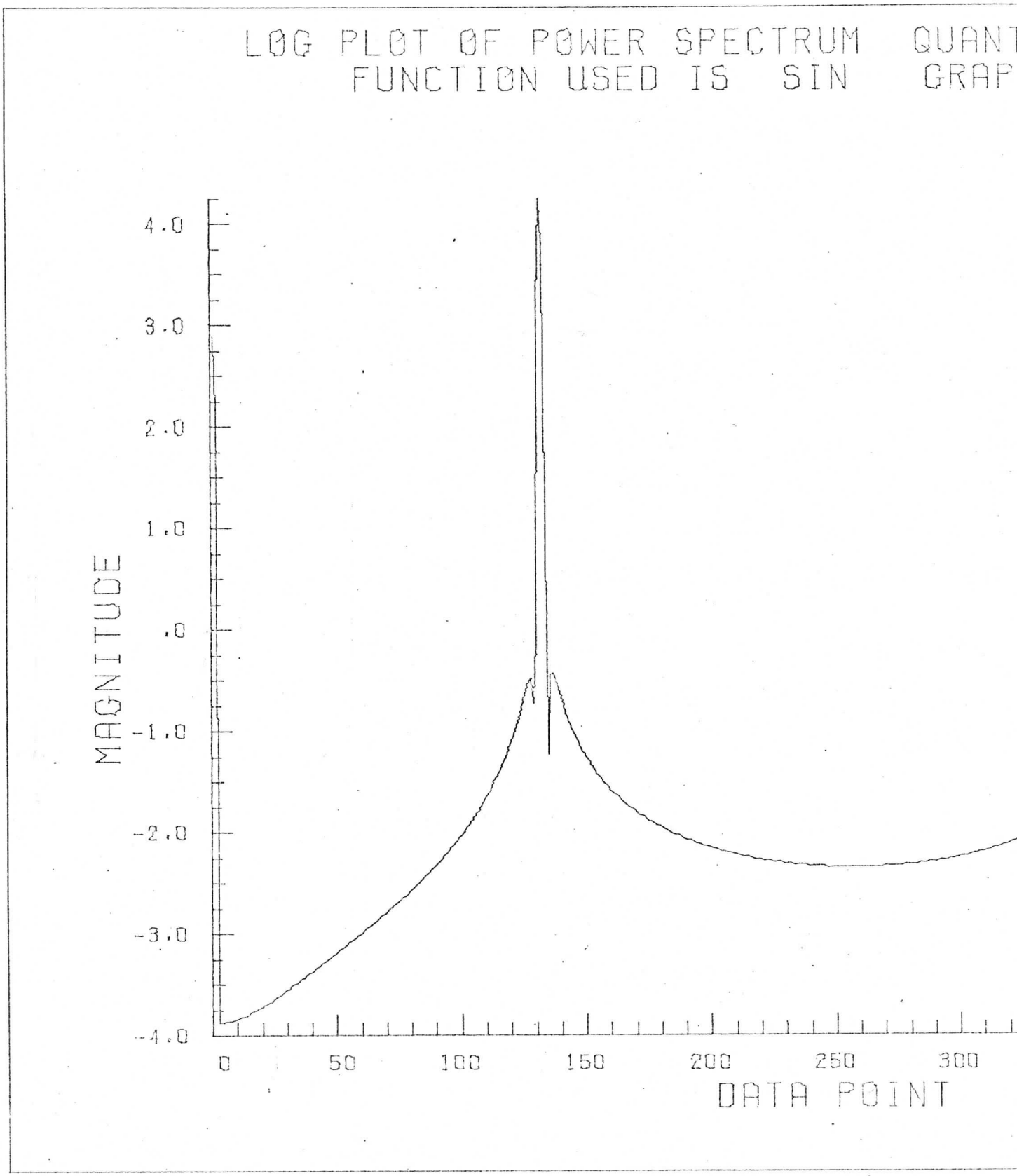

Cycles: 132.20
Window: Papoulis
Avg. Value: 0.0000
Date: 2/15/73-8

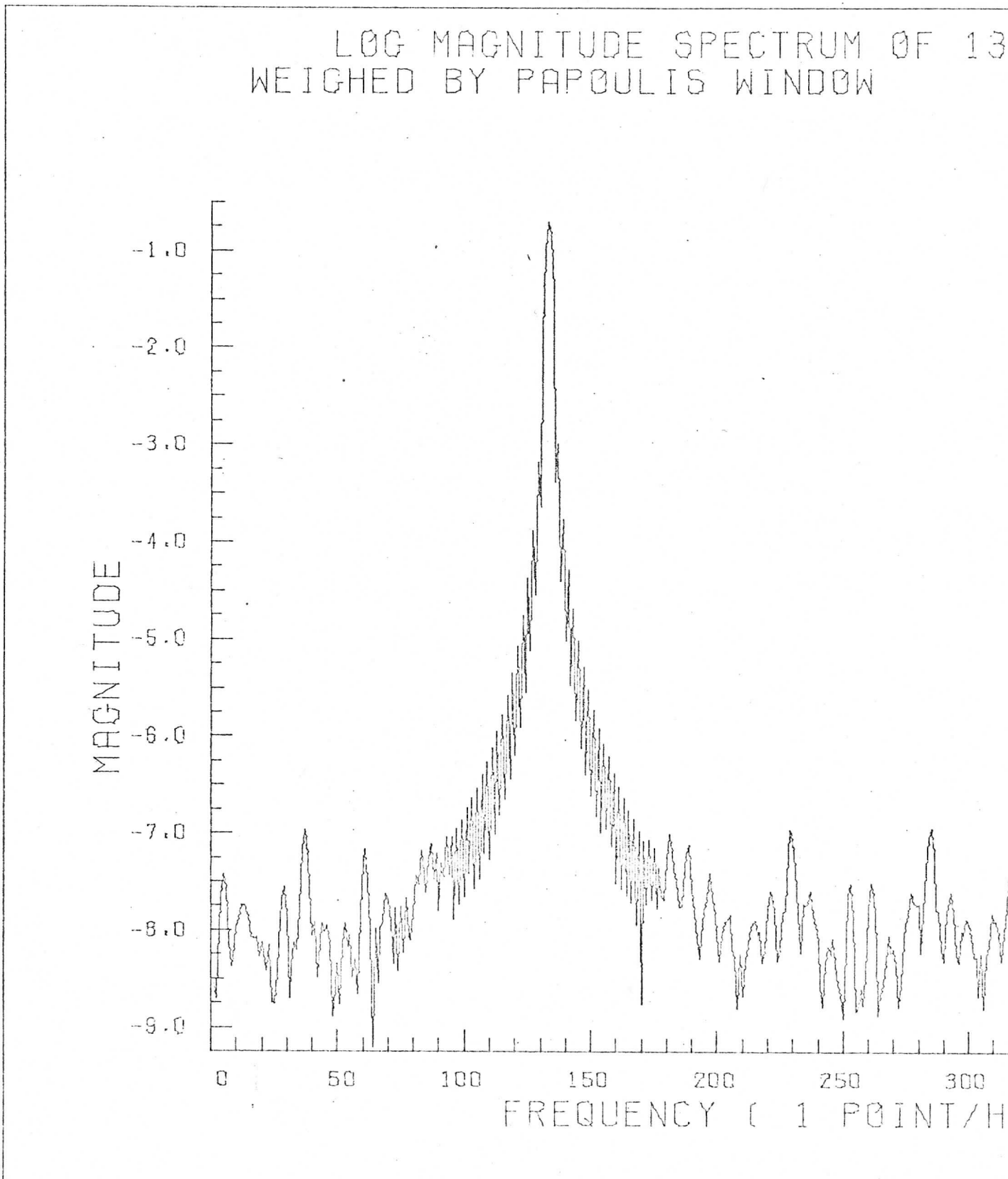

Cycles: 203.000
Window: Rectangular
Avg. Value: 0.50000
Date: 12/30/72-21

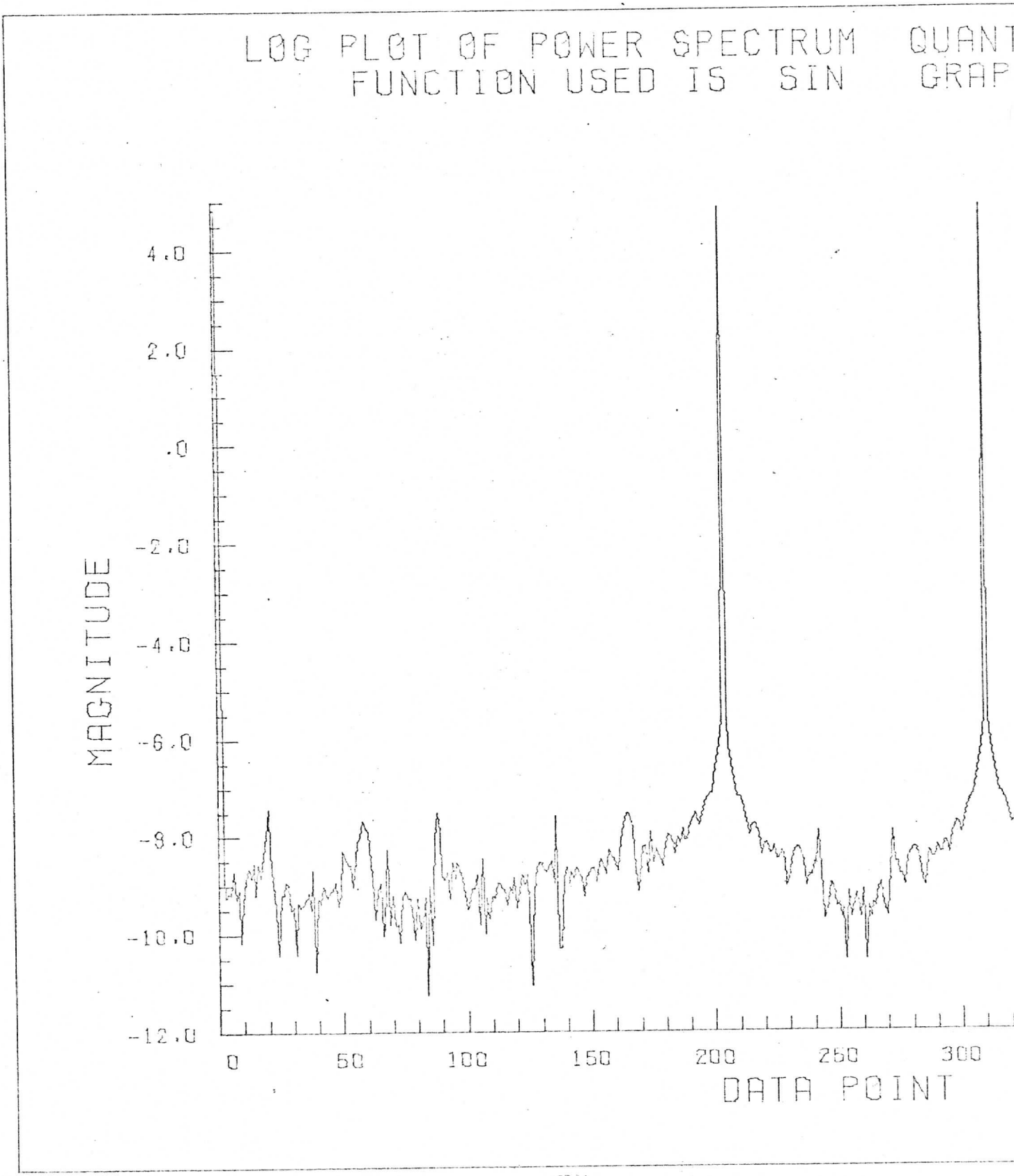

Cycles: 203.000
Window: Hanning
Avg. Value: 0.50000
Date: 12/30/72-22

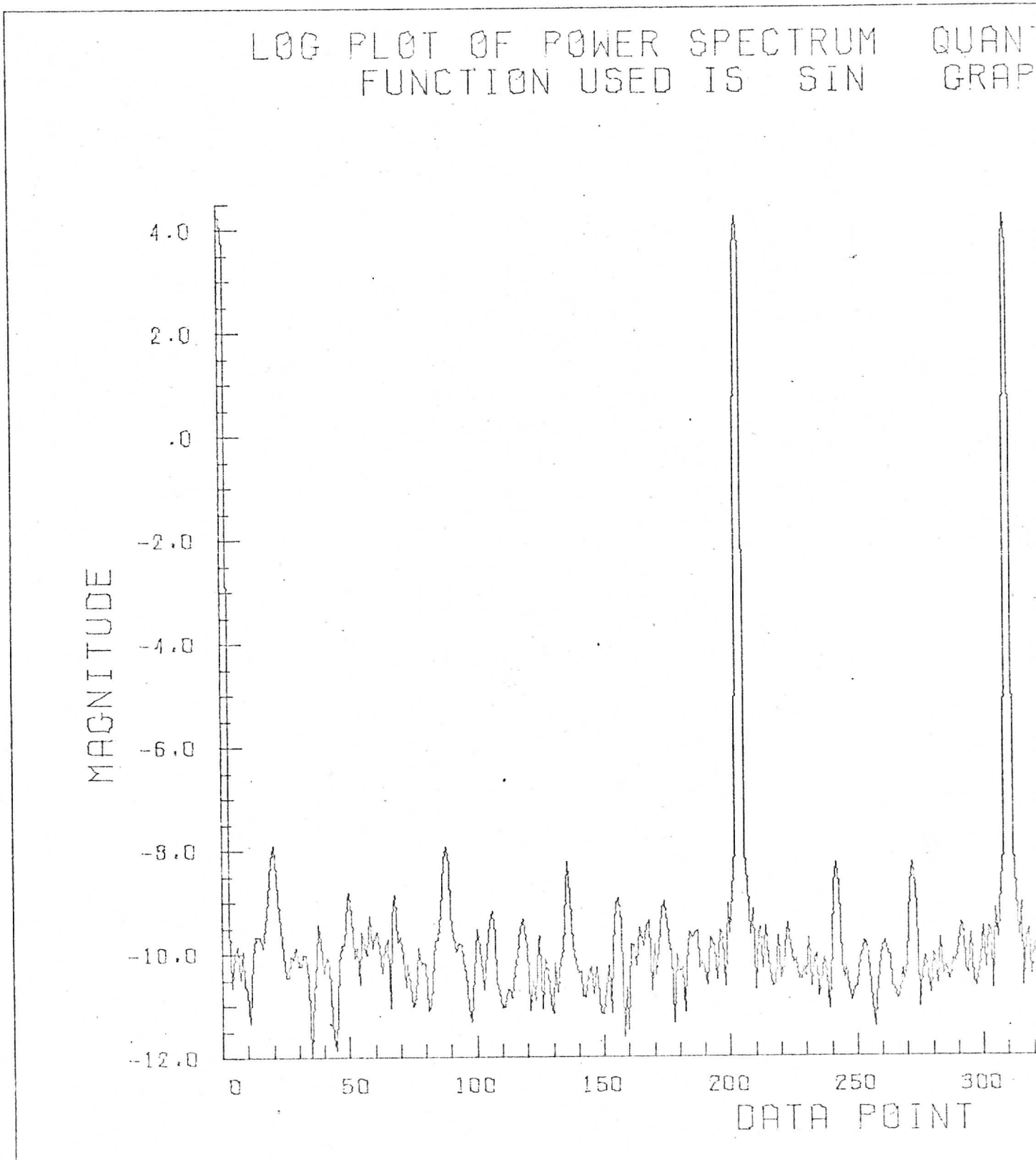

Cycles: 203.000
Window: Hamming
Avg. Value: 0.50000
Date: 12/30/72-23

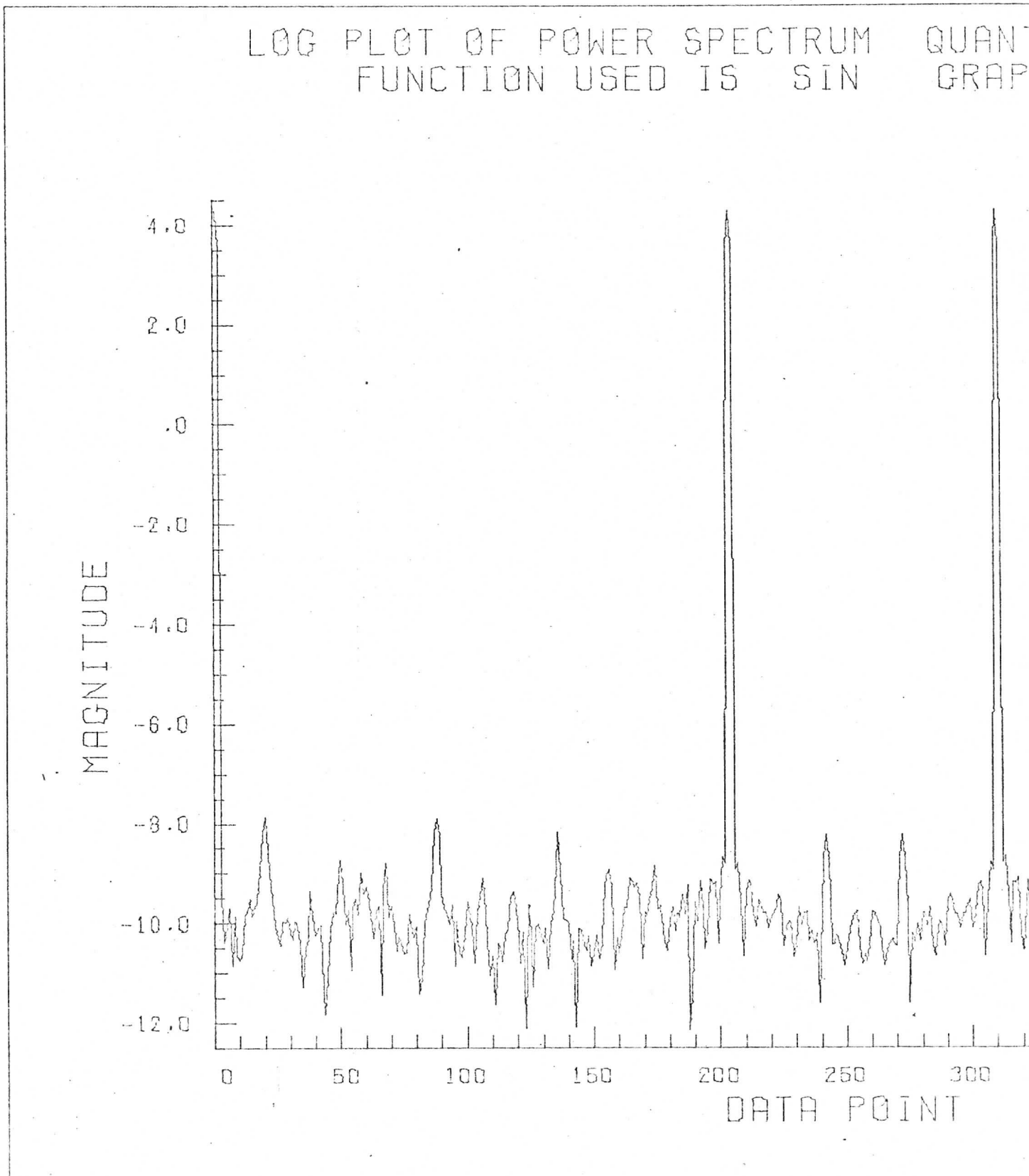

Cycles: 202.68
Window: Rectangular
Avg. Value: 0.00000
Date: 12/30/72-25

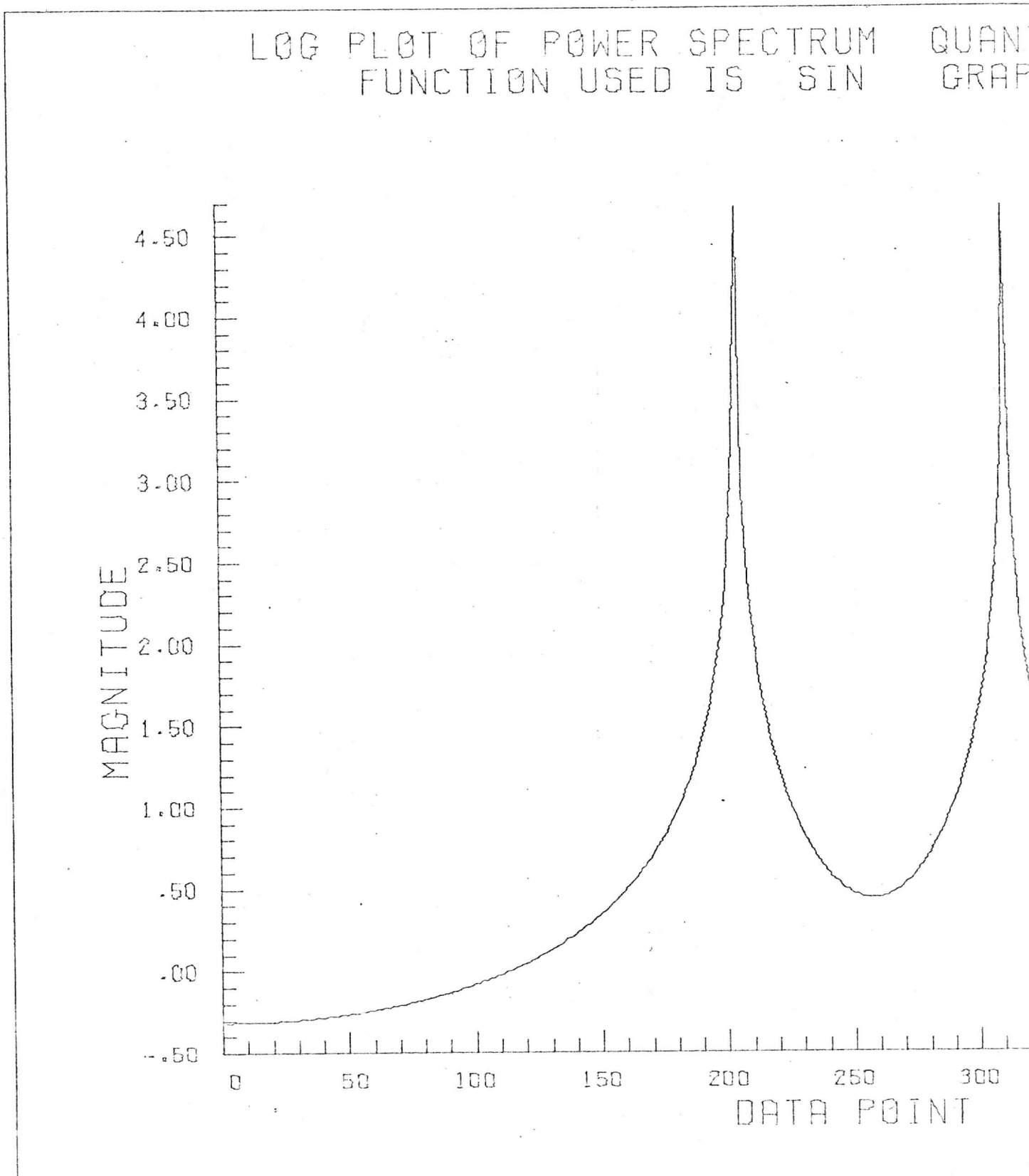

Cycles: 202.68
Window: Hanning
Avg. Value: 0.00000
Date: 12/30/72-26

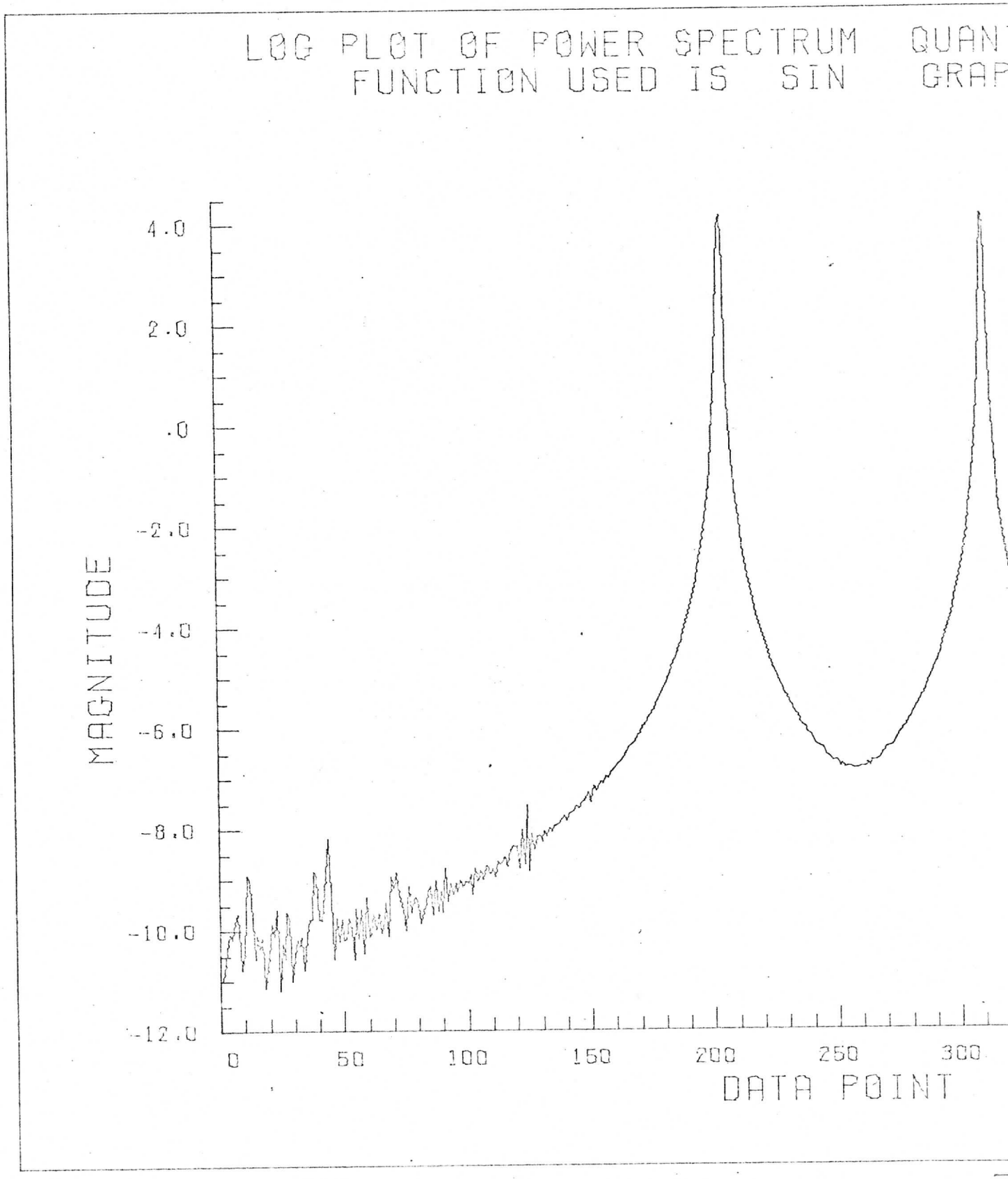

Cycles: 202.68
Window: Hamming
Avg. Value: 0.00000
Date: 12/30/72-27

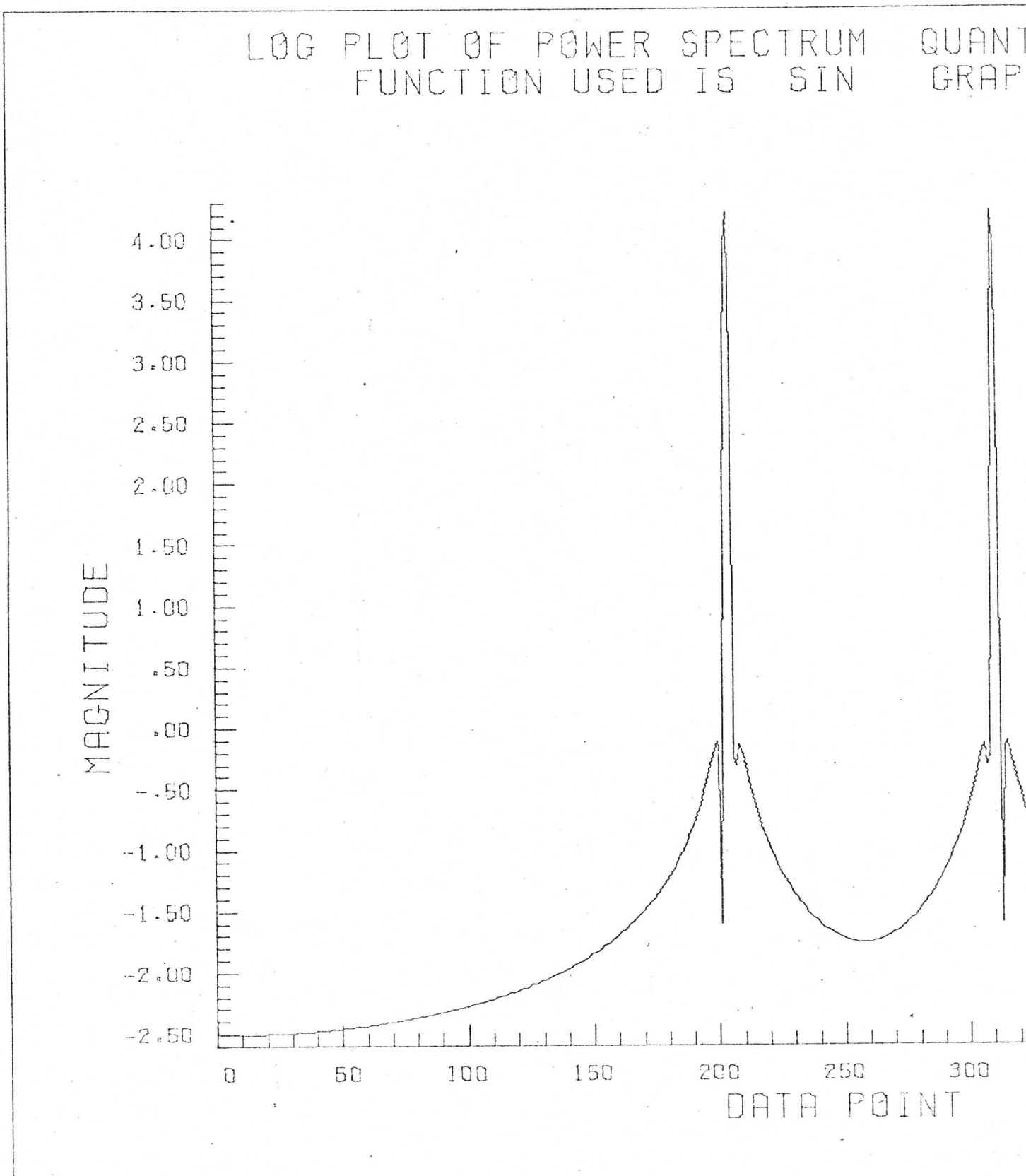

Cycles: 202.68
Window: Papoulis
Avg. Value: 0.0000
Date: 2/15/73-10

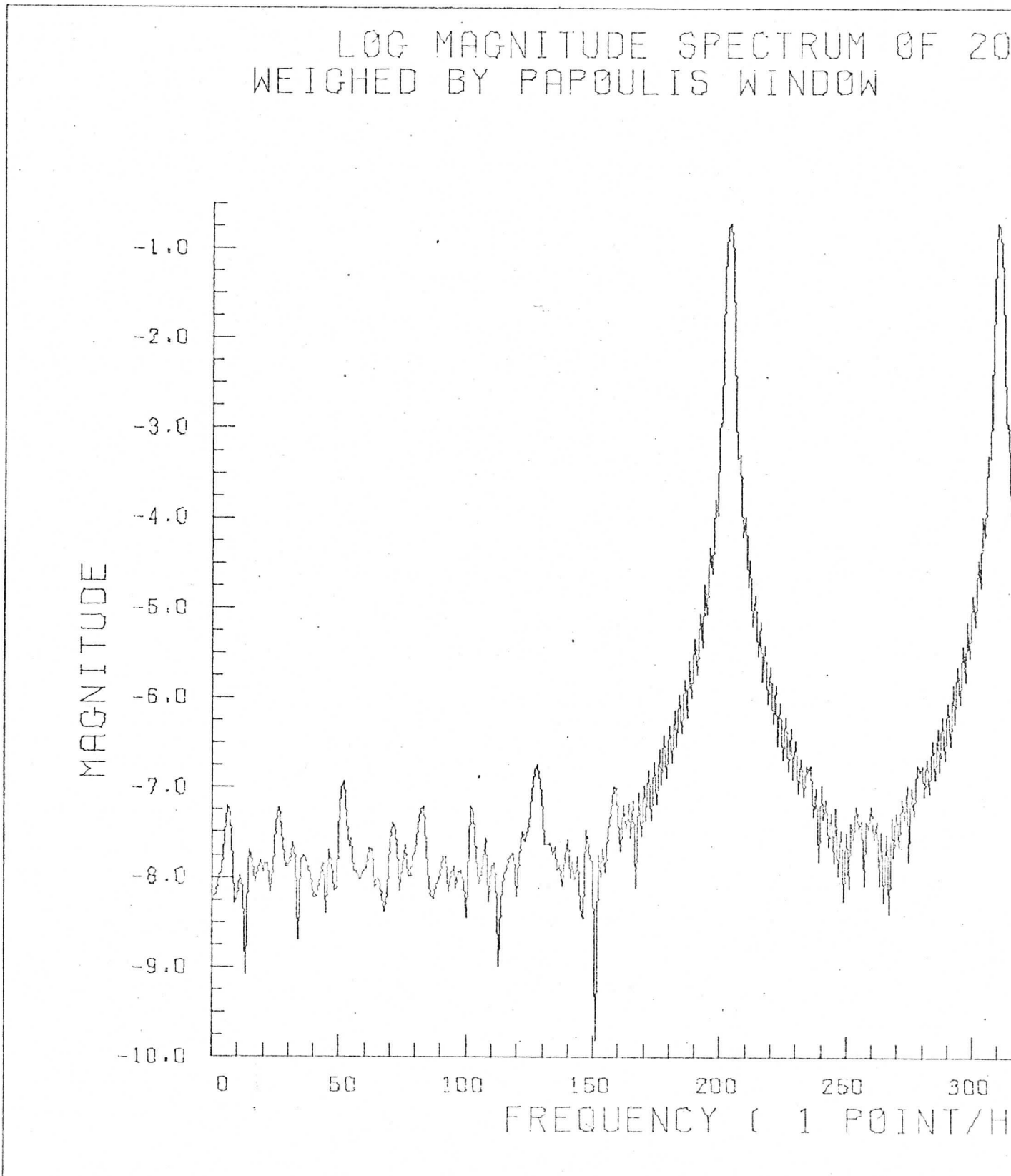

APPENDIX C

CALCULATION OF SMS SPATIAL FREQUENCY CONVERSIONS

Here we briefly outline the type of conversion necessary to convert spatial frequency content measured on the earth's surface to the apparent frequency content as viewed by the SMS. We restrict the analysis to the plane passing through the center of the earth and perpendicular to the satellite spin axis. The geometry is shown in Figure C.1.

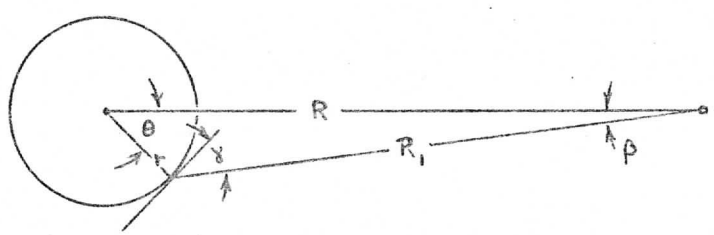

Figure C.1. Earth-Satellite Geometry

Let R be the distance between centers of the earth and the satellite, r the radius of the earth, and let R_1 be the distance between the observed point on the surface of a spherical earth and the satellite. From the figure, we can write:

$$\tan \beta = \frac{r \sin \theta}{R - r \cos \theta} = \frac{(r/R) \sin \theta}{1 - (r/R) \cos \theta} . \qquad \text{(C-1)}$$

From this, we can determine β for a given θ.

Using the law of sines, we can write:

$$\frac{R - r \sec \theta}{\sin \gamma} = \frac{r \tan \theta}{\sin \beta} \qquad \text{(C-2)}$$

or,

$$\frac{1}{\sin \gamma} = \frac{r \tan \theta}{\sin \beta (R - r \sec \theta)} \quad . \tag{C-3}$$

For a constant angular rate $\dot{\beta}$, the phase velocity along the earth's surface is:

$$v_p = v/\sin \gamma \tag{C-4}$$

where v is the tangential velocity:

$$v = \dot{\beta} R_1 . \tag{C-5}$$

We can also write, referring to Figure C.1 and using the law of sines,

$$\frac{R_1}{\sin\theta} = \frac{r}{\sin\beta}$$

or,

$$R_1 = \frac{r \sin\theta}{\sin \beta} \quad . \tag{C-6}$$

The relative increase in the phase velocity v_p over that at the satellite subpoint, v_{p_0}, is then:

$$\Gamma = \frac{v_p}{v_{p_0}} = \frac{\dfrac{\dot{\beta} R_1}{\sin \gamma}}{\dfrac{\dot{\beta}(R-r)}{\sin(\pi/2)}}$$

$$= \frac{R_1}{(R-r) \sin \gamma} \quad . \tag{C-7}$$

Substituting Eq. C-6 in Eq. C-7,

$$\Gamma = \frac{r \sin \theta}{(R-r) \sin \beta \sin \gamma} \tag{C-8}$$

and substituting Eq. C-3 in Eq. C-8, we get:

$$\Gamma = \frac{(r/R)^2 \sin \theta \tan \theta}{[1 - (r/R)][1 - (r/R) \sec \theta] \sin^2 \beta} \quad . \tag{C-9}$$

This is about all the farther we can go in general. Given a value of θ, the angle β can be determined from Eq. C-1. This in turn can be used to solve Eq. C-8 for the correction factor Γ. Considerable simplification can be made if β is assumed to be small. In this case, we can use the approximation $\sin \beta \approx \tan \beta$. Using this approximation, we can substitute Eq. C-1 directly into C-8 yielding:

$$\Gamma = \frac{[1 - (r/R) \cos \theta]^2}{[1 - (r/R)][\cos \theta - (r/R)]} . \qquad \text{(C-10)}$$

These approximations are good to within about 1% for the case of interest: $r/R = 4/26.3 = 0.152$. A graph of Γ is shown in Figure 4.

The apparent instantaneous frequency f_1 viewed from the satellite is proportional to the satellite spin rate times the phase velocity correction factor Γ:

$$f_1 = f \dot{\beta} (R-r)\Gamma. \qquad \text{(C-11)}$$

Because the satellite spin rate is a constant,

$$\dot{\beta} = 100 \text{ rpm} = 10.47 \text{ rad./sec.}$$

we can conveniently normalize everything to the satellite subpoint:

$$\dot{\beta}(R-r) = (10.47)(19{,}360) = 0.202 \text{ n.mi./}\mu\text{-sec.}$$

Thus the frequency conversion is:

$$f_1 = 0.202 \, \Gamma f \qquad \text{(C-12)}$$

where:

f_1 = apparent instantaneous frequency in MHz

f = spatial frequency in cycles per nautical mile

Γ = phase velocity correction factor.

The above analysis has not included the effects of a variation across the satellite IGFOV nor has it included the effects of an azimuthal angle. It is intended merely to show the variations in satellite scaling between the spatial frequencies displayed in the power spectra in this report and the spectra of the electrical signals out of the photomultiplier tube. These electrical signals are bandlimited by the pre-aliasing filter in the satellite. Clearly if there is an aliasing problem for data at the satellite subpoint the aliasing problem will become more serious as θ increases.

REFERENCES

M. Born and E. Wolf, Principles of Optics, Third Ed., Pergamon Press, N.Y., 1965, Ch. 8.

Computer Sciences Corp., Synchronous Meteorological Satellite Image Quality Analysis, Final Report, September 1972, Section 3.

J. W. Goodman, Introduction to Fourier Optics, McGraw-Hill, N.Y., 1968, Ch. 6.

C. D. McGillem and G. R. Cooper, Continuous and Discrete Signal and System Analysis. New York: Holt, Rinehart and Winston, 1973, Chapter 5.

R. K. Otnes and L. Enochson, Digital Time Series Analysis. New York: John Wiley & Sons, 1972, Chapter 7.

A. Papoulis, Probability, Random Variables, and Stochastic Processes. New York: McGraw-Hill, 1965, Chapter 10.

A. Papoulis, "Minimum Bias Windows for High Resolution Spectral Estimates," IEEE Transactions on Information Theory, Vol. IT-19, pp. 9-12, 1973.

ACKNOWLEDGEMENTS

We wish to thank Mr. Nim-Yau Chu for his very valuable help in performing the computer calculations for this report.